

OpenMolcas: From Source Code to Insight

Ignacio Fdez. Galván,^{1,2} Morgane Vacher,¹ Ali Alavi,³ Celestino Angeli,⁴ Francesco Aquilante,⁵ Jochen Autschbach,⁶ Jie J. Bao,⁷ Sergey I. Bokarev,⁸ Nikolay A. Bogdanov,³ Rebecca K. Carlson,^{7,9} Liviu F. Chibotaru,¹⁰ Joel Creutzberg,^{11,12} Nike Dattani,¹³ Mickaël G. Delcey,¹ Sijia S. Dong,^{7,14} Andreas Dreuw,¹⁵ Leon Freitag,¹⁶ Luis Manuel Frutos,¹⁷ Laura Gagliardi,⁷ Frédéric Gendron,⁶ Angelo Giussani,^{18,19} Leticia González,²⁰ Gilbert Grell,⁸ Meiyuan Guo,^{1,21} Chad E. Hoyer,^{7,22} Marcus Johansson,¹² Sebastian Keller,¹⁶ Stefan Knecht,¹⁶ Goran Kovačević,²³ Erik Källman,¹ Giovanni Li Manni,³ Marcus Lundberg,¹ Yingjin Ma,¹⁶ Sebastian Mai,²⁰ João Pedro Malhado,²⁴ Per Åke Malmqvist,¹² Philipp Marquetand,²⁰ Stefanie A. Mewes,^{15,25} Jesper Norell,¹¹ Massimo Olivucci,^{26,27,28} Markus Oppel,²⁰ Quan Manh Phung,²⁹ Kristine Pierloot,²⁹ Felix Plasser,³⁰ Markus Reiher,¹⁶ Andrew M. Sand,^{7,31} Igor Schapiro,³² Prachi Sharma,⁷ Christopher J. Stein,^{16,33} Lasse Kragh Sørensen,^{1,34} Donald G. Truhlar,⁷ Mihkel Ugandi,^{1,35} Liviu Ungur,³⁶ Alessio Valentini,³⁷ Steven Vancouillie,¹² Valera Veryazov,¹² Oskar Weser,³ Tomasz A. Wesolowski,⁵ Per-Olof Widmark,¹² Sebastian Wouters,³⁸ Alexander Zech,⁵ J. Patrick Zobel,¹² and Roland Lindh^{*,2,39}

¹Department of Chemistry – Ångström Laboratory, Uppsala University, P.O. Box 538, SE-751 21 Uppsala, Sweden

²Department of Chemistry – BMC, Uppsala University, P.O. Box 576, SE-751 23 Uppsala, Sweden

³Max Planck Institut für Festkörperforschung, Heisenbergstraße 1, 70569 Stuttgart, Germany

⁴Dipartimento di Scienze Chimiche e Farmaceutiche, Università di Ferrara, Via Luigi Borsari 46, 44121 Ferrara, Italy

⁵Département de Chimie Physique, Université de Genève, 30 quai Ernest-Ansermet, CH-1211 Genève 4, Switzerland

⁶Department of Chemistry, University at Buffalo, State University of New York, Buffalo, New York 14260-3000, United States

⁷Department of Chemistry, Chemical Theory Center, and Minnesota Supercomputing Institute, University of Minnesota, Minneapolis, Minnesota 55455-0431, United States

⁸Institut für Physik, Universität Rostock, Albert-Einstein-Straße 23-24, 18059 Rostock, Germany

¹⁰Theory of Nanomaterials Group, University of Leuven, Celestijnenlaan 200F, Leuven 3001, Belgium

¹¹Department of Physics, AlbaNova University Center, Stockholm University, SE-106 91 Stockholm, Sweden

¹²Division of Theoretical Chemistry, Kemiteknik, Lund University, P.O. Box 124, SE-221 00 Lund, Sweden

¹³Harvard Smithsonian Center for Astrophysics, Cambridge, Massachusetts 02138, United States

¹⁵Interdisciplinary Center for Scientific Computing, Heidelberg University, Im Neuenheimer Feld 205 A, 69120 Heidelberg, Germany

¹⁶Laboratorium für Physikalische Chemie, ETH Zürich, Vladimir-Prelog-Weg 2, 8093 Zürich, Switzerland

¹⁷Departamento de Química Analítica, Química Física e Ingeniería Química, and Instituto de Investigación Química “Andrés M. del Río”, Universidad de Alcalá, E-28871 Alcalá de Henares, Madrid, Spain

¹⁸Department of Chemistry, University College London, 20 Gordon Street, London WC1H 0AJ, United Kingdom

¹⁹Instituto de Ciencia Molecular, Universitat de València, Apartado 22085, ES-46071 Valencia, Spain

²⁰Institute of Theoretical Chemistry, Faculty of Chemistry, University of Vienna, Währinger Straße 17, 1090 Vienna, Austria

²³Division of Materials Physics, Ruđer Bošković Institute, P.O.B. 180, Bijenička 54, HR-10002 Zagreb, Croatia

²⁴Department of Chemistry, Imperial College London, London SW7 2AZ, United Kingdom

²⁵Centre for Theoretical Chemistry and Physics, The New Zealand Institute for Advanced Study (NZIAS), Massey University Albany, Private Bag 102904, Auckland 0632, New Zealand

²⁶Department of Biotechnology, Chemistry and Pharmacy, University of Siena, via A. Moro 2, 53100 Siena, Italy

²⁷Department of Chemistry, Bowling Green State University, Bowling Green, Ohio 43403, United States

²⁸USIAS and Institut de Physique et Chimie des Matériaux de Strasbourg, Université de Strasbourg-CNRS, 67034 Strasbourg, France

Received: May 31, 2019

Published: September 11, 2019



²⁹Department of Chemistry, KU Leuven, Celestijnenlaan 200F, Leuven 3001, Belgium

³⁰Department of Chemistry, Loughborough University, Loughborough LE11 3TU, United Kingdom

³²Institute of Chemistry, The Hebrew University of Jerusalem, Jerusalem, Israel

³⁶Department of Chemistry, National University of Singapore, 117543 Singapore

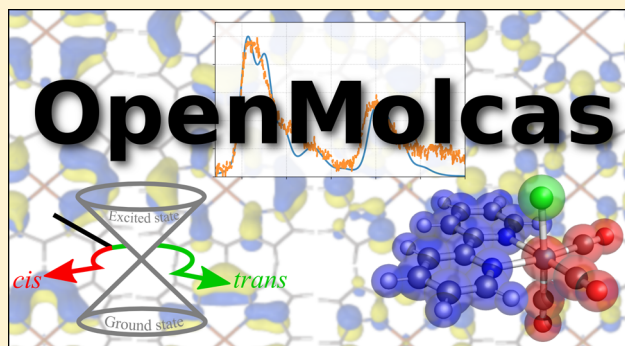
³⁷Theoretical Physical Chemistry, Research Unit MolSys, Allée du 6 Août, 11, 4000 Liège, Belgium

³⁸Brantsandpatents, Pauline van Pottelsberghelaan 24, 9051 Sint-Denijs-Westrem, Belgium

³⁹Uppsala Center for Computational Chemistry (UC₃), Uppsala University, P.O. Box 596, SE-751 24 Uppsala, Sweden

S Supporting Information

ABSTRACT: In this Article we describe the OpenMolcas environment and invite the computational chemistry community to collaborate. The open-source project already includes a large number of new developments realized during the transition from the commercial MOLCAS product to the open-source platform. The paper initially describes the technical details of the new software development platform. This is followed by brief presentations of many new methods, implementations, and features of the OpenMolcas program suite. These developments include novel wave function methods such as stochastic complete active space self-consistent field, density matrix renormalization group (DMRG) methods, and hybrid multiconfigurational wave function and density functional theory models. Some of these



implementations include an array of additional options and functionalities. The paper proceeds and describes developments related to explorations of potential energy surfaces. Here we present methods for the optimization of conical intersections, the simulation of adiabatic and nonadiabatic molecular dynamics, and interfaces to tools for semiclassical and quantum mechanical nuclear dynamics. Furthermore, the Article describes features unique to simulations of spectroscopic and magnetic phenomena such as the exact semiclassical description of the interaction between light and matter, various X-ray processes, magnetic circular dichroism, and properties. Finally, the paper describes a number of built-in and add-on features to support the OpenMolcas platform with postcalculation analysis and visualization, a multiscale simulation option using frozen-density embedding theory, and new electronic and muonic basis sets.

1. INTRODUCTION

At the 4th MOLCAS developers' workshop, 30 March–1 April 2016, in Vienna, Austria, the MOLCAS developer community decided that the source code of the MOLCAS project would be released, where the authors agree, as an open-source project under the GNU Lesser General Public License (LGPL)¹ – the OpenMolcas project. This decision was followed by intensive work to adapt to this new format and context. An open-source repository was established September 2017. In late 2018 the transition to the new open-source format and integration platform was completed. The history of the OpenMolcas codebase dates back much earlier in time, and for a summary of it we refer to previous MOLCAS publications.^{2–8} Here we report on the new and recent developments and options available in OpenMolcas.

OpenMolcas is a software package capable of performing state-of-the-art quantum chemical calculations, but it is not the only one. Other packages, some of them open source, with similar or overlapping capabilities are (a necessarily non-exhaustive list) as follows: ACES,⁹ ADF,¹⁰ BAGEL,¹¹ BigDFT,¹² CFOUR,¹³ Columbus,¹⁴ Dalton,¹⁵ deMon2k,¹⁶ DIRAC,¹⁷ Firefly,¹⁸ GAMESS,¹⁹ GAMESS-UK,²⁰ Gaussian,²¹ HONDOPLUS,²² Jaguar,²³ Molpro,²⁴ MRCC,²⁵ NWChem,²⁶ NRLMOL,²⁷ ORCA,²⁸ PQS,²⁹ Psi4,³⁰ PySCF,³¹ Q-Chem,³² TeraChem,³³ Turbomole.³⁴ A more comprehensive relation, but restricted to open-source programs, can be found in ref 35. A detailed comparison of the OpenMolcas features with these other packages is out of the scope of this report, but it can be

stated that the main strength and focus of OpenMolcas is on multiconfigurational wave function methods, and applications and properties for which these methods are appropriately suited, as reflected in the contents of this article.

Apart from scientific and methodological improvements, the release of OpenMolcas incorporates a series of changes in code management and tools. These changes, as presented here, are aimed at an optimal interface for software accessibility for new developers and facilitating interaction with other codes. In this report the new developments are subdivided into five different categories: novel wave function and density functional methods, approaches to explore potential energy surfaces (PESs), implementations associated with various types of spectroscopy, tools for postanalysis of orbitals and wave functions, and finally a set of some miscellaneous developments.

On the issue of resolving the prohibitive exponential scaling of the multiconfigurational wave function a number of new techniques have been introduced to eliminate this bottleneck. In particular, the Stochastic-CASSCF method has been implemented. Furthermore, two interfaces are introduced—with the CheMPS2 and QCMAQUIS programs—that greatly expand the potential of multiconfigurational wave functions by allowing much larger active spaces as well as speeding up calculations with usual active spaces. This is achieved by supplementing the full configuration interaction (full CI, FCI) solver in the RASSCF module by the density matrix renormalization group (DMRG). With these interfaces it is

possible to perform DMRG-SCF, DMRG-CASPT2, and DMRG-NEVPT2 calculations, obtain analytical DMRG-SCF gradients, or compute state interaction. Moreover, the multiconfiguration pair-density functional theory (MC-PDFT) option has been further developed. This includes translating several KS-DFT functionals not previously available, introducing analytical gradients for state-specific CAS-PDFT, state-interaction PDFT (SI-PDFT) for situations where two electronic states are strongly interacting and the use of PDFT in association with DMRG technology.

The exploration of the PESs is a significant part of any sophisticated tool for electronic structure calculations. In spite of being a leading package for the computational study of electronic excited states, MOLCAS has for a long time lacked the ability of computing nonadiabatic coupling vectors. The recent implementation of analytical nonadiabatic coupling vectors for state-averaged CASSCF wave functions is now available, together with practical methods for optimizing and characterizing conical intersections, and the use in simulations of nonadiabatic processes. Furthermore, simulating the time evolution of matter in the vicinity of electronic degeneracy regions is essential for understanding the rate and the product distribution of photochemical reactions and for complementing time-resolved experiments. Direct dynamics methods were developed to avoid the required computation and fitting of the PESs prior to dynamics simulations and to address the issue of the exponential scaling with the system size. OpenMolcas now supports three different tools for this. First, the DYNAMIX and SURFACEHOP modules of OpenMolcas allow molecular dynamics (MD) simulations of adiabatic and nonadiabatic processes; there are now options for generating starting conditions, adding external forces to the molecular system for steered MD simulations, and simulating isotope effects. Second, the SHARC–OpenMolcas interface allows the simulation of nonadiabatic trajectory surface hopping dynamics including any arbitrary coupling; this means it can deal with photochemical events involving internal conversion and intersystem crossing on the same footing. Third, we report here a new interface to the Quantics package. Dynamics code for classical nuclei is rather straightforward since information is only needed at a given position in space; a quantum description of the nuclei has more problems because of delocalization of the wavepacket. The new interface with the Quantics code allows a quantum mechanical treatment of both electronic and nuclear dynamics via the direct-dynamics variational multiconfiguration Gaussian (DD-vMCG) method.

The OpenMolcas package can generate operator matrix elements between spin–orbit-coupled electronic states and is thus frequently used in simulation of various spectroscopic processes. Recently, these tools have been improved. For high-energy photons the short wavelength means that the electric field can no longer be treated as constant—as in the dipole approximation—and electric-dipole forbidden transitions can be observed. The solution, as presented here, is to either introduce higher orders in the multipole expansion or, more elegantly, use the exact exponential form of the wave vector. Core-hole states are notoriously problematic to handle in standard computations, since these states are high up in energy. Now there is a simple option to use projection during the CI optimization to prevent the core-hole being filled. Moreover, spectroscopy typically involves transitions between an initial state and several final states. The standard CI algorithms are designed to calculate ground and a relatively

small number of low-lying excited states. However, to simulate experiments as X-ray spectroscopy, hundreds of high-energy states are needed. A new approach to the CI problem, which efficiently handles this case, is presented here. We report also the implementation of multiconfigurational Dyson orbitals for accurate simulations of molecular ionization processes. Another example is magnetic circular dichroism (MCD) as one of the prime tools to study the electronic states of complicated metal complexes and metalloproteins. Software tools have now been created for the easy generation of MCD spectral intensities with OpenMolcas. We will also discuss the computation of magnetic properties for transition metal and lanthanide compounds. Moreover, an example in which the OpenMolcas platform has been used as an alternative to experiments, to generate microhartree accuracy of ionization potentials, is given.

Any quantum chemical simulation needs the support of postcalculation analysis tools to render the simulations to be more than just the matter of computing a numerical value of the energy or some other molecular property. Such tools enable the scientist to make qualitative conclusions from the simulations and to obtain insight in addition to quantitative predictions. They typically involve the generation of orbitals, which could be natural, canonical, or localized, and the graphical representation of these. In that respect, OpenMolcas has recently been enhanced with the following new utilities. The graphical user interface LUSCUS is a next generation of GV (Graphical Viewer) code; it is a lightweight viewer of input and output data produced by various quantum chemical codes, in particular the OpenMolcas program suite. One of the bottlenecks in the graphical visualization procedure is the size of the intermediate data. The ability to on-demand compute the data for visualization is now implemented in a stand-alone code, SAGIT. Furthermore, Pegamoid is a new orbital viewer that can read and write the native OpenMolcas orbital formats, simplifying the process of selecting and analyzing the active space for MCSCF calculations. Moreover, binatural orbitals, also called natural transition orbitals, are now available in order to characterize the nature of an electronic excitation. This can be computed by singular value decomposition of a transition density matrix using RASSCF wave functions in the RASSI module. Finally, the WFA (wave function analysis) module not only provides visualization tools but also computes quantitative descriptors, which allow for a rigorous and completely automatized analysis of excited-state computations.

In addition, as listed below, miscellaneous utilities and functionalities have been added to the program suite. The relativistic ANO-RCC basis set has been the spearhead of the MOLCAS/OpenMolcas program since its introduction a decade ago. It is now accompanied by an extremely small relativistic alternative, the ANO-XS basis set. The small size of ANO-XS greatly reduces integral computation times yet still predicts, e.g., geometries or excitation energies with only small differences as compared to the larger ANO-RCC basis sets. Moreover, OpenMolcas is adapted to use point groups beyond D_{2h} . Thus, for highly symmetrical molecules OpenMolcas can occasionally generate wave functions with broken symmetry. It is a problematic programming task to adapt a computational code to use higher point groups. However, a code for a posteriori symmetrization of the wave function, msym, has been developed and implemented in OpenMolcas. As a further development we report on the ability to simulate muonic atoms and molecules, i.e., systems containing one muon—a

Fermion with a mass about 207 times heavier than an electron. This includes developments of muonic basis sets, bookkeeping of two types of Fermionic particles and basis sets in integral and wave function code, diagonal finite mass correction, and analysis of parameters associated with the finite-nucleus approximation. Finally, a new method for multiscale electronic structure calculations has been implemented which is based on frozen-density embedding theory (FDET).

Thus, below we will in some detail describe and discuss these new tools in the OpenMolcas program suite. The structure of the Article will in all respects follow the order as presented above. This will be followed with a brief summary.

2. CODE DEVELOPMENT AND TOOLS

The tools and culture in software development have changed dramatically in the last three decades since the initial versions of MOLCAS. The original code “would only run on the IBM 3090 computers under the JCL operating system”,⁶ and although later versions made it more versatile and user-friendly, it remained for a long time a project developed mainly in Lund (Sweden), using a set of custom-written tools for debugging, configuring, updating, and documenting the code.⁵ In the past few years, particularly since the establishment of annual MOLCAS developers workshops in 2013, the MOLCAS project has become a much more international and collaborative project and has tried to keep up with the times and embrace the new tools and technologies that are available for code management. Perhaps the most significant of the changes, and the one that triggers the need for this publication, is the choice of an open-source model, as discussed in the [Introduction](#).

The main codebase of OpenMolcas is written in Fortran language, something that reflects its history and background and the popularity of Fortran in scientific programming. Newer code is increasingly written in other languages: a number of libraries and interfaces recently added to OpenMolcas are written in C or C++, and the main input parser and driver has been rewritten in Python. The most significant changes introduced in OpenMolcas with respect to the development environment are the use of third-party open-source tools for code management, compilation, and testing. Already in 2013 it was decided to use git³⁶ as a version control system for MOLCAS; in connection with the release of OpenMolcas, it was considered important to have a source code repository that is publicly accessible and not only for developers. As a build and configuration system, OpenMolcas now uses CMake,³⁷ a system that also simplifies the combination of different packages such as some of the interfaces reported in this paper. For testing, OpenMolcas uses the verification tools (test suite and scripts) that were already available in MOLCAS, but it additionally benefits from the continuous integration facilities in GitLab,³⁸ the chosen hosting platform, to ensure fast and reliable test runs with minimal maintenance for OpenMolcas developers.

Historically, communication between the different programs in MOLCAS has been mostly done through files, in text or binary format. MOLCAS users will be familiar with names like “RunFile”, “InpOrb”, or “JobIph”. These files have the inconvenience that they are specific to MOLCAS and in some cases incompatible between different versions and/or platforms. With the release of OpenMolcas there is also an increased effort to make use of more portable and standardized file formats for transferring data between programs and for

storing the results of calculations—orbital and CI coefficients, geometries, and energies. In particular, the most important results can now be stored in the HDF5 (hierarchical data format) format,³⁹ which allows efficient storage and access of structured data, including its description. HDF5 files can then be accessed in any platform without knowledge of the program that generated them, since the size and structure of the data are also part of the format. We consider this an important step forward toward interoperability with other scientific codes.

3. MULTICONFIGURATIONAL WAVE FUNCTION METHODS

Important conceptual bases for understanding the motivations for some of the most important features of OpenMolcas are provided by the definition of configuration and the distinction between static correlation and dynamic correlation. A configuration is a particular way to assign electrons to orbitals, which may be doubly occupied, singly occupied, or unoccupied, and a configuration state function (CSF) is an approximate wave function with appropriate spin symmetry (singlet, doublet, etc.) and a definite set of orbital occupancies. Static correlation is also called near-degeneracy correlation, left–right correlation, and strong correlation, and it is due to the interaction of nearly degenerate configurations. A good zeroth-order wave function for a system with significant static correlation will have appreciable coefficients for two or more CSFs. Dynamic correlation is the rest of the correlation energy; it includes a variety of correlation effects ranging from very short-range (due to the cusp in the correct many-electron wave function when two electrons approach one another) to very long-range (as in dispersion interactions). The slow convergence of dynamic correlation with respect to adding more CSFs is often the bottleneck in making accurate calculations, and the most common way to calculate dynamic correlation is usually to optimize the orbitals with a self-consistent-field (SCF) calculation and then include dynamic correlation by adding CSFs that are excited from a reference SCF wave function (single excitations, double excitations, triple excitations, etc.); the addition of excited CSFs may be done by perturbation theory, configuration interaction, or coupled cluster^{40–42} theory. When static correlation is negligible, good results can often be obtained with a single-CSF reference wave function (typically a Hartree–Fock,^{43–46} HF, wave function); methods employing this scheme are called single-reference methods. For strongly correlated systems, this method might be inaccurate unless one uses very high excitation levels (quadruple excitations or higher), which are often unaffordable. A more efficient way to treat strongly correlated systems is to use a multiconfiguration reference wave function; such methods are called multireference methods. Systems well treated by single-reference methods with low levels of excitation are sometimes called single-reference systems, and systems that are much more efficiently treated with multiconfiguration reference wave functions are sometimes called multireference systems or strongly correlated systems. Because many chemical systems of practical interest feature electronic structures dominated by more than one electronic configuration in their ground or excited states, as well as along reaction pathways in which they are involved, the development of efficient methods for multiconfiguration wave functions and multireference correlation methods is a key challenge for quantum chemistry; it was one of the primary motivations for the original development of MOLCAS, and it

remains a key strength of OpenMolcas. Multiconfigurational self-consistent field (MCSCF) methods, capable of dealing with these cases, have been known since the early days of quantum chemistry, but they gained popularity only when the complete active space self-consistent field method (CASSCF) was developed.^{47–50}

Density functional theory presents a similar but conceptually distinct scenario. Kohn–Sham density functional theory (KS-DFT)⁵¹ does not involve a wave function for the system under study, but it does involve a Slater determinant that has the same electron density as the system under study. This Slater determinant may be considered to be a reference wave function, and in that sense KS-DFT is a single-reference theory. Unlike Hartree–Fock theory, though, KS-DFT is in principle exact, in that there is an existence theorem for an exact density functional that would yield the correct electron density and energy. However, this density functional is unknown and probably unknowable. We must rely on approximate density functionals (ADFs), and currently available ADFs are less accurate for strongly correlated systems than for single-reference systems.^{52,53} One way to overcome this is to develop density functional theories that use multiconfigurational reference wave functions, and OpenMolcas includes multiconfiguration pair-density functional theory (MC-PDFT)⁵⁴ as an example of this kind of theory.

MOLCAS⁸ (and now OpenMolcas) has always had a strong focus in multiconfigurational wave function methods and has pioneered the development of cutting-edge methods aiming at circumventing the exponential scaling limitation in CASSCF. The restricted active space (RAS) SCF,^{55,56} the generalized active space (GAS)⁵⁷ SCF, and the SplitGAS⁵⁸ methods are examples.

Multiconfigurational SCF methods, such as the above, explicitly recover electron correlation within the active space and, via the self-consistent orbital relaxation procedure, part of the electron correlation outside the active space. In this respect it is to be noticed that the orbital relaxation in MCSCF procedures is not to be compared to the self-consistent orbital optimization in the single-reference HF procedure, as the MCSCF orbital gradient directly depends on the multiconfigurational wave function via the generalized Fock operator. Correlation effects not included at the MCSCF level are usually recovered by a posteriori treatments that use the preceding MCSCF wave function as reference. Examples of these methods within the OpenMolcas package are the multiconfiguration pair-density functional theory, MC-PDFT,^{54,59–61} and second-order perturbation theory methods, such as CASPT2, RASPT2,^{62–64} and NEVPT2.^{65–71} Despite their broad applicability, these methods rely on the qualitative correctness of the reference wave function, or, in the case of MC-PDFT, its electron density, on-top pair-density, and the ratio of these two.⁷²

The rest of this section describes with more detail some of the newest approaches implemented in OpenMolcas to work around the exponential scaling of CASSCF, while keeping its conceptual simplicity. In particular, the Stochastic-CASSCF method (section 3.1) uses a Monte Carlo algorithm to solve the CI problem in the active space; the density matrix renormalization group (DMRG)—for which two different interfaces are presented (section 3.2)—expresses the wave function as a product of matrices, with a reduced number of free parameters with respect to a linear combination of configuration state functions. In addition, the MC-PDFT

capabilities in OpenMolcas (section 3.3) are enhanced with analytic gradients and state-interaction functionalities.

3.1. The Stochastic-CASSCF Approach. The Stochastic-CASSCF^{73–76} has been developed since 2015, initially for MOLCAS,⁸ and is now available in OpenMolcas. The method retains the simplicity of CASSCF, while circumventing the exponential scaling of the latter. This is obtained by replacing the Davidson diagonalization technique,⁷⁷ in its direct-CI implementation,^{55,78} with the full-CI quantum Monte Carlo (FCIQMC) algorithm,^{79–87} while the Super-CI method^{47–50} is used for the orbital optimization. Starting from the *decoupled* two-step Newton–Raphson method⁸⁸ for the optimization of the orbitals and CI coefficients, the Stochastic-CASSCF procedure can be summarized in two conceptually simple steps—(i) the FCIQMC approach to optimize the CI-coefficients and obtain the one- and two-body density matrices and (ii) the Super-CI algorithm for the orbital coefficients optimization. The Super-CI step is done according to standard procedures^{47,48,50} and will not be described here. The FCIQMC approach for the optimization of the CI coefficients, instead, will be described below in more detail.

The FCIQMC algorithm is a projector technique based on the imaginary-time Schrödinger equation

$$\frac{\partial \Psi}{\partial \tau} = -(\hat{H} - E_S)\Psi \quad (1)$$

In this equation the term E_S is an energy offset, referred to as the *shift*, that is updated iteratively, converging to the ground-state correlation energy. In the context of FCIQMC, E_S plays the role of population control. Expanding the wave function, $\Psi(\tau)$, into a linear combination of Slater determinants, and integrating eq 1, with a short time step, $\Delta\tau$, such that the full propagator $e^{-\tau(\hat{H}-E_S)}$ can be approximated to first-order, an iterable working equation is obtained

$$C_i(\tau + \Delta\tau) = C_i(\tau) - \Delta\tau(H_{ii} - E_S)C_i(\tau) - \Delta\tau \sum_{j \neq i} H_{ij}C_j(\tau) \quad (2)$$

A deterministic update of the CI vector from the time τ to $(\tau + \Delta\tau)$ would require the storage of several arrays of the size of the CI vector and would face the same exponential scaling limitation of the standard direct-CI approach. Instead, in FCIQMC the concept of *walkers* is introduced. Walkers are signed Kronecker delta functions that reside on a specific determinant. We define $\delta_{i,\alpha}$ as the α th walker residing on determinant $|i\rangle$. A sign is assigned to each walker, $s_\alpha = \pm 1$, associated with it. Thus, the signed number of walkers, N_i , which reside on $|i\rangle$ is given by $N_i = \sum_\alpha s_\alpha \delta_{i,\alpha}$. The total number of walkers residing in all relevant determinants is kept to a fixed value, $N_w = \sum_i |N_i|$. This value is to be considered an optimization parameter in addition to the basis set and the active space. The larger the total number of walkers, the smaller the error due to the initiator approximation.⁸⁰ In practice, this parameter is gradually increased until convergence over the energy estimate is reached.

The key point of FCIQMC is to allocate memory only for the populated determinants, instead of allocating memory for the entire CI vector. The purpose of FCIQMC is to generate distributions of walkers such that for a large number of total walkers and long imaginary time limit the expectation value of the number of walkers on each determinant becomes

proportional to the CI coefficient of that determinant, $C_i \propto \langle N_i \rangle_\tau$. In FCIQMC, walker population dynamics simulates the imaginary-time evolution as given in eq 2. The dynamics consists of three steps. In the *spawning* step child particles are generated from their parents into various locations of the Hilbert space. In the *death* step parent walkers are stochastically removed from the simulation. In the *annihilation step* parents and newly created walkers residing on the same determinant with opposite sign are eliminated.

The expectation value of the number of walkers on each determinant in practical calculations is never explicitly calculated. Instead derived properties are accumulated once the walker population has reached a dynamical equilibrium. One of these properties is the projected energy

$$E_p = \frac{\langle \sum_i N_i \langle D_0 | \hat{H} | D_i \rangle \rangle_\tau}{\langle N_0 \rangle_\tau} \quad (3)$$

where the numerator and denominator are accumulated and averaged separately, D_0 is the reference determinant, and $\langle N_0 \rangle_\tau$ is the time-averaged number of walkers on D_0 . One- and two-body reduced density matrices (RDMs) are similarly accumulated⁸² to evaluate the CASSCF energy as the expectation value of the Hamiltonian operator and to compute the matrices required for the orbital optimization step.

Electron correlation outside the active space, also known as dynamic correlation, can be recovered via MC-PDFT,^{54,59–61} using the Stochastic-CASSCF wave function as reference.

3.1.1. Technical Details. The Stochastic-CASSCF method in OpenMolcas relies on the interface of the NECI program, responsible for the FCIQMC CI algorithm, and the RASSCF program of OpenMolcas, responsible for the Super-CI method as an orbital optimizer. In principle, two installation protocols can be adopted that are referred to as *embedded* and *uncoupled* forms. In the *embedded* form, the NECI program is treated as a subroutine of the RASSCF program. This form effectively leads to an automatized version of the Stochastic-CASSCF within the OpenMolcas software. In the *uncoupled* form of Stochastic-CASSCF, NECI is installed as a stand-alone program, and the OpenMolcas–NECI interface is controlled manually by the user. Dedicated keywords are required in the OpenMolcas input file to let OpenMolcas produce the relevant files, namely the file containing one- and two-electron integrals in the MO basis (FCIDUMP) and an input file for the NECI program (see section S1). FCIQMC is then started externally, and the population is grown and stabilized before one- and two-body density matrices are accumulated. Walker population and other parameters can be tuned at this stage within the FCIQMC calculation if necessary. Density matrices are then transferred back to OpenMolcas and used to evaluate the Fock matrices necessary for the Super-CI step. After orbitals have been rotated, the integral file is updated, and a new FCIQMC dynamics in the active space can be performed. The *embedded* OpenMolcas–NECI form is the recommended form for simple cases (small active spaces, small number of walkers, loose convergence). The *uncoupled* OpenMolcas–NECI form is the recommended form for difficult applications (large active spaces, large number of walkers, tight convergence).

Geometry, spatial symmetry, AO integral evaluation, scalar relativistic effects, and additional external potentials are evaluated at the OpenMolcas level, and corrections are made to the FCIDUMP provided to the NECI program.

With the choice of the FCIQMC algorithm as CI eigensolver, the Stochastic-CASSCF method can be applied to larger active spaces, when compared to the deterministic analog. Active spaces containing up to 40 electrons and 38 orbitals have been reported.⁷⁵ Integral evaluations and AO–MO transformations can be carried out via resolution-of-identity (RI) Cholesky decomposition (CD) techniques,^{89–93} available within the OpenMolcas package. The choice of the Super-CI method for the orbital relaxation together with the density fitting techniques enable Stochastic-CASSCF calculations easily with up to 5000 basis functions.

3.1.2. Applications of the Stochastic-CASSCF Method. The Stochastic-CASSCF method has been applied to a number of chemical problems. Two very recent cases will be summarized in this section, namely the correlation mechanism leading to the large effective antiferromagnetic spin coupling, J , in corner-sharing cuprate solids and the enhanced σ -donation/ π -back-donation mechanism that explains the stabilization of the intermediate spin-states over the high spin-states in Fe(II)-porphyrin model systems. For a more detailed description of these systems and the strategy used within the Stochastic-CASSCF framework we refer to the literature.^{74–76}

Corner-sharing cuprates are of great interest, as they host high-temperature superconductivity upon doping.⁹⁴ Magnetic properties of undoped cuprates have been rationalized on the basis of the Heisenberg–Dirac–Van Vleck Hamiltonian with antiferromagnetic nearest-neighbor magnetic coupling constant J . The values of J in these systems are among the largest known, with some variations upon rather small geometrical differences.⁹⁵ From a quantum-chemical standpoint understanding how J directly depends on electron correlation is a challenging problem that has been investigated by several research groups.^{96–100} Conventional wave function theory treatment greatly underestimates the J value. The Stochastic-CASSCF method has been used to investigate this aspect. A cluster containing two CuO_4 (or CuO_6) units and all adjacent Cu^{2+} and Sr^{2+} (or La^{2+}) ions has been employed in these calculations. The rest of the solid has been modeled by an array of point charges fitted to reproduce the Madelung potential due to infinite crystal in the cluster region. It has been demonstrated that to capture the essential elements of the superexchange mechanism it is necessary to explicitly correlate the 20 valence 3d and *double-shell* d' orbitals on the Cu sites together with the six 2p and p' orbitals on the bridging O ion, with a total of 24 electrons, resulting in a CAS(24,26). Calculations with this size of active space would be impossible with standard CASSCF technology, the corresponding CI wave function containing $\sim 9 \times 10^{13}$ Slater determinants. The calculation is carried out with ease using the Stochastic-CASSCF method.⁷⁶

Metal-porphyrins are crucial active sites in many enzymes responsible for electron transfer, oxygen transport and oxygen reduction. For example, the Fe(II)-porphyrin is the active species in cytochrome P450, that binds molecular oxygen and reduces it, leading to *P450 Compound 1*, responsible for the hydroxylation reaction (insertion of an oxygen atom in a C–H bond) in alkyl chains. In spite of the numerous experimental and theoretical data, a definitive understanding of the ground-state electronic structure and its changes along the reaction pathway remain ambiguous, and an electronic explanation for the relative ordering of the low-lying spin-states remains unknown. Via large Stochastic-CASSCF(32,34) calculations,⁷⁴ a complex mechanism has been proposed that demonstrates

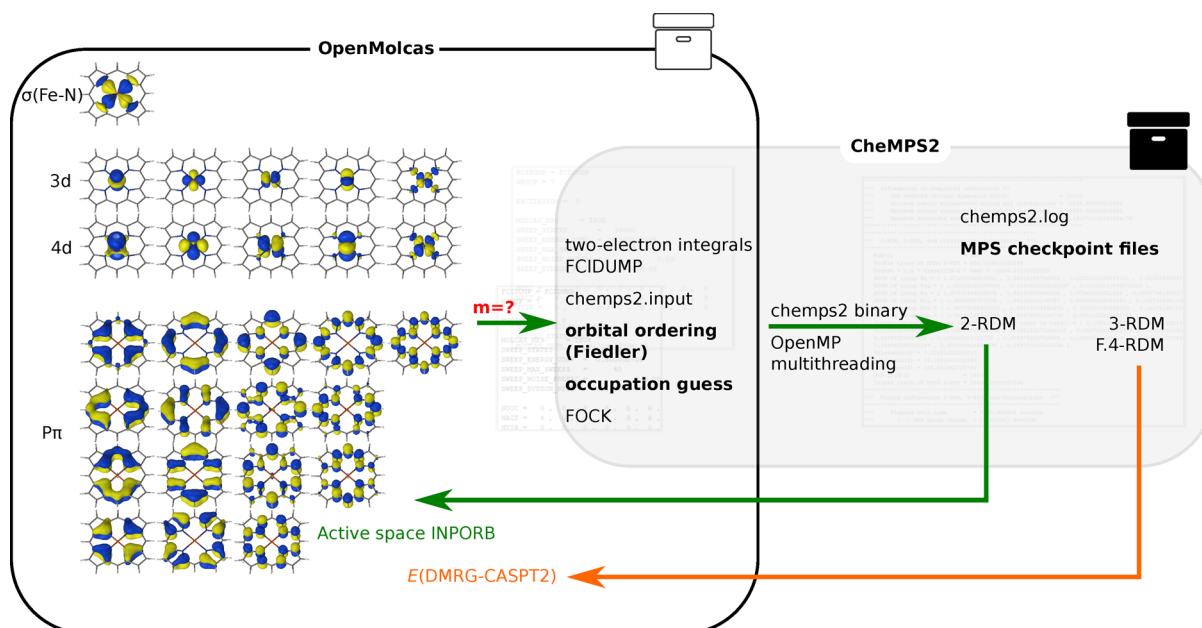


Figure 1. Schematic representation of a DMRG-SCF/DMRG-CASPT2 calculation performed by the OpenMolcas–CheMPS2 interface. Only the number of renormalized states m must be specified. The user can define optional parameters to speed up the calculation, e.g., orbital ordering, occupation guess, the matrix product state (MPS) checkpoint files from a previous calculation, etc.

the differential stability of the intermediate triplet spin-state over the quintet spin-state in a model system of the Fe(II)-porphyrin. This mechanism involves ring correlation at the level of the π -system, a correlated breathing process at the metal center and charge-density redistribution. The large (32,34) active space includes the entire π -system and nitrogen lone pairs, the 3d and d' orbitals at the metal center, and the (4s4p) shell. It has been demonstrated that ring correlation reduces the electron repulsion among the π electrons, making the macrocycle a better electron acceptor. The correlating d' orbitals provide the necessary flexibility for the orbital relaxation induced by charge-transfer processes from the lone-pairs of the ligand to the metal center. They also account for radial correlation, responsible for a lower on-site electron repulsion at the level of the metal center, and provide a larger overlap with the π orbitals thus favoring charge-transfer from the metal center to the ligand. This complex mechanism can be related to a correlation enhanced σ -donation/ π -back-donation process and it is stronger for the triplet spin-state. It was suggested in ref 74 that smaller active spaces, even upon second-order perturbative correction, such as in the conventional CASPT2(8,11) are not capable of fully capturing this mechanism (see section 3.2.5 for further discussion). The Stochastic-CASSCF technique has been also used to understand the role of semicore electrons. This analysis has been performed via a large CAS(40,38) active space.⁷⁵

3.2. Density Matrix Renormalization Group Interfaces. After White proposed the DMRG^{101,102} in 1992, subsequent work^{103–109} established that DMRG optimizes a matrix product state (MPS). The flexible nature of MPSs allows one to calculate excited states in an efficient manner¹¹⁰ and provides easy access to higher-order reduced density matrices and the evaluation of arbitrary correlation functions. The standard definition of an MPS describing a state over L orbitals or sites is given by

$$|\psi\rangle = \sum_{\sigma} \sum_{a_1, \dots, a_{L-1}} M_{1a_1}^{\sigma_1} M_{a_1 a_2}^{\sigma_2} \dots M_{a_{L-1} 1}^{\sigma_L} |\sigma\rangle \quad (4)$$

with basis states $|\sigma\rangle = |\sigma_1, \dots, \sigma_L\rangle$ and $\sigma_i = |\uparrow\downarrow\rangle, |\uparrow\rangle, |\downarrow\rangle, |0\rangle$ for spatial orbitals. In systems with symmetries, the matrix indices a_i are complemented with a quantum number label $a_i \rightarrow q_i \alpha_i$,¹¹¹ leading to a block-sparse structure. Matrix product states will encode a full CI wave function exactly if the matrix dimension m (the maximum size of the indices a_i , called “number of renormalized block states” or “bond dimension”) is allowed to grow unrestrictedly. In practice, a finite m is chosen which limits the amount of entanglement that the resulting MPS is able to describe between any bipartition of an L -orbital active space. For one-dimensional systems, so-called area laws^{112,113} prove that the amount of entanglement is constant irrespective of L and that limiting m is therefore a good approximation. For the general case in quantum chemistry, the convergence rate in m depends on molecular topology and the choice of the orbital basis, influencing the sparsity of the one- and two-electron integrals.¹¹⁴

Analogously to MPS, matrix product operators (MPOs)^{110,115,116} are defined as

$$\hat{W} = \sum_{\sigma\sigma'} \sum_{b_1, \dots, b_{L-1}} W_{1b_1}^{\sigma_1 \sigma'_1} \dots W_{b_{l-1} b_l}^{\sigma_{l-1} \sigma'_{l-1}} \dots W_{b_{L-1} 1}^{\sigma_{L-1} \sigma'_{L-1}} |\sigma\rangle \langle \sigma'| \quad (5)$$

The efficient determination of the W matrices for Hamiltonian operators with long-range interactions such as Coulomb interactions is a nontrivial task.^{117–119} The DMRG algorithm formulated explicitly in terms of MPS and MPO is sometimes referred to as second-generation DMRG. Compared to the original formulation, a pure MPS/MPO implementation provides additional flexibility by allowing arithmetic operations to be performed on wave functions and operators independently. These properties are exploited, for instance, to implement a fully relativistic DMRG variant¹²⁰ in QCMAQUIS (the first such implementation was presented earlier¹²¹), for interfacing with multireference perturbation

theory^{122,123} (see section 3.2.3) and for MPS state-interaction¹²⁴ (see section 3.2.4).

This section presents the interface of OpenMolcas with two established DMRG codes: the CheMPS2 library,¹²⁵ a first-generation DMRG implementation, based on a MPS representation of wave functions (eq 4), and QCMAQUIS,^{111,117,126} a second-generation program that additionally makes use of a MPO representation of operators (eq 5). In a nutshell, both interfaces can replace the FCI solver from CASSCF with a DMRG implementation and be used to obtain state-specific or state-averaged DMRG-SCF wave functions and perform single-state DMRG-CASPT2 calculations,¹²⁷ while QCMAQUIS also supports DMRG-NEVPT2, MPSSI, and analytical state-specific gradients for DMRG-SCF, support for the recently published analytical state-averaged DMRG-SCF gradients¹²⁸ will be added in the near future.

The CheMPS2 library is a free open-source spin-adapted implementation of DMRG for *ab initio* quantum chemistry. It is designed for high-performance computing, allowing for hybrid MPI and OpenMP parallelization, and can handle a general active space up to 40 electrons in 40 orbitals in a DMRG-SCF calculation. In a DMRG-CASPT2 calculation^{122,127,129,130} requiring the 2- and 3-particle reduced density matrices (2- and 3-RDM) as well as the generalized Fock matrix contracted with the 4-RDM (*F.4*-RDM), an active space of ~ 30 active orbitals can be treated. Figure 1 illustrates a schematic representation of a DMRG-SCF/DMRG-CASPT2 calculation performed by the OpenMolcas–CheMPS2 interface. DMRG-SCF calculations are performed in a manner similar to standard CASSCF calculations except that the number of renormalized state m must be provided by the user. Additionally, other parameters controlling the cost and accuracy of the calculations, e.g., the initial guess of the matrix product state, the orbital ordering, the MPS checkpoint files, etc., can be optionally specified. The shared-memory (OMP) CheMPS2 binary is then called and executed. CheMPS2 outputs, such as the 2-RDM, are then fed to the RASSCF module, allowing the active orbitals to be optimized with the super-CI method. If a subsequent DMRG-CASPT2 calculation is required, the active orbitals are transformed into pseudocanonical orbitals in the last DMRG-SCF iteration, and the 3-RDM and *F.4*-RDM are calculated by CheMPS2 based on this pseudocanonical orbital basis. Because the generalized Fock matrix is diagonal in the pseudocanonical orbital basis, the calculation of the full 4-RDM is avoided, which drastically reduces the computational cost.¹²²

Regarding the other DMRG interface described in this paper, the OpenMolcas–QCMAQUIS interface, it has been designed to (i) steer a DMRG calculation with the MPS/MPO program QCMAQUIS^{111,117,126} and (ii) exchange data such as N -particle reduced density matrices (N -RDMs), from QCMAQUIS to OpenMolcas. Figure 2 illustrates the capabilities of the OpenMolcas–QCMAQUIS interface. DMRG-SCF calculations with QCMAQUIS are enabled in OpenMolcas within the DMRGSCF module by specifying the `ActiveSpaceOptimizer=QCMAquis` keyword which sets QCMAQUIS as default active space solver. Note that the DMRGSCF module shares the same subset of keywords, e.g., for the wave function model specification, orbital-optimizer convergence acceleration, and MO analysis, that are available in OpenMolcas within the complete active space SCF optimizer module RASSCF. The core of the OpenMolcas–QCMAQUIS interface comprises a subset of Fortran90 modules

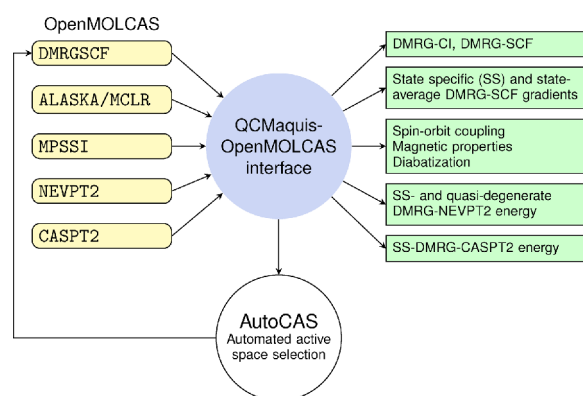


Figure 2. Schematic representation of the capabilities of the OpenMolcas–QCMAQUIS interface. OpenMolcas modules that are interfaced with QCMAQUIS are listed on the left, and the properties that can be obtained are listed on the right.

which (i) “translate” in an automated fashion the user-provided wave function input data of OpenMolcas into the corresponding DMRG input for QCMAQUIS, (ii) generate on the fly the one- and two-electron integrals in the MO basis in the commonly used format defined by Knowles and Handy,¹³¹ (iii) invoke the actual DMRG wave function optimization with QCMAQUIS, and (iv) convert any (user-)requested N -RDM or N' -particle reduced transition density matrix (with $N = \{1,2,3,4\}$ and $N' = \{1,2,3\}$) from QCMAQUIS to OpenMolcas format. The complete MPS wave function, optimization input, and output data as well as all molecular properties calculated by QCMAQUIS are stored in external files in HDF5 format and are therefore available in OpenMolcas for further external processing.

3.2.1. Active Space Selection Based on Entanglement Measures. The selection of an appropriate active space for multiconfigurational calculations is a task as important as it is difficult. While several guidelines exist for this selection,^{132–136} it still requires expertise with trial and error and, hence, constitutes a considerable entry barrier to such calculations.¹³⁷ An automated protocol has been proposed¹³⁸ and implemented in combination with the OpenMolcas–QCMAQUIS interface, which selects orbitals for the active space based on orbital entanglement entropies^{139,140} from a partially converged DMRG calculation. This protocol has become possible owing to (i) the feature of DMRG that allows one to consider large active spaces in an exploratory fashion through limiting the number of sweeps and the block dimension and owing to (ii) the spread of entanglement measures defined for one or a pair of orbitals so that rather robust thresholds can be defined that separate strongly from weakly correlated orbitals, the former to be chosen for an active space in a final well-converged DMRG or CASSCF calculation.

The orbital entanglement entropies are calculated from the one- and two-orbital reduced density matrices. The elements of these matrices can be expressed as expectation values of strings of creation and annihilation operators and are efficiently calculated within a DMRG algorithm. The explicit equation for the single-orbital entropy, on which the selection protocol is based, reads

$$s_i(1) = - \sum_{\alpha=1}^4 w_{\alpha,i} \ln w_{\alpha,i} \quad (6)$$

whereas the two-orbital entropy follows in close analogy as

$$s_{ij}(2) = - \sum_{\alpha=1}^{16} w_{\alpha,ij} \ln w_{\alpha,ij} \quad (7)$$

In these equations, $w_{\alpha,i}$ and $w_{\alpha,ij}$ are the eigenvalues of the one- and two-orbital reduced density matrices, respectively, i, j are orbital indices, and α is one of the four (or 16) possible occupations of a spatial orbital (or a pair of spatial orbitals). Both quantities can be combined to give the mutual information which quantifies the entanglement of an orbital pair

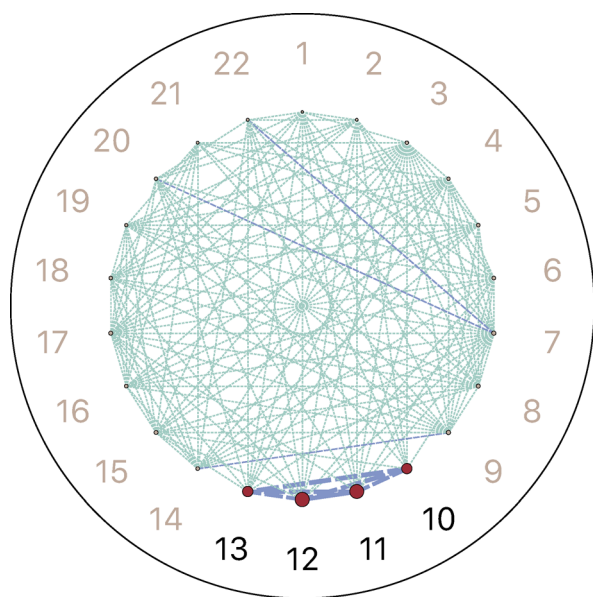


Figure 3. Entanglement diagram obtained from a DMRG wave function optimized with the QCMAQUIS program with $m = 250$ and 10 sweeps including all valence orbitals of butadiene that were obtained from a minimal basis Hartree–Fock calculation. A circle with an area proportional to the single-orbital entropy is associated with each orbital. The thickness of the connecting lines is proportional to the mutual information of an orbital pair. The π -orbitals are those with numbers 10–13 and would be selected by the automated protocol as implemented in AUTOCAS.

$$I_{ij} = \frac{1}{2} [s_i(1) + s_j(1) - s_{ij}(2)] (1 - \delta_{ij}) \quad (8)$$

Both the mutual information and the single-orbital entropies are collected in entanglement diagrams such as the one in Figure 3 that provide an intuitive interpretation of the orbital entanglement.

It was demonstrated that CAS wave functions calculated from these automatically selected active spaces are suitable zeroth-order wave functions for subsequent CASPT2 calculations.¹⁴¹ Furthermore, consistent active spaces for several electronic states and along reaction coordinates can be identified.¹⁴² The automated active orbital space selection has been implemented as a graphical user interface (GUI) called AUTOCAS^{143,144} that drives OpenMolcas and QCMAQUIS. AUTOCAS is the first computer program that allows one to run multiconfigurational calculations, for which an active space must be selected, in a fully automated way. It can be

downloaded separately free of charge from the SCINE Web page.¹⁴⁵

3.2.2. Analytic Ground- and Excited-State DMRG-SCF Gradients. A central feature of the traditional multiconfigurational wave function toolbox of OpenMolcas is the availability of analytic energy gradients (with respect to the nuclear coordinates) for a single (“state-specific”) or an ensemble (“state-averaged”) of electronic states.^{146–148} State-specific and state-averaged gradients are, for instance, key for the calculation of ground- and excited-state equilibrium structures, reaction paths, and for molecular dynamics simulations. Likewise, excited-state gradients are vital for modeling a wide range of photochemical phenomena, such as photochemical and photophysical pathways or resonance Raman spectra. Whereas a state-specific DMRG-SCF gradient is rather straightforward to implement,¹⁴⁹ a formalism for state-averaged DMRG-SCF gradient theory has only been recently presented and applied to an optimization of a conical intersection in the study of the photochemistry of 1,2-dioxetane.¹²⁸ The applicability of state-specific DMRG-SCF gradients has been demonstrated for optical spectroscopy, in particular, for resonance Raman spectroscopy,¹⁵⁰ and that of the state-averaged DMRG-SCF gradients in a conical intersection optimization.¹²⁸

In analogy to CASSCF, the calculation of a state-specific DMRG-SCF analytic gradient, available with the OpenMolcas–QCMAQUIS interface, requires the one- and two-particle reduced density matrices for a given target state in addition to the derivatives of the Hamiltonian, i.e., the derivatives of one- and two-electron integrals, with respect to the nuclear coordinates.^{149,150} The latter quantities can be calculated independently of the parent multiconfigurational wave function. Their calculation is carried out most efficiently in the AO-basis (to which the reduced density matrices are backtransformed from the MO basis) which is implemented in the ALASKA module of the OpenMolcas framework.

3.2.3. Perturbation Theory with DMRG Reference. While DMRG-SCF is capable of describing static correlation for large active spaces, a significant contribution to electron correlation required for quantitative results, namely the *dynamic* correlation, must be accounted for separately. Traditionally, second-order perturbation theory with a zeroth-order Hamiltonian that describes the static correlation effects has been most popular (but coupled-cluster models combined with a DMRG reference have also been considered^{151–153}). Multiconfigurational second-order perturbation theory in the form of CASSCF/CASPT2 became the flagship method of the (Open)Molcas quantum chemistry package.¹⁵⁴ In the early 2000s, Angeli et al.^{65–68} introduced another formulation of a CAS-based multireference perturbation theory, the (second-order) n -electron valence state perturbation theory (NEVPT2). The main difference of NEVPT2 with respect to CASPT2 is the definition of the zeroth-order Hamiltonian: NEVPT2 uses the Dyll Hamiltonian as a model Hamiltonian,¹⁵⁵ which explicitly considers two-electron interactions among the electrons in the active space. The two-electron interactions in the reference ensure that NEVPT2 is intruder-state free and size consistent.⁷¹ NEVPT2 allows for two different contraction schemes to construct the first-order wave function: the *partially contracted* (PC) scheme is identical to the one in CASPT2, while the *strongly contracted* (SC) scheme introduces additional contractions, further simplifying the formalism.

The majority of the DMRG-based perturbation-theory methods encompass DMRG-CASPT2^{122,130} (available with both the OpenMolcas–CheMPS2 and OpenMolcas–QCMAQUIS interfaces) and DMRG-NEVPT2^{123,156} (available with the OpenMolcas–QCMAQUIS interface). One of the major drawbacks of these approaches (or rather of the internal contraction formalism^{157–159} on which these theories are based) is their dependence on higher-order N -RDMs ($N > 2$), whose evaluation scales as $O(L^{2N})$ with the number of active orbitals L . For instance, in the case of the four-particle RDM, its evaluation scales formally as $O(L^8)$. While for small active spaces (small L) this is not a problem, the fourth-order RDM evaluation becomes quickly the computational bottleneck for active spaces of more than 20 to 22 orbitals.

Apart from the RDM scaling problem, the ability to deal with large basis sets is crucial for increasing active space sizes. In particular, the transformation of the two-electron integrals from the AO to the MO basis becomes a bottleneck. One of the flagship features of the OpenMolcas program package is the Cholesky decomposition of the two-electron integral matrix, initially proposed by Beebe and Linderberg¹⁶⁰ and developed over the years by Aquilante, Lindh, Pedersen, and co-workers for various single- and multireference electronic structure methods.^{90,93,161,162} The DMRG-NEVPT2 implementation in QCMAQUIS¹²³ and the DMRG-CASPT2 calculations with the OpenMolcas–CheMPS2 and OpenMolcas–QCMAQUIS interfaces take full advantage of the Cholesky decomposition to handle the two-electron integrals¹⁶² and the DMRG reference wave function (CD-DMRG-NEVPT2, CD-DMRG-CASPT2).

3.2.4. State Interaction for Matrix Product States. In the restricted active space state-interaction (RASSI) approach of Malmqvist,¹⁶³ sets of spin-free (SF) eigenstates can be coupled under the influence of the spin–orbit (SO) coupling, and a variety of highly important molecular properties can be evaluated. A critically important feature of the RASSI program is that the state interaction can be performed among different sets of SF states with different spin or spatial symmetry, with the molecular orbitals (MOs) optimized for each set of states individually. This implies mutual nonorthogonality of the respective MO bases and requires the transformation of pairs of MO sets to a biorthonormal basis.¹⁶³ These nonunitary transformations require a countertransformation of the representations of the wave functions such that the physical content of the latter remains intact. This feature was, until recently, only available for CI-type wave functions but not for MPSS.

The formalism and implementation for MPS-based state interaction (MPSSI) within QCMAQUIS¹²⁴ includes the critical capability to work with nonorthogonal MO sets. The approach differs considerably from Malmqvist's but is likewise based on constructing biorthogonal MO bases and concomitant countertransformations of the MPSs. An MPSSI flowchart for generating SO-coupled wave functions and matrix elements of operators for molecular properties is shown in Figure 4. Very importantly, the MPSs serve as a complete substitute for the CI-type states in calculations of SO-coupled wave functions as well as SF and SO molecular properties with the RASSI program. For instance, ref 124 reported relative SF and SO valence state energies and state compositions for Te_2 , NpO_2^{2+} , and PuO_2^{2+} , as well as EPR g -factors for the actinyl species, from MPS-SO calculations with QCMAQUIS and the RASSI

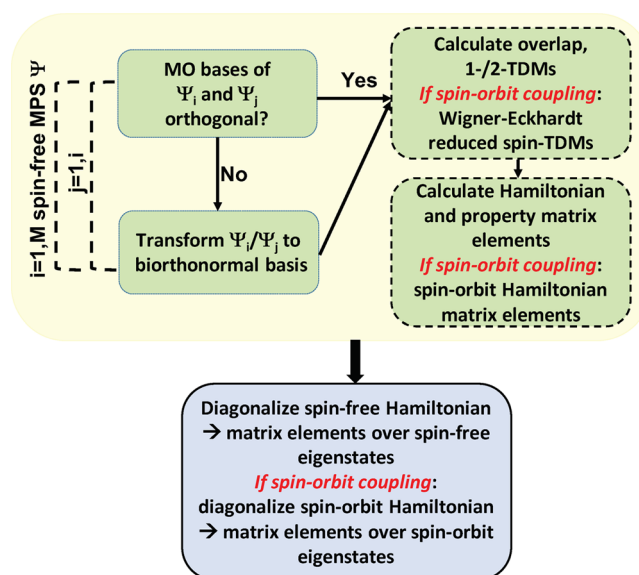


Figure 4. Flowchart illustrating the MPS state-interaction (MPSSI) approach to calculate property matrix elements of spin-free and spin–orbit coupled MPS wave functions according to ref 124.

program. The MPSSI results were in full agreement with CASSCF and CASPT2.¹⁶⁴ Therefore, the full suite of SO-level molecular properties and spectra previously available in the RASSI program can now be calculated with the potentially very large active spaces that are accessible with MPS wave functions.

3.2.5. Applications of DMRG-MRPT2. The case of the spin states of Fe(II)-porphyrin (FeP) has already been mentioned in the context of Stochastic-CASSCF (section 3.1.2), where it was proposed (for a smaller model system) that a small CAS(8,11) active space might be insufficient and a much larger active space, including all ligand π as well as extra nitrogen orbitals and the 4s4p shell on the metal center, is needed.⁷⁴ Here we discuss a series of DMRG-SCF and DMRG-CASPT2 calculations performed on the lowest triplet ($^3A_{2g}$) and quintet ($^5A_{1g}$) states of FeP with the OpenMolcas–CheMPS2 interface. The active space used is CAS(26,27), containing, next to the CAS(8,11) space, 16 P (π, π^*) orbitals (all but the $2p_z$ of the β carbons of the pyrrole rings). The best DMRG calculations, using $m = 10000$ for the CAS(26,27) active space, differ by less than 0.4 kJ/mol from the CAS(8,11) results, giving a quintet–triplet gap of -68.53 kJ/mol with DMRG-SCF and -19.46 kJ/mol with DMRG-CASPT2. The conclusion is that including the P (π, π^*) orbitals on top of the CAS(8,11) space has a minor impact on the CASSCF/CASPT2 description of the spin state energetics in FeP. In refs 165 and 166 it was shown that an improved description should instead come from more extensive basis sets (extrapolated to the complete basis set limit) as well as a special (CCSD(T)) treatment of the Fe (3s,3p) semicore electrons. All details of the calculations, a plot of the active natural orbitals, and a discussion on the convergence and performance can be found in the SI.

Another example of the OpenMolcas–CheMPS2 interface shown in the SI is the geometry optimization of ferrocene ($\text{Fe}(\text{C}_5\text{H}_5)_2$ or FeCp_2) at the DMRG-CASPT2 level; this demonstrates that the interface can easily be coupled with other modules that require either the 2-RDM or CASPT2 total energy. The equilibrium structure of FeCp_2 was optimized

(with numerical gradients) employing both standard CASPT2, with a CAS(10,10) active space, and DMRG-CASPT2, with an extended CAS(14,18) active space. The number of renormal-

Table 1. Structural Parameters of the Eclipsed Conformation of Ferrocene^a

	CASPT2 ^b	DMRG-CASPT2 ^c	CCSD(T) ^d
$d(\text{Fe}-\text{Cp})$ (Å)	1.610	1.615	1.648
$d(\text{Fe}-\text{C})$ (Å)	2.016	2.020	2.047
$d(\text{C}-\text{C})$ (Å)	1.426	1.426	1.427
$d(\text{C}-\text{H})$ (Å)	1.077	1.076	1.079
$\angle(\text{Cp}-\text{H})$ (deg) ^e	0.89	1.08	0.52

^aIn CASPT2, DMRG-CASPT2, and CCSD(T) calculations, the cc-pwCVTZ basis set (672 basis functions) was used, and all 96 electrons were correlated. ^bStandard CASPT2 calculation with CAS(10,10). ^cDMRG-CASPT2 [$m = 1000$] calculation with CAS(14,18). ^dReference 167. ^eAngle between hydrogens and cyclopentadienyl ring, positive values mean hydrogen is bent toward metal.

ized states m is 1000, which gives converged DMRG-CASPT2 energies for medium-sized active spaces.¹²⁹ Further computational details and active natural orbitals can be found in the SI. The key structural parameters of ferrocene, calculated with CASPT2, DMRG-CASPT2, and CCSD(T),¹⁶⁷ are shown in Table 1. Interestingly, the results indicate that CASPT2 and DMRG-CASPT2 give almost the same structure. As compared to CASPT2, DMRG-CASPT2 predicts slightly longer Fe–C and Fe–Cp bond distances by less than 0.005 Å. The results imply that in this simple case, the size of the active space has a minor impact on the optimized geometry. As compared to the CCSD(T) results,¹⁶⁷ both CASPT2 and DMRG-CASPT2 predict the same $d(\text{C}-\text{C})$ and $d(\text{C}-\text{H})$, whereas they underestimate the Fe–C and Fe–Cp bond distances by ~ 0.03 Å. All calculations were performed on a single Intel(R) Xeon(R) CPU E5-2680 v3 @ 2.50 GHz machine, 256GB RAM, and 16 MPI processes. A numerical gradient calculation with the CAS(10,10) active space finishes in around 2 h, while it takes ~ 9 h for the DMRG CAS(14,18) active space. For

comparison purposes, a standard CASPT2 calculation employing the large active space requires a fairly large amount of memory (~ 20 GB per process), consequently, only 12 MPI processes can fit the machine, and a numerical gradient calculation takes almost 8 days with this setting. It is also worth noting that a geometry optimization cycle using CCSD(T) analytical gradients can take almost 9 days.¹⁶⁷

As an example of a DMRG-NEVPT2 calculation with the OpenMolcas–QCMAQUIS interface, we show here results of CD-DMRG-NEVPT2 for the energy gaps between the lowest quintet, triplet, and singlet states of a large iron(II) complex, $\text{FeN}_2\text{C}_{72}\text{H}_{100}$, shown in Figure 5. This complex was chosen by Guo et al. in reference calculations¹⁶⁸ for their DLPNO-NEVPT2 approach¹⁶⁹ and by Coughtrie et al. in their paper on embedded multireference coupled cluster theory.¹⁷⁰ As the PC-variant of the CD-DMRG-NEVPT2 approach is known to be unreliable for large active spaces and small bond dimensions m (due to the incomplete convergence of the zeroth-order wave function),¹²³ the CD-DMRG-SC-NEVPT2 variant was applied, given that it is much less sensitive to the convergence of the zeroth-order wave function. The active orbitals for the initial DMRG-SCF step were determined with the automated active space selection protocol¹³⁸ using the AUTOCAS program (see section 3.2.1). The active spaces for all spin states must be equal and, according to the selection protocol, comprise the union of the active spaces selected for the individual spin states. In this way, 17 orbitals were selected by the protocol, resulting in an active space of 14 electrons in 17 orbitals. However, upon orbital optimization of the triplet wave function, one orbital rotated out of the active space, and hence, the active spaces for different spin states would no longer be consistent, so the orbital was removed from the active space for all spin states, resulting in an active space of 14 electrons in 16 orbitals. In all calculations, the maximum bond dimension was set to $m = 512$. Although this is a rather small value for the bond dimension, it was found to be a suitable approximation in certain cases,^{123,156} especially if an accuracy

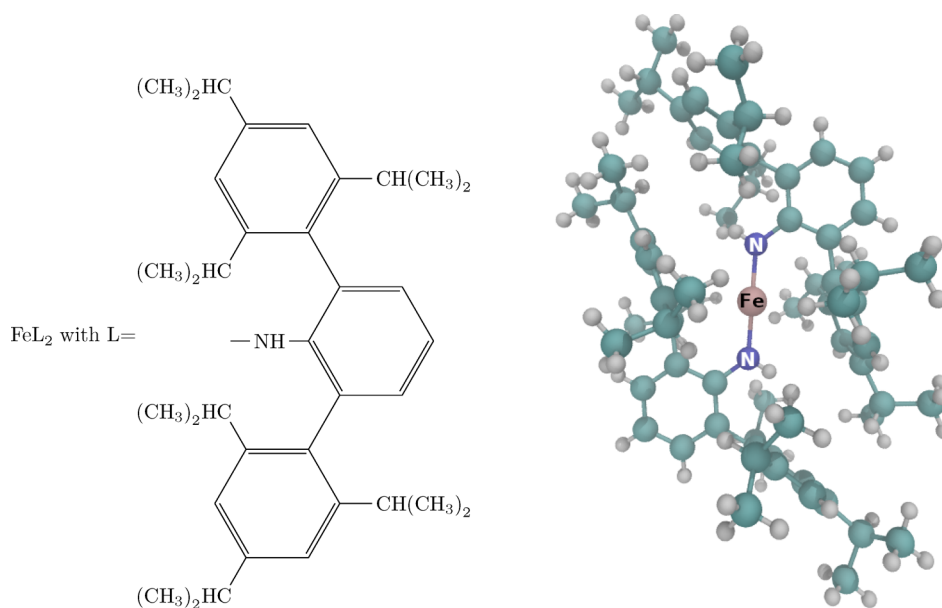


Figure 5. Lewis and molecular structure of the $\text{FeN}_2\text{C}_{72}\text{H}_{100}$ complex in ref 169 (Cartesian coordinates were taken from that reference). Color code: turquoise—carbon, white—hydrogen.

Table 2. Excitation Energy in kJ/mol Relative to the Quintet (A5) Ground State of FeN₂C₇₂H₁₀₀^a

St	DMRG-SC-NEVPT2 this work	SC-NEVPT2 ref 169	DLPNO-SC- NEVPT2 ref 169	NEVPT2 emb CASSCF ref 170	ic-MRCCSD(T) emb CASPT2 ref 170	PNO- CASSCF ref 170	DMRG-SCF this work
A3	165.8	177.2	178.6	178.4	176.6	218.6	146.3
A1	241.7			290.3	262.4	346.1	197.8

^aResults in refs 169 and 170 were obtained with a CAS(6,5) (and with a def2-TZVP basis set), whereas we chose a CAS(14,16) (and an ANO basis set; see text for further discussion) for the CD-DMRG-SC-NEVPT2 and DMRG-SCF calculations. Abbreviation: “emb”, “embedded in”.

of about 8 kJ/mol is considered to be sufficient. Further computational details are available in the SI.

Table 2 contains the quintet–triplet and quintet–singlet excitation energies calculated with CD-DMRG-SC-NEVPT2 and DMRG-SCF along with results from refs 169 and 170 obtained with several NEVPT2 and embedded MRCC variants. The quintet–triplet gap of 165.8 kJ/mol deviates only by approximately 10 kJ/mol from the embedded ic-MRCCSD(T) result from ref 170 which may be attributed to the different basis sets (ANO-RCC-VDZP/VQZP vs def2-TZVP) and the different active orbital spaces from which the reference wave function was constructed. The quality of the reference wave function may be assessed from a comparison of the CASSCF and DMRG-SCF excitation energies with the final results that include the NEVPT2 contribution: DMRG-SCF excitation energies show a significantly smaller deviation from the DMRG-SCF plus NEVPT2 results than their CASSCF counterparts, which indicates that NEVPT2 benefits from an improved active space for the reference wave function calculation and that this can be provided by the suggested automated active-orbital selection algorithm. However, the quintet–singlet excitation shows a much larger discrepancy between the DMRG-NEVPT2 results and those from the literature. First of all, the CASSCF result for the small active space deviates even more from the DMRG-SCF result than what was observed for the quintet–triplet excitation. Unfortunately, no NEVPT2 reference data are available for this higher excitation. Still, the embedded NEVPT2 result from Coughtrie et al.¹⁷⁰ is about 30 kJ/mol larger than the embedded MRCC result, whereas they were very similar in the singlet–triplet case. This may also be taken as an indication that the CAS of the reference was too small because the MRCC approach may compensate for a small-CAS reference wave function through the coupled-cluster excitation hierarchy. Accordingly, the DMRG-NEVPT2 result obtained for the larger active space is only about 20 kJ/mol smaller than the embedded MRCC result.

3.3. Multiconfiguration Pair-Density Functional Theory. Multiconfiguration pair-density functional theory (MC-PDFT)^{54,61} combines the advantages of wave function theory and density functional theory to provide a method for efficient evaluation of the electronic energy of strongly correlated systems. In MC-PDFT the first step is to calculate a multiconfiguration wave function, and in OpenMolcas, this wave function may be calculated by CASSCF,⁴⁷ RASSCF,⁵⁶ GASSCF,⁵⁷ CAS-CI,⁵⁵ RAS-CI,⁵⁵ GAS-CI,¹⁷¹ stochastic-CASSCF⁷³ (section 3.1), and DMRG^{101,102,109,172,173} (section 3.2). CASSCF, RASSCF, and GASSCF are special cases of the multiconfiguration self-consistent-field (MCSCF) method, and one can use either state-specific¹⁷⁴ SCF or state-averaged^{175,176} SCF. The total MC-PDFT energy is expressed as

$$E = V_{\text{nn}} + \langle \Psi^{\text{MC}} | \hat{T} | \Psi^{\text{MC}} \rangle + V_{\text{ne}} + V_{\text{C}} + E_{\text{ot}}[\rho, \Pi] \quad (9)$$

where the first term corresponds to the nuclear–nuclear interaction; the second, the third, and the fourth terms, respectively, correspond to the kinetic energy, the nuclear–electron attraction, and the classical Coulomb interaction of the electronic charge cloud with itself; and the final term is the on-top energy. In eq 9 the kinetic energy and the classical electrostatic energy (nuclear–nuclear repulsion energy, nuclear–electron attraction energy, and classical electron–electron Coulomb energy) are directly obtained from the multiconfigurational wave function, Ψ , while the rest of the electronic energy is calculated from an on-top density functional that is a functional of the electron density ρ and on-top pair density Π (which represents the probability of finding two electrons on top of each other) of that reference wave function.

Computationally, eq 9 reduces to

$$E = V_{\text{nn}} + \sum_{pq} h_{pq} D_{pq} + \frac{1}{2} \sum_{pqrs} g_{pqrs} D_{pq} D_{rs} + E_{\text{ot}}[\rho, \Pi, \nabla\rho, \nabla\Pi] \quad (10)$$

where D is the one-electron density matrix, h and g contain respectively the one- and two-electron integrals, and p, q, r , and s are general orbital indices including inactive and active orbitals. An MC-PDFT calculation involves two steps: (1) calculation of the multiconfiguration wave function and (2) calculation of the on-top density functional energy. Because the postself-consistent-field step is a calculation based on a density functional, the computational effort for step 2 is generally negligible compared to the cost of step 1, and this makes MC-PDFT computationally more affordable than other multireference methods such as those based on perturbation theory or multireference configuration interaction.

An MC-PDFT calculation always uses multiconfiguration wave functions that are spin eigenfunctions. MC-PDFT is free from delocalization error,¹⁷⁷ which is sometimes considered to be the most fundamental source of error in KS-DFT with approximate exchange–correlation functionals. MC-PDFT is also less prone than KS-DFT to self-interaction error.¹⁷⁸

The decomposition of the MC-PDFT energy expression of eq 9 into its individual components is sometimes important for understanding chemical and physical phenomena in molecular systems.^{72,179} This decomposition is available in OpenMolcas, along with the tabulation of ρ and Π in Cartesian coordinates for plotting and visualization.

3.3.1. On-Top Functionals for MC-PDFT. Due to the symmetry dilemma, the spin-polarized exchange–correlation functionals of KS-DFT are not compatible with the spin densities of a multiconfiguration wave function. To bypass the symmetry dilemma, one uses translated⁵⁴ and fully translated⁶⁰ on-top functionals, which are obtained by translation of KS-DFT exchange–correlation functionals of the spin densities and their gradients. Translated functionals are denoted with the prefix “t”, and fully translated functionals are denoted with the prefix “ft”. If $E_{\text{xc}}[\rho_{\alpha}(\mathbf{r}), \rho_{\beta}(\mathbf{r}), \nabla\rho_{\alpha}(\mathbf{r}), \nabla\rho_{\beta}(\mathbf{r})]$ denotes a KS-

DFT exchange–correlation functional, in which ρ_σ is the spin density ($\sigma = \alpha, \beta$), and $\nabla\rho_\sigma$ is the gradient of the density, the translated functional is given by

$$E_{\text{ot}}[\rho(\mathbf{r}), |\nabla\rho(\mathbf{r})|, \Pi(\mathbf{r})] = E_{\text{xc}}[\rho_\alpha^t(\mathbf{r}), \rho_\beta^t(\mathbf{r}), \nabla\rho_\alpha^t(\mathbf{r}), \nabla\rho_\beta^t(\mathbf{r})] \quad (11)$$

where

$$\rho_\alpha^t(\mathbf{r}) = \frac{\rho}{2}(1 + f(\rho, \Pi)) \quad \nabla\rho_\alpha^t(\mathbf{r}) = \frac{\nabla\rho}{2}(1 + f(\rho, \Pi))$$

$$\rho_\beta^t(\mathbf{r}) = \frac{\rho}{2}(1 - f(\rho, \Pi)) \quad \nabla\rho_\beta^t(\mathbf{r}) = \frac{\nabla\rho}{2}(1 - f(\rho, \Pi))$$

$$f(\rho, \Pi) = \sqrt{\max\left(0, 1 - \frac{4\Pi}{\rho^2}\right)}$$

in which $\nabla\rho$ is the gradient of that spin density. For a single-determinant wave function, $\frac{4\Pi}{\rho^2} \leq 1$ in all space. However, for a multiconfiguration wave function, this ratio can be greater than one. Notice that the translated functionals depend on Π but not on its gradient and that the left and right derivatives of f are not equal at $\frac{4\Pi}{\rho^2} = 1$, making the gradient of f discontinuous.

Fully translated functionals also depend on $\nabla\Pi$, and the first and the second derivatives of the functional are continuous. Both kinds of functionals have been found to give reasonably good results for multireference systems.

OpenMolcas supports the use of several different on-top functionals, including a translated local spin-density approximation (LSDA), various translated generalized gradient approximations, and various fully translated generalized gradient approximations. The following is a list of currently supported functionals: tLSDA,^{54,180,181} ftLSDA,^{60,180,181} tPBE,^{54,182} ftPBE,^{60,182} trevPBE,^{183,184} ftrevPBE,^{183,184} tBLYP,^{54,185,186} ftBLYP,^{60,185,186} tOPBE,^{182,187,188} and ftOPBE.^{60,182,187,188}

OpenMolcas also supports functionals obtained by scaling the exchange and/or correlation components of the exchange–correlation functionals prior to translation. The scaling factors may be input by the user. This allows the functionals to be modified into an HLE-type functional,^{189,190} where the standard scaling factors are 1.25 for exchange and 0.5 for correlation, but other scaling factors may be chosen.

3.3.2. Performance of MC-PDFT. MC-PDFT generally produces results that are comparable in accuracy to complete active space second-order perturbation theory (CASPT2) but at significantly lower computational cost¹⁹¹ for bond energies,^{59,60,177,192,193} spin-multiplet splittings,^{194–197} and other excitation energies.^{198–201} These results are summarized in Table 3. A review containing references for tests and validations on electronically excited states up to mid-2018 is available in ref 202.

3.3.3. Analytical Gradients for SS-CAS-PDFT. OpenMolcas includes analytical gradients for MC-PDFT when a state-specific CASSCF (SS-CASSCF) wave function is used as a reference (SS-CAS-PDFT), and these gradients enable the fast and efficient determination of equilibrium and transition state structures.²⁰⁵ Because MC-PDFT is a nonvariational method, the computation of the gradient requires the construction of a Lagrangian. In general, the computation of analytical gradients can be performed at least an order of magnitude faster than the corresponding gradient calculation using a numerical finite-difference method. SS-CAS-PDFT shows good accuracy compared to experimental data for both equilibrium and

Table 3. Mean Unsigned Error (MUE) of MC-PDFT Using the tPBE Functional and CASPT2

ref	system/property	MUE (eV)	
		PT2	tPBE
54	6 covalent or ionic diatomics/ dissociation energy	0.3	0.3
59	10 transition metals with ligand/ average bond energy	0.24	0.19
194	11 <i>n</i> -acenes (from naphthalene to dodecacene)/ singlet–triplet gap	0.06 ^a	0.13 ^a
193	13 main-group atoms or compounds/ singlet–triplet gap	0.12 ^b	0.24 ^b
196	8 organic rings/ singlet–triplet gap	0.01 ^b	0.10 ^b
199	19 main-group atoms/ first excitation energy	0.22	0.42
201	10 doublet radicals/ first 5 vertical excitation energies	0.14	0.19

^aThe reference wave function is optimized from a GASSCF calculation.^{57,203} ^bThe active space for the reference wave function uses the correlated-participating-orbital (CPO) scheme.²⁰⁴

Table 4. Illustrative Timings (in s) for a Single Gradient Computation^a Using a Single Processor

	active space	symmetry	cc-pVDZ		cc-pVTZ	
			CASPT2	tPBE	CASPT2	tPBE
NH ₃	(6,6)	C _s	16	7	32	14
HCN	(8,8)	C _{2v}	9	4	17	10
CH ₂ O	(12,9)	C _{2v}	29	9	29	15
HCCH	(10,10)	D _{2h}	20	6	20	11
oxirane	(10,10)	C _{2v}	55	27	136	45
pyrrole	(6,5)	C _{2v}	87	39	1082	212
acrolein	(4,4)	C _s	558	117	3390	160
butadiene	(4,4)	C _{2h}	85	29	933	137
pyridine	(6,6)	C _{2v}	183	32	2256	156
maleic anhydride	(8,7)	C _{2v}	123	36	1148	218

^aCASPT2: numerical gradient. tPBE: analytical MC-PDFT gradient.

transition-state structures. Some illustrative single-processor timings for MC-PDFT calculations employing the tPBE on-top functional are shown in Table 4.

3.3.4. Density Matrix Renormalization Group Pair-Density Functional Theory (DMRG-PDFT). DMRG (see section 3.2) is a powerful method to treat static correlation, especially in molecular systems requiring large active spaces. MC-PDFT can be used in conjunction with DMRG to add additional dynamic correlation in an inexpensive way. The first applications^{206,207} of DMRG-PDFT were based on an interface between the existing MC-PDFT code in OpenMolcas and the DMRG code in the QCMAQUIS^{117,126,208} program. An illustrative example²⁰⁶ of singlet–triplet gaps in polyacenes is shown in Figure 6. The tPBE/6-31G+(d,p) combination of on-top functional and basis set was used.

3.3.5. State-Interaction Pair-Density Functional Theory. The accurate description of ground- and excited-state PESs in cases where two electronic states are strongly interacting (such as near conical intersections or locally avoided crossings) is a challenge for many electronic structure methods. A new framework, called state-interaction PDFT (SI-PDFT),²⁰⁹ has

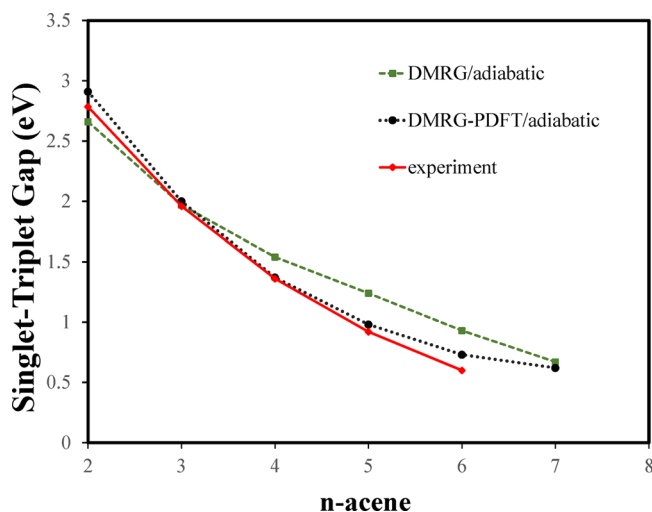


Figure 6. Singlet–triplet gaps in polyacenes.

been introduced to handle these situations in the case of MC-PDFT. This has been recently implemented in OpenMolcas and successfully applied to several cases, such as the dissociation of LiF^{209} and the charge-transfer reaction path of a mixed-valence compound.²¹⁰ SI-PDFT is an extension of MC-PDFT that involves the diagonalization of an $N \times N$

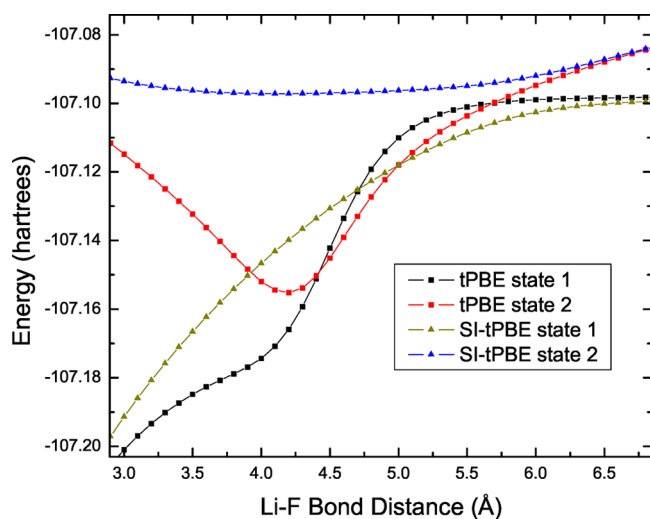


Figure 7. Dissociation of LiF calculated with a (6e,6o) active space.

effective Hamiltonian to generate a new set of N electronic states with proper PES topology in regions of strong state interaction. This method is similar in objectives and application to the “perturb-then-diagonalize” approaches in multireference perturbation theories such as MS-CASPT2^{211,212} or MC-QDPT.^{213,214} An illustrative example is shown in Figure 7. The tPBE functional was used for both a standard MC-PDFT calculation and a SI-PDFT calculation. While unphysical curve crossings are present in the standard MC-PDFT treatment, these vanish when the SI-PDFT methodology is used because the final step in the SI-PDFT method is a diagonalization.

4. EXPLORATION OF POTENTIAL ENERGY SURFACES

Understanding the mechanism, rate, and yield of chemical reactions requires exploring the potential energy surfaces of

interest. A photochemical reaction involves by definition several PESs; the strong coupling between the different electronic states promotes efficient nonradiative electronic transitions.^{215,216} One distinguishes between *internal conversion* caused by nonadiabatic coupling between states of same spin multiplicity and *intersystem crossing* caused by spin–orbit coupling between states of different spin multiplicity. Exploration of PESs can be performed either through optimization of specific geometries and paths along the reaction or through simulations of the actual dynamics of the reaction in time.

Regarding optimization calculations, OpenMolcas allows one to optimize minima and transition states, as well as minimum-energy paths and intrinsic reaction paths, using the SLAPAF program. Since recently, it is also possible to optimize conical intersections thanks to the implementation of the nonadiabatic coupling vector. This new feature is detailed in section 4.1. We mention in passing that the SHARC suite (described in section 4.3) provides a module, alternative to the SLAPAF program in OpenMolcas, that allows the optimization of excited-state minima, minimum-energy crossing points, and conical intersections, using OpenMolcas for calculating the needed electronic quantities.

Regarding dynamics simulations, direct methods calculate the PESs as needed along trajectories, sampling only the relevant regions of the PESs. These nuclear trajectories are then used to describe the nuclear wavepacket motion. One major feature that differentiates the several direct methods able to describe (nonadiabatic) dynamics is the treatment of the nuclear motion through the basis of nuclear trajectories.²¹⁷ OpenMolcas allows one to simulate Born–Oppenheimer and surface-hopping dynamics, by treating the nuclei classically. New features presented in section 4.2 include thermal sampling of the initial conditions, application of external mechanical forces, and study of isotopic effects. As an electronic structure package, OpenMolcas is also interfaced to other open-source dynamics codes. The interfaces to SHARC and Quantics are presented in sections 4.3 and 4.4, respectively. SHARC contains a general surface-hopping algorithm with arbitrary couplings such as the spin–orbit coupling, while Quantics allows a quantum treatment of the nuclear motion with the direct dynamics variational multi-configuration Gaussian (DD-vMCG) method.

4.1. Conical Intersection Optimization and Characterization. A key quantity for describing photochemical processes and near-degeneracy between electronic states is the nonadiabatic or derivative coupling vector. However, until now it was not possible to obtain this quantity with the MOLCAS package, and some approximations had to be employed for nonadiabatic molecular dynamics⁸ or for the location of conical intersections.²¹⁸

Since its release, OpenMolcas includes analytical non-adiabatic couplings between state-average CASSCF wave functions, as described in ref 219. The implementation is based on the algorithm used for energy gradients,^{146,148,220} and it is compatible with both conventional and density-fitted two-electron integrals. The availability of nonadiabatic couplings allows the use of the projected constrained optimization (PCO) method^{221,222} for locating minimum-energy conical intersections (MECI). From the user’s perspective, the only change with respect to a single-surface geometry optimization is the addition of an energy difference constraint—gradients, and nonadiabatic couplings are computed automatically as

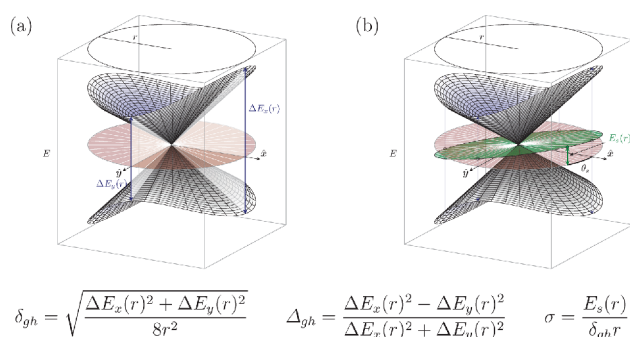


Figure 8. Illustration of the parameters characterizing a conical intersection. The red disc represents the horizontal plane $E = E^*$. (a) Energy differences in the \hat{x} and \hat{y} directions define the pitch δ_{gh} and asymmetry Δ_{gh} . (b) The green disc represents the average energy plane, as indicated by the small circles on its edge, and the amount and orientation of its maximum deviation from the red disc define the relative tilt σ and the tilt heading θ_s .

needed. Furthermore, the first-order conical intersection characterization proposed in ref 219 is also reported upon convergence, allowing the unambiguous description and comparison of conical intersection topographies. The meaning of the characterization parameters is illustrated in Figure 8. From these, it is possible to determine whether the intersection is *peaked* or *sloped*—in the latter case, it is not a minimum on the upper surface—and this is available in the output as well.

4.2. Dynamics Simulations within OpenMolcas.

Born–Oppenheimer and nonadiabatic dynamics can be performed within OpenMolcas using the DYNAMIX and SURFACEHOP modules. Transitions between different electronic states can be treated by two different approaches: (a) according to the quantification of the temporal rate of mixing between electronic states²²³ and (b) following Tully’s fewest switches approach²²⁴ where the initial population density matrix is defined at the beginning of the propagation. The modular structure of OpenMolcas allows combining other features in OpenMolcas with dynamics simulations. For example, the ESPF module enables hybrid quantum mechanics/molecular mechanics (QM/MM) simulations, or any other electronic structure method available in OpenMolcas can be used to obtain the energy and gradients. Recent developments for molecular dynamics simulations have been included in OpenMolcas. They are summarized below.

4.2.1. Initial Thermal Sampling. In order to obtain statistically significant predictions using molecular dynamics simulations, an ensemble of trajectories has to be computed (usually hundreds of trajectories, even in simple reactions like *trans*–*cis* photoisomerization^{225–230}). The initial state of the system has to be appropriately sampled in order to get a good representation of nuclear positions and momenta. OpenMolcas allows sampling of the phase-space for a thermally equilibrated state according to the Boltzmann distribution. Given the minimum energy structure of the system, the absolute temperature, and a second-order expansion of the potential energy as determined with a frequency calculation, initial conditions (i.e., nuclear coordinates and momenta) are generated; they can be subsequently used for running individual trajectories.

4.2.2. Steered Molecular Dynamics. DYNAMIX has the possibility of including multiple external force pairs, each one applied on a specific couple of nuclei. The external forces are

added to the molecular force field defined by the electronic state. This new feature allows the user to simulate the action of external forces (i.e., mechanical effects) acting over a molecular system. The magnitude of each force pair is defined as the magnitude of each force vector acting on each of the two atoms. Many force pairs can be added, generating a final external force vector by summing up all the components on each atom. Finally, the applied force pairs can be defined as extension or compression forces. In this way different mechanochemical setups (e.g., polymer mechanochemistry, sonochemistry, or force probes) can be simulated, in a first approach, by adding external forces.

Steered molecular dynamics can be performed in ground and excited states, permitting the study of photochemical processes in strained systems. Photochemistry of mechanically affected systems, i.e., mechanophotochemistry, still remains quite unexplored, and only a few studies show the interesting properties of these processes. In this regard, it has been shown that photochemistry can be effectively modified by mechanical means,²³¹ where the interplay between excited-state dynamics and external forces is far from being simple and intuitive, as is the case of a *trans* to *cis* photoisomerization of a retinal model system, where an extension force, expected to oppose the formation of the *cis* isomer, is found to enhance the photoisomerization, significantly increasing the photoreaction quantum yield.²²⁹

4.2.3. Isotope Effect. DYNAMIX is making use of the isotope feature in OpenMolcas which enables the consideration of specific isotopes in molecular dynamics simulations. Typically, replacing an atom with an isotope is associated with a kinetic isotope effect which affects the reaction rate of a chemical process.

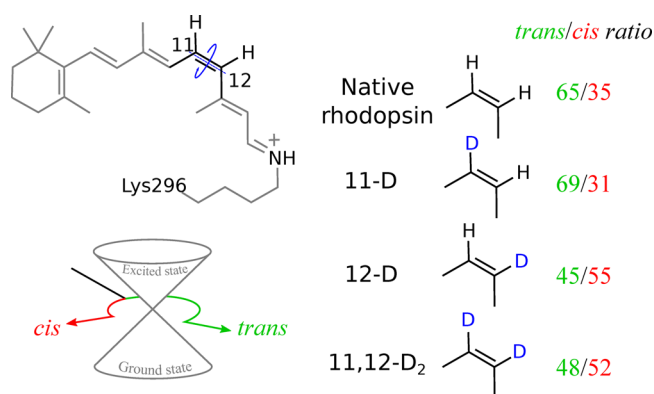


Figure 9. 11-*cis*-Retinal protonated Schiff base and the three studied isotopomers.

In a recent study of the photoisomerization in rhodopsin, the new feature helped to reveal a new type of kinetic isotope effect.²³² In this specific case, the hydrogen atoms of the 11-*cis* isomerizing double bond were replaced by deuterium in three different ways: at both hydrogens and at the hydrogen at either the 11 or 12 position (Figure 9). The molecular dynamics simulations together with time-resolved measurements showed that while the reaction rate was mainly unaffected, the isomerization quantum yield was significantly altered by the deuterium replacements. In fact, remarkably, the quantum yield was found to decrease and increase in the monodeuterated and bideuterated cases, respectively. This study provided further evidence on the importance of the “hydrogen

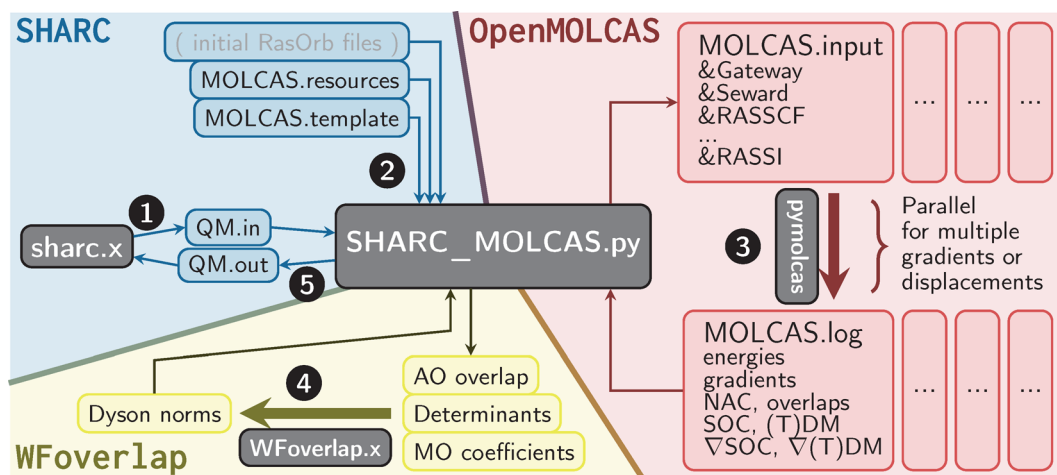


Figure 10. Flowchart of the SHARC–OpenMolcas interface. In step (1), the SHARC dynamics driver `sharc.x` writes a file with the current geometry and requests for quantities (e.g., energies E , spin–orbit couplings (SOC)). This file is read by the interface, together with the template and resource files that define the level of theory and the computational parameters, respectively. In step (2), all necessary OpenMolcas input files are written, and step (3) executes the `pymolcas` driver. The resulting output files are parsed for all requested quantities. Optionally (4), the WFOVERLAP program is executed to obtain Dyson norms. Finally (5), all obtained results are handed back to the SHARC driver.

out of plane” mode for the description of the reaction coordinate of the photoisomerization of the 11-*cis*-retinal protonated Schiff base chromophore of vertebrate visual rhodopsins.^{233,234}

Changing the masses of atoms to “artificial” values may also be a useful simulation tool to get insights into the factors that determine the yield of chemical reactions. In a recent study of the dissociation of dioxetane compounds, this functionality was used to understand the effect of methylation.²³⁵ Substitution of hydrogen atoms by methyl groups in dioxetane had been shown to lead to a longer dissociation time, and it had been previously suggested that this was due to the increase in the number of degrees of freedom. To investigate further the effect of methylation, dynamics was simulated for the unmethylated 1,2-dioxetane, but where the mass of the four hydrogen atoms was increased to reproduce the moment of inertia of the methyl groups. The simulations suggest that approximately 75% of the increase in the dissociation time is actually due to a pure mass effect (in contrast to the hypothesis put forward in a previous theoretical study).

4.3. Nonadiabatic Semiclassical Dynamics Interface.

OpenMolcas is interfaced with the ab initio molecular dynamics software suite SHARC (Surface Hopping including ARbitrary Couplings).^{236–240} Through this interface, non-adiabatic dynamics can be carried out based on the CASSCF and CASPT2 electronic structure methods of OpenMolcas.

SHARC is a generalization of the surface hopping method.²²⁴ This allows describing processes such as inter-system crossing or laser-induced transitions, which is not possible with standard Tully surface hopping. Furthermore, the SHARC software suite can manage large trajectory ensembles and features many analysis tools.

The interface between SHARC and OpenMolcas is based on file communication between the two programs, see the flowchart in Figure 10. The SHARC dynamics driver (the master process) writes a request file at each simulation time step, containing the current geometry and a list of required electronic quantities, such as energies, gradients, spin–orbit couplings, etc. The interface, a Python script, combines the request information with the electronic structure settings and

computational parameters. The interface writes the OpenMolcas input files, allowing for computation of multiple gradients or displacements for numerical gradients in a task parallel fashion. The automatically generated OpenMolcas input employs the GATEWAY and SEWARD modules for setup and integrals, the RASSCF module for wave functions and energies, RASSI for transition dipole moments, spin–orbit couplings, and wave function overlaps (for nonadiabatic interactions, see below), and MCLR and ALASKA for gradients. For CASPT2 or MS-CASPT2, the calculation of numerical gradients is directly controlled by the SHARC–OpenMolcas interface, allowing a simultaneous calculation of all gradients of all states and the derivatives of dipole moments and spin–orbit couplings in a single loop. The nonadiabatic interaction between the different states is described by employing wave function overlaps²⁴¹ from the RASSI module or by nonadiabatic coupling vectors from MCLR/ALASKA. QM/MM dynamics (CASSCF/force fields) can also be performed through the OpenMolcas–Tinker interface. All collected electronic structure data is finally communicated back through the interface to the dynamics driver, which propagates the trajectory to the next time step.

It is noted that the SHARC–OpenMolcas interface can also produce Dyson norms to approximately describe ionization probabilities (see also section 5.3) by feeding the relevant wave function data into the WFOVERLAP program²⁴² within the SHARC suite.

4.4. Quantum Dynamics Interface. While implementing a direct dynamics code for classical nuclei is rather straightforward since information is only needed at a given position in space, a quantum description of the nuclei has more problems. We report here a new interface between OpenMolcas and the Quantics package²⁴³ (grown out of the Heidelberg MCTDH package²⁴⁴), which allows a quantum mechanical treatment of both electronic and nuclear dynamics via the direct dynamics variational multiconfiguration Gaussian (DD-vMCG) method.^{217,245,246} In practice, Quantics uses OpenMolcas to build a local harmonic approximation of the coupled PESs, as represented in Figure 11. The dynamics can be run either in Cartesian coordinates or in normal modes. If

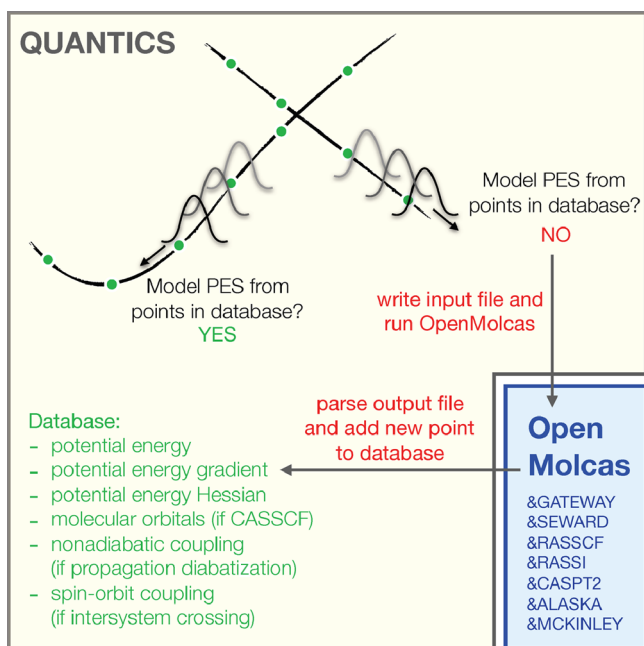


Figure 11. Quantics–OpenMolcas interface. At each time step, the database of previously run quantum chemistry calculations is probed to build model coupled potential energy surfaces (PESs). If suitable points exist around the desired geometry (Gaussian basis function on the left-hand side of the figure), a representation of the PES is constructed using those points. If that region of the coordinate space has not been previously explored (right-hand side), an OpenMolcas calculation is performed, and information about this new point is added to the database.

the latter, transformation matrices between the two systems of coordinates are set up by reading the output file of a frequency calculation (using the MCKINLEY module with OpenMolcas).

Along the dynamics simulation, Quantics writes input files from a template input file to run OpenMolcas and compute the adiabatic energies, gradients, Hessians, and couplings for all electronic states involved. The electronic structure calculations are performed at the center point of each Gaussian basis function, and subroutines in Quantics parse the OpenMolcas output files to extract the relevant information.²⁴⁷ Currently possible electronic structures methods are HF, CASSCF, and CASPT2. In the latter case, it is only the CASPT2 potential energies that are used, while the corresponding energy derivatives and couplings are approximated with their values at the CASSCF level.

If several electronic states are included in the simulation, the dynamics is performed in a diabatic basis in order to avoid singularity issues. A diabaticization operation is then realized to transform the adiabatic quantities provided by OpenMolcas into diabatic ones. Two diabaticization schemes are available: the regularization diabaticization method,²⁴⁸ which limits the application to two electronic states, and the propagation diabaticization method implemented more recently.²⁴⁹ The former method requires information about a reference conical intersection geometry (which can be optimized using the SLAPAF module with OpenMolcas). The latter method requires the calculation of the nonadiabatic coupling vector (which can be done using the ALASKA module with OpenMolcas) at every new electronic structure point. When dealing with states of different spin multiplicity, a diabaticization

is performed in each spin-multiplicity subset, and internal conversion within each subset is accounted for as usual in same-spin dynamics. Intersystem crossing is treated by calculating the spin–orbit coupling terms (which can be done using the RASSI module in OpenMolcas) at every new electronic structure point.¹⁶³

In order to save time and avoid redundant electronic structure calculations, the electronic quantities calculated by OpenMolcas are stored in a database. New database points are only calculated if the new nuclear geometry differs by some predetermined amount from all database geometries (right basis function in Figure 11). If it is close enough to some database points (left basis function in Figure 11), the quantities are interpolated from the values present in the database.²⁵⁰ It is noted that the molecular orbital coefficients of the CASSCF calculations are also stored in the database and used as initial guesses for new electronic structure calculations. Also, instead of calculating the Hessian at every point, after the first point, an update procedure can be performed using the database according to the Powell method.^{246,251} By running the dynamics calculation several times, more and more points are added to the database. The database “grows” iteratively and reaches convergence once no new database points are needed.

5. SPECTROSCOPIC AND MAGNETIC PROPERTIES

The strong focus of the OpenMolcas package in multi-configurational wave function methods makes it an excellent tool for the computational study of systems where multiple electronic states play an important role. An obvious case is the study of electronic spectra, involving transitions between different electronic states. A paradigmatic example is the study of transition metal complexes, where the presence of partially filled d and/or f shells gives rise to many close-lying electronic states of various spin multiplicities.

The workhorse for these investigations, once accurate spin-adapted wave functions and energies are obtained, is the RASSI program.¹⁶³ This program can compute the spin–orbit interaction to yield a set of spin–orbit eigenstates, with the use of atomic mean-field integrals,²⁵² as well as transition properties between different wave functions.

In this section we report some recent developments and improvements for the computation of spectroscopic and magnetic properties in OpenMolcas, from the exact semi-classical treatment of light–matter interaction (section 5.1) to applications in X-ray spectroscopy (section 5.2), photoelectron spectroscopy (section 5.3), magnetic circular dichroism (section 5.4), molecular magnetism (section 5.5), and in the context of ultra-accurate calculations (section 5.6).

5.1. Light–Matter Interaction and beyond the Multipole Expansion. All spectroscopies depend on the interaction between the system and an external electromagnetic field. For weak fields that can be treated as perturbations, the oscillator strength for a transition from an initial state i to a final state f is

$$f_{if}(\omega) \propto |\langle i | \hat{U} | f \rangle|^2 \delta(\omega - \omega_{if}) \quad (12)$$

where $\omega_{if} = (E_f - E_i)/\hbar$ is the resonance angular frequency, and \hat{U} is the time-independent part of the electromagnetic perturbation. Usually, the field is described by a plane wave, and using only terms linear in field strength \hat{U} then becomes

$$\hat{U} \propto \sum_j \left[\exp(i\mathbf{k} \cdot \mathbf{r}_j) (\mathbf{e} \cdot \hat{\mathbf{p}}_j) + i \frac{g}{2} \exp(i\mathbf{k} \cdot \mathbf{r}_j) (\mathbf{k} \times \mathbf{e}) \cdot \hat{\mathbf{s}}_j \right] + \text{c.c.} \quad (13)$$

where the sum goes over all the electrons, \mathbf{k} is the wave vector, \mathbf{r}_j is the position, $\boldsymbol{\varepsilon}$ is the polarization vector, $\hat{\mathbf{p}}_j$ is the momentum operator, g is the electronic spin g -factor, and $\hat{\mathbf{s}}_j$ is the spin operator, and c.c. is the complex conjugate of the previous terms.

Traditionally, the integrals in eq 12 are evaluated using a multipole expansion of the electromagnetic wave:

$$\exp(i\mathbf{k}\cdot\mathbf{r}_j) = 1 + i(\mathbf{k}\cdot\mathbf{r}_j) - \frac{1}{2}(\mathbf{k}\cdot\mathbf{r}_j)^2 + \dots \quad (14)$$

For the transition moments, taking only the zeroth-order term amounts to the electric dipole approximation, while the first-order term is associated with electric quadrupole and magnetic dipole interactions. The multipole expansion leads to well-recognized selection rules that for certain systems and specific choices of coordinate systems can be directly related to electronic structure. While the dipole approximation is often sufficient for the low-energy photons in the optical region, high-energy photons have large \mathbf{k} vectors, rapidly oscillating fields, and higher-order terms in the multipole expansion cannot be ignored. These higher-order terms depend on the choice of origin, at least in cases where there are nonzero terms of lower order. For weak fields the problem of origin dependence was recently solved by Bernadotte et al., by including all terms to the same order in the oscillator strength and not in the transition moments, which for the second order requires calculations up to magnetic quadrupoles and electric octupoles.²⁵³ The complete second-order expansion is implemented in OpenMolcas and has been used to calculate X-ray spectra of several mono- and binuclear iron complexes.^{254,255} Although origin independence was first proven for the velocity gauge,²⁵³ origin independence in a finite basis set can also be accomplished in the length gauge.²⁵⁶ However, what is usually referred to as the length gauge is actually a mixed gauge, with the electric components in the length gauge and magnetic components in the velocity gauge.²⁵⁶ Origin independence, in finite basis sets, is not conserved in this mixed gauge.²⁵⁷ Furthermore, when using the complete second-order expansion the increased basis set requirements for higher-order terms in the multipole expansion must be considered.²⁵⁷

A solution to the problems with the multipole expansion is to instead use the plane-wave form of the wave vector directly: the exact semiclassical light–matter interaction²⁵⁸ is origin independent, cannot give negative oscillator strengths, and gives what all terms in the multipole expansion ideally should converge to.²⁵⁸ Further, it shows better numerical stability with respect to the choice of basis set.²⁵⁹ OpenMolcas now includes an elegant and efficient procedure using a standard Gauß–Hermite quadrature to evaluate the integrals in eq 12 in this formalism.²⁵⁹ Both electric and magnetic terms are calculated this way, with the spin-magnetic term in eq 13 being nonzero when the spin–orbit operator in the RASSI module is used.

With the exact operator OpenMolcas now calculates the angular dependence on the transition intensities with respect to both polarization and wave propagation direction. This can be used to simulate experiments where the system is oriented relative to the photon beam, e.g., in single crystals or molecules on surfaces. Although no closed formula for the isotropically tensor averaged oscillator strengths is known, the exact value can be approximated by averaging over different directions using a Lebedev grid.^{259,260} Although the averaging over a grid increases the computational time compared to the multipole

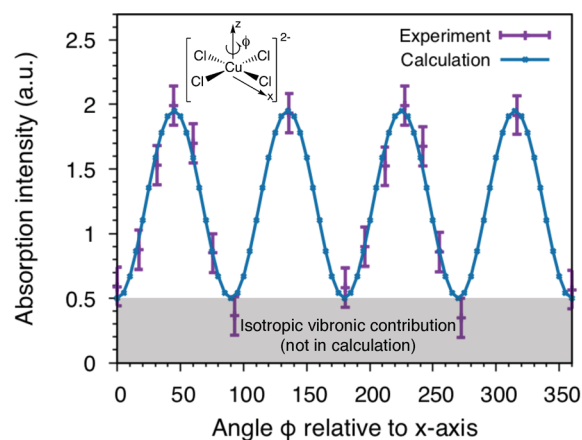


Figure 12. Angular dependence of the 1s \rightarrow 3d copper K pre-edge transition in $[\text{CuCl}_4]^{2-}$. Experimental data are normalized K pre-edge peak heights.²⁶¹ Calculated values are from the exact semiclassical light–matter interaction with intensity uniformly scaled to match experiment.²⁵⁹ The isotropic contributions are due to vibronic coupling, which are not included in the calculations.

expansion, this will only rarely affect the timing of the full electronic structure calculation. To illustrate the capabilities of the exact operator, the angular dependence of the single Cu 1s \rightarrow 3d transition in single-crystal $[\text{CuCl}_4]^{2-}$ has been calculated and compared to the experimental values, see Figure 12.²⁵⁹ The experimental intensity is distinguished by a 4-fold periodicity, which was used to assign the electric quadrupole contributions.²⁶¹ Further, the orientation of the peak maxima can also be used to identify the symmetry of the singly occupied 3d orbital. Calculations with the exact operator show the same angular dependence, including the 4-fold periodicity, which illustrates how the exact operator includes any information that traditionally has been assigned to multipole contributions.

5.2. X-ray Spectroscopy and Calculations of Many Core-Hole Excited States. X-ray spectroscopy involves core-hole states that are at least hundreds of eV higher in energy than the valence excited states. In a complete-active-space approach, these states can be included in the CI expansion by placing the relevant core orbitals in the active space. As the number of excitations from these orbitals can be restricted to one, it is convenient to use a restricted active space (RAS) wave function to simulate X-ray spectra.^{262–265} For such processes, the usual bottom-up approach that includes all states is problematic because to reach core-hole excited states all possible valence excited configurations must be calculated first. A few strategies for generating core-hole states are available, for example, for some systems where it is possible to use symmetry considerations or for very small active spaces.²⁶⁶ However, for a standard-size active space there can be millions of valence states. Strategies that only reach core-hole states are needed. Two of them recently implemented in OpenMolcas are reported here.

A convenient solution to this problem is to define a fixed orbital function χ and a parameter λ and add a term to the molecular Hamiltonian

$$\hat{H}_{\text{sh}} = \hat{H} + \lambda \hat{P}[\chi] \quad (15)$$

Here, \hat{H}_{sh} is the shifted Hamiltonian, and $\hat{P}[\chi]$ is an orthogonal projection on the space of wave functions where orbital χ is doubly occupied. This is multiplied by λ and can be

Table 5. Orbitals Used for H₂O^a

	1a'	2a'	3a'	4a'	5a'*	6a'*	7a'*	1a''	2a''*
ground	-20.6	-1.36	-0.72	-0.59	0.03	0.03	0.04	-0.51	0.04
excited	-21.3	-1.78	-1.13	-1.02	-0.07	-0.01	0.01	-0.97	0.01

^aAsterisked are valence/Rydberg orbitals, unoccupied in the ground state. Orbital energies (E_h), for the ground state and for the excited states (average, hence approximate).

implemented by modifying the two-electron MO integrals at the CI step. These integrals are recomputed at each macroiteration while the added term is using the same fixed function χ all the time. The penalty term has the effect of raising the energy of those configurations with a filled core-hole to be above those with a single hole, which are now the lowest in energy. Our experience shows that it is easy to find a suitable shift λ , such that this scheme is stable across changing orbitals and structure, and it has been observed to give only a slight energy variation with the input shift parameter. Obviously, special basis functions may have to be supplied to allow the orbitals of the core-hole states to relax accurately, or if inner-valence correlation is important, e.g., for Auger. The following example shows the calculation of core–valence excitations for H₂O close to equilibrium, using a specifically prepared basis set. Two calculations were performed: one without the projected shift and the other with the shift. The orbital energies in Table 5 show large differences between

Table 6. States, Excitation Energies (eV), Dipole and Velocity Einstein A Coefficients (ps⁻¹), and Polarization (C_s)

excitation (RASSI)	energy	dipole	velocity	polarization
5a' ← 1a' (O 1s)	537.2	0.124	0.139	A'
6a' ← 1a' (O 1s)	539.1	0.316	0.289	A'
7a' ← 1a' (O 1s)	539.8	0.065	0.052	A'
2a'' ← 1a' (O 1s)	537.7	0.075	0.065	A''

without and with the core-hole present. The results of the subsequent RASSI calculation are displayed in Table 6, showing that it is possible to access states very high in energy (compared with typical valence excitations). For other examples, please see the online poster in ref 267.

For the general case, another simple technique is to remove from the CI all configurations with fully occupied core orbitals, the so-called core–valence separation (CVS).²⁶⁸ Because of the large energy separation between configurations with and without core-holes, the latter do not contribute significantly to the core-hole excited states. For active-space methods the CVS is closely related to the generalized active space method.⁵⁷ Using the special case of RAS, the core orbitals can be placed in RAS1 allowing at least singles, for single-core-hole excited states, or doubles, for double-core-hole excited states. The core-hole excited states are found by applying a core-hole (ch) projection operator P_{ch}

$$P_{ch}\Psi = \Psi_{ch} \quad (16)$$

on the RASSCF calculation, which for single-core-hole excited states removes all configurations in Ψ that are fully occupied in RAS1.^{254,269} This ensures that the lowest-energy state in Ψ_{ch} is a core-hole excited state in the RASSCF optimization. It is noted that although the core-hole and valence states are calculated separately and are thus not orthogonal, transition

intensities can still be calculated in the RASSI module^{163,270} since the different wave functions use the same CI expansion.

In X-ray spectroscopy, even if the computation of all valence states can be avoided using one of the two strategies discussed above, the number of excited states needed to describe the process of interest can be very large. In transition metal complexes, the density of states is very high so that, for an X-ray absorption spectrum that typically spans 10 eV, several hundred final states are required.²⁶⁶ This creates difficulties for standard techniques such as a multiroot Davidson⁷⁷ or Davidson–Olsen algorithm.²⁷¹ A modified CI algorithm has therefore been implemented to allow for more efficient calculations of a large number of states.

The Davidson–Olsen algorithm is the quasi-Newton method applied to the CI problem. It uses an approximate Hamiltonian H_0 , typically diagonal, to compute successive corrections to an approximate CI vector $C_j^{(i)}$. The next CI vector $C_j^{(i+1)}$ is then found by diagonalizing a small Hamiltonian in the basis of all CI vectors at the current iteration and their corresponding correction vectors. To improve convergence, the correction vectors of a few previous iterations are often included. When calculating a very large number of states, this scheme (hereafter called Version 1) encounters some problems. First, storing several hundred CI or correction vectors from a few iterations can put severe constraints on memory. Second, the higher-lying states typically get increasingly difficult to converge, which leads to a large number of CI iterations and makes the CI calculation very costly. Finally, as the number of previous correction vectors stored increases, they tend to have significant linear dependence, which can lead to numerical instability during the orthonormalization and sometimes even divergence.

The OpenMolcas CI algorithm has been significantly improved for calculations with hundreds of states. The first aim was to improve stability of the algorithm to better deal with linear dependencies in the correction vectors. A simple and quick fix in order to have a more reliable (but slower) convergence was to reduce the number of past iterations for which the CI vectors were saved to two instead of five. This version of the algorithm is called hereafter Version 2. As a more general alternative to this, a more comprehensive change of the code was realized. While the original implementation (Version 1) saved the last five correction vectors for each state, this new implementation instead sets an upper limit to the total number of correction vectors to around 400, which was found to be the best compromise between speed, flexibility, and stability. Improvements were also made to reduce the risk of divergence in case of near-linear dependency by performing additional orthogonalizations and normalizations. This leads to what we call Version 3 of the algorithm. Finally, a very important improvement is to stop computing correction vectors for converged states. As lower roots converge significantly faster than the higher ones, this leads to a drastic reduction of the number of vectors to compute during the majority of the Davidson–Olsen iterations. This final version is

referred to as Version 4 and is now the new default option in OpenMolcas.

Savings in computational time with the modified CI algorithm depend on the size of the system and the active space. The improvement is most significant with a larger active space because then the CI step dominates the computational cost. As an example, we simulated the X-ray $K\alpha$ emission spectrum of $[\text{Fe}(\text{bmip})_2]^{2+}$, a calculation with ten valence and four Fe 2p and 1s core orbitals in the active space (145404 CSFs for the ground state), using up to 90 core-hole excited states in each irreducible representation, which was needed to get the desired orbitals in the active space. The calculation consists of 1 calculation of the initial 1s core-ionized state and 3 independent calculations of the $2p \rightarrow 1s$ final states of different irreducible representations. RASSCF failed to

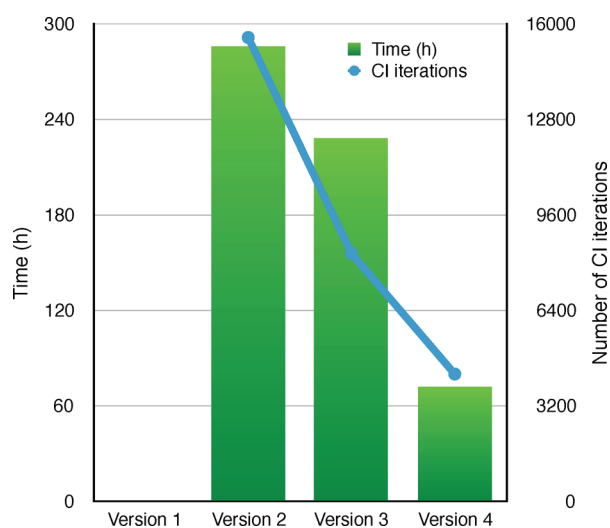


Figure 13. Total RASSCF time and total number of CI iterations for the calculation of X-ray emission spectrum of $[\text{Fe}(\text{bmip})_2]^{2+}$. Version 1 refers to the original algorithm. In Version 2, the number of past iterations for which the correction vectors are saved is reduced. Version 3 contains stability improvements and a cap on the number of stored vectors instead. Additionally, in Version 4, the corrections are not computed for the already converged lower-energy states.

converge in the old MOLCAS/OpenMolcas implementation (Version 1) because of numerical instabilities. The new algorithm does not suffer from such issues, and compared to the Version 2 calculation, the number of CI iterations is reduced by a factor of 3.6, while the saving in computational time is a factor of 4, see Figure 13.²⁶⁹ Skipping the calculation of correction vectors for the converged low-lying states reduces significantly not only the computational time but also the number of iterations. The reason is that as the lowest states converge, more and more of the vectors used as basis for the Davidson diagonalization correspond to the remaining higher states, which can thus converge faster.

5.3. Photoelectron Spectroscopy and Dyson Orbitals.

For the simulation of molecular ionization processes and photoelectron spectroscopy, it is routinely necessary to evaluate integrals between wave functions with N and $N-1$ bound electrons. The information about the molecular system may then be conveniently compressed into a one-electron quantity

$$\phi_{fi}^{\text{DO}}(x_i) = \sqrt{N} \int \Psi_f^{N-1}(x_2, x_3, \dots, x_N) \Psi_i^N(x_1, x_2, \dots, x_N) dx_2 \dots dx_N \quad (17)$$

commonly known as the Dyson orbital (DO). In the second quantization formalism, the Dyson orbital ϕ_{fi}^{DO} may in a given orbital basis ϕ_m be computed as

$$\phi_{fi}^{\text{DO}} = \sum_m c_{fi,m} \phi_m \quad (18)$$

$$c_{fi,m} = \langle \Psi_f^{N-1} | \hat{a}_m \Psi_i^N \rangle \quad (19)$$

where \hat{a}_m annihilates a single electron from orbital ϕ_m .

A new feature now natively available in the RASSI module is the calculation of multiconfigurational Dyson orbitals including spin-orbit (SO) coupling, similarly to what has previously been implemented with an external software.^{272,273} Within the RASSI framework for spin-free (SF) states, eq 19 is efficiently evaluated within a biorthonormal basis²⁷⁴ ϕ_A to obtain $c_{fi,A}^{\text{SF}}$. As the basis ϕ_A may vary for different combinations of f and i , the Dyson orbitals are subsequently re-expressed as $c_{fi,Z}^{\text{SF}}$ in the atomic basis ϕ_Z through standard transformations. Dyson orbitals for spin-orbit coupled states are obtained as superpositions of those computed for the spin-free states

$$c_{fi,Z}^{\text{SO}} = \sum_{k,l} \xi_{f,l}^* \xi_{k,i} c_{kl,Z}^{\text{SF}} \quad (20)$$

where $\xi_{f,l}$ denotes expansion coefficient l of spin-orbit state f in the basis of the spin-free states.¹⁶³ Both types of Dyson orbitals are, optionally, exported in Molden format for further use. The current implementation supports states obtained from RASSCF and RASPT2 calculations, both with and without the explicit use of symmetry.

Applied to photoelectron spectroscopy, the ionization cross section σ_{fi} of the transition $\Psi_i^N \rightarrow \Psi_f^{N-1}$ is within the dipole approximation proportional to the squared photoelectron matrix element $|D_{fi}|^2$. Assuming a simple factorization $\psi_k^{\text{el}} \Psi_f^{N-1}$ for the final state and the strong orthogonality condition,²⁷⁵ it can be written as

$$\sigma_{fi} \propto |D_{fi}|^2 = \langle \psi_k^{\text{el}} \Psi_f^{N-1} | \hat{\mu} | \Psi_i^N \rangle \text{str. orth.} \left| \langle \psi_k^{\text{el}} | \hat{\mu} | \phi_{fi}^{\text{DO}} \rangle \right|^2 \quad (21)$$

where ψ_k^{el} is the continuum wave function of the ejected photoelectron. As ψ_k^{el} is currently not representable within OpenMolcas, eq 21 cannot be directly evaluated. However, assuming the transition dipole integral between ψ_k^{el} and the normalized Dyson orbital to be constant, commonly called the sudden approximation, the ionization cross section σ_{fi} can be approximated by the squared norm of the Dyson orbital:

$$\sigma_{fi} \propto |D_{fi}|^2 = \|\phi_{fi}^{\text{DO}}\|^2 \left| \underbrace{\langle \psi_k^{\text{el}} | \hat{\mu} | \frac{\phi_{fi}^{\text{DO}}}{\|\phi_{fi}^{\text{DO}}\|} \rangle}_{\approx \text{constant}} \right|^2 \approx \|\phi_{fi}^{\text{DO}}\|^2 \quad (22)$$

The approximate cross sections obtained from eq 22 are in the RASSI output referred to as *Dyson amplitudes* and provide a direct estimate of the relative cross sections. Note that the sudden approximation is inadvisable in cases where, e.g., the photoelectron has a low kinetic energy or the Dyson orbitals of the relevant transitions have strongly differing characters. Still, Figure 14(a)–(c) illustrates how accurate photoelectron spectra may be obtained even for complex molecules from

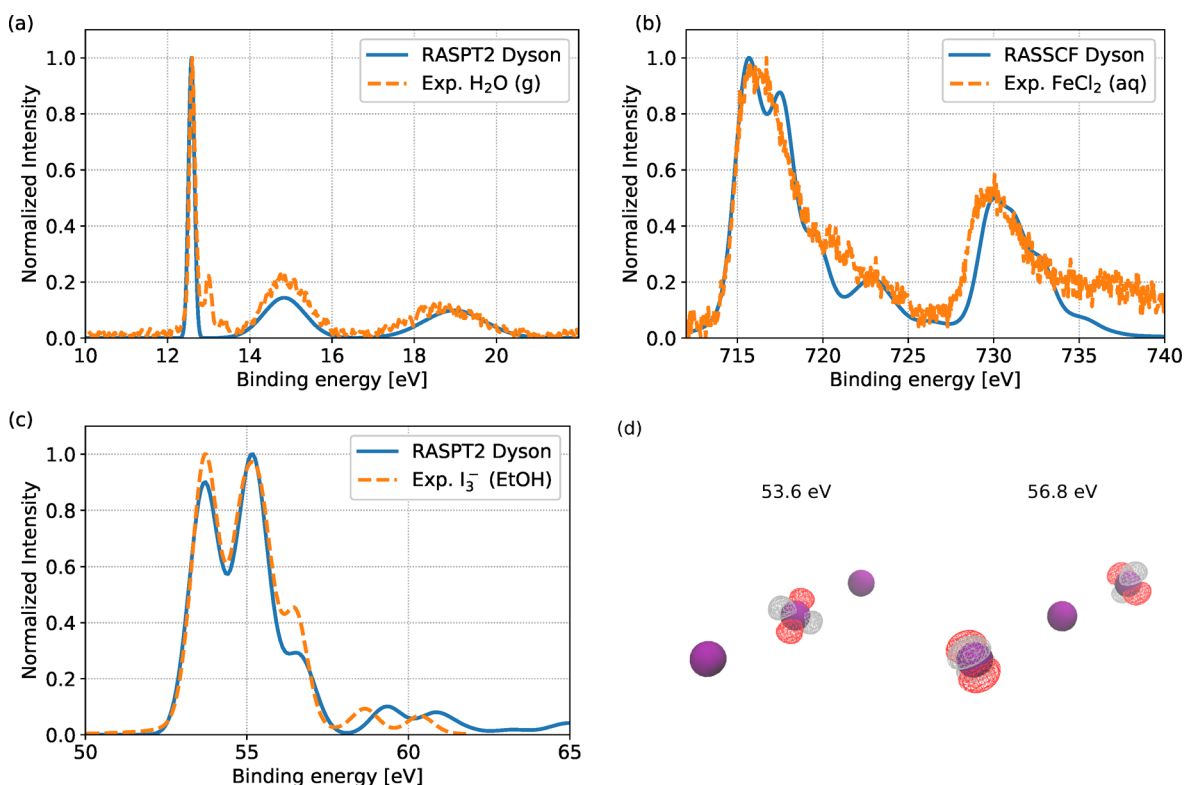


Figure 14. Comparison of photoelectron spectra obtained from Dyson amplitudes as implemented in RASSI and from cited measurements. (a) Valence extreme ultraviolet photoelectron spectrum of H_2O (g).²⁷² (b) Fe 2p X-ray photoelectron spectrum of $[\text{Fe}(\text{H}_2\text{O})_6]^{2+}$.²⁷² (c) I 4d X-ray photoelectron spectrum of I_3^- .²⁷⁹ (d) Dyson orbitals (real part) for selected transitions (53.6 and 56.8 eV) from the I_3^- calculation shown in panel (c), clearly assigning the features to I 4d ionization from the central (53.6 eV) and terminal (56.8 eV) sites.

the RASSI Dyson amplitudes. Figure 14(d) shows in addition how the shape of the Dyson orbitals facilitates spectral assignments. Recent publications have further demonstrated the applicability of the Dyson orbitals for simulation and analysis of photoelectron spectra,^{272,273,276–278} and we expected them to find their use also for simulations of, for instance, Auger-electron and nonresonant X-ray emission spectra.

5.4. Magnetic Circular Dichroism Spectroscopy. Magnetic circular dichroism²⁸⁰ (MCD) spectroscopy probes the differential absorption coefficient $\Delta\epsilon$ for left versus right circular polarized light in the presence of a static magnetic field B pointing in the light wave's propagation direction. It may reveal more information than regular absorption spectra, especially when spectral bands overlap,²⁸¹ because the MCD intensities of different transitions may have different signs. MCD is also able to provide information about the magnetic properties of the electronic states. However, MCD spectra can be complicated to analyze, and the analysis benefits greatly from theoretical support. With commonly applied approximations, the MCD for an electronic transition is given by

$$\frac{\Delta\epsilon}{E} = \gamma B \left[-\mathcal{A} \left(\frac{\partial f(E)}{\partial E} \right) + \left(\mathcal{B} + \frac{1}{k_B T} C \right) f(E) \right] \quad (23)$$

Here, $\gamma = 2\mu_B N_A \pi^3 \log e / (250hc)$ in Gaussian units, and $f(E)$ is a line shape function in terms of the photon energy E . Equation 23 and the expressions for the \mathcal{A} , \mathcal{B} , and C terms were provided by Buckingham and Stephens.^{282,283} We focus here on the C term, which dominates the MCD for a molecule with a degenerate ground state, especially at low temperature.

For a transition from a populated state A with components $|Aa\rangle$ and degeneracy g_A to state J with components $|J\lambda\rangle$, the isotropic C term in eq 23 reads²⁸⁰

$$C = -\frac{i}{3g_A} \sum_{a,a',\lambda} \langle Aa' | \hat{L} + 2\hat{S} | Aa \rangle \cdot \{ \langle Aa | \hat{D} | J\lambda \rangle \times \langle J\lambda | \hat{D} | Aa' \rangle \} \quad (24)$$

Here, \hat{L} and \hat{S} are the dimensionless orbital and spin angular momentum one-electron operators, and \hat{D} is the one-electron electric dipole moment operator. The “nonrelativistic with spin” level of theory used for the operators in eq 24 is commonly applied in calculations of absorption spectra and magnetic susceptibilities of compounds with even the heaviest elements, and therefore it should be adequate for MCD as well. An orbital angular momentum in the ground state is required for a nonvanishing MCD C -term spectrum. Consequently, if the ground state at the nonrelativistic or scalar relativistic (SR) level has only spin degeneracy, the C term is zero. In such a case, MCD C terms may appear via spin–orbit coupling (SOC), if it mixes components of other–orbitally degenerate–spin states into the ground state. Other systems may already have a ground state orbital angular momentum in the nonrelativistic limit.

The functionality of OpenMolcas is very powerful for investigating MCD spectra theoretically.²⁸⁵ Reference 284 reported the first *ab initio* wave function-based MCD calculation for an actinide complex, namely for the octahedral $5f^1$ system $[\text{UCl}_6]^-$, using RASSCF and multistate RASPT2 calculations followed by treating the SOC via state interaction. $[\text{UCl}_6]^-$ is one of the aforementioned cases where the C term spectrum is entirely a relativistic effect, i.e., due to SOC. The calculated and experimental UV–vis range MCD spectra are

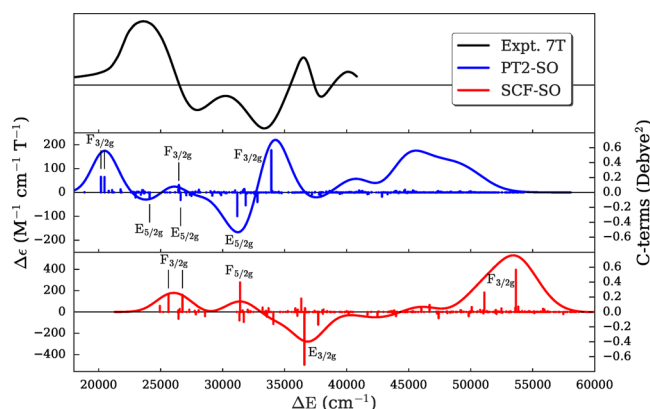


Figure 15. MCD spectrum (5K) of $[\text{UCl}_6]^{3-}$. MCD C term calculations based on RASSCF and RASPT2 calculations of doublet and quartet spin states and treatment of SOC by state interaction with the RASSI module. Calculated $\Delta\epsilon$ generated from Gaussian-broadened vertical C term spectra. Experiment taken at 7T field strength. Reprinted with permission from ref 284. Copyright 2017 PCCP Owner Societies.

compared in Figure 15. The PT2 spectrum, although overcorrecting the blue-shifted SCF spectrum, is in reasonably good agreement with the experimental MCD (also first reported in ref 284). A collection of open-source utility codes and scripts²⁸⁶ was developed for the purpose of generating MCD intensities conveniently for a large number of transitions from SO-RASSI calculations. When the keyword PRPR is present in the RASSI input, the matrix elements for the electric dipole moment, the electron spin, and the orbital angular momentum for the calculated set of SO states are printed to a set of files, which is convenient for postprocessing. The MCD intensities for vertical transitions, and broadened spectra, are then generated with the software tools of ref 286. Code for \mathcal{A} and \mathcal{B} terms²⁸⁷ is also available in the repository.

5.5. Molecular Magnetic Properties. In the field of molecular magnetism, the SINGLE_ANISO module⁸ has allowed the computation of the parameters of all magnetic Hamiltonians and the field- and temperature-dependent thermodynamic properties for mononuclear complexes and fragments. The POLY_ANISO module now allows the computation of the magnetic properties of polynuclear complexes using a semi-*ab initio* approach. The necessity for such an approach is dictated by the current computational difficulties with a full *ab initio* treatment of polynuclear compounds containing several transition metals or lanthanide ions. In the proposed approach, the first step consists of dividing the investigated polynuclear compound in several mononuclear fragments containing one magnetic center only. This fragmentation does not imply that the ligand framework needs to be altered: replacing a neighboring magnetic center with its diamagnetic closely related metal ion suffices. For example, the effect of a neighboring Er^{3+} site could be reasonably well simulated by a diamagnetic Lu^{3+} , containing a completely filled 4f shell. *Ab initio* calculations using the SINGLE_ANISO module are then performed for each of such fragments. The features of POLY_ANISO can be divided into three groups: modeling of magnetic exchange interactions, decomposition of magnetic exchange interactions, and computation of magnetic thermodynamic properties. Both SINGLE_ANISO and POLY_ANISO also have the ability to

generate in an automatic way various plots, via an interface to gnuplot utility.²⁸⁸

5.5.1. Modeling of Exchange. The total magnetic interaction between two metal centers is a sum of the anisotropic exchange interaction and dipole–dipole magnetic interaction. The dipole–dipole magnetic interaction is evaluated exactly by using the total magnetic dipole moment matrix elements calculated on the basis of local multiplets of the corresponding metal sites available from the fragment SINGLE_ANISO calculations.

The easiest simulation of anisotropic exchange interaction is achieved within the Lines model,²⁸⁹ involving one effective exchange (Lines) parameter per interacting pair. This parameter quantifies the hypothetical isotropic exchange interaction between the ground-state spins of the corresponding magnetic ions, which would arise in the absence of spin–orbit coupling. The anisotropic exchange is modeled via the projection of this effective isotropic model over chosen spin–orbit multiplets of individual metal centers obtained in the corresponding fragment SINGLE_ANISO calculations. The Lines model is expected to be accurate in three cases: (i) the two interacting sites have uniaxial (Ising) magnetic anisotropy (reduces to generally noncollinear Ising exchange), (ii) the two interacting sites are completely isotropic (obviously reduces to Heisenberg exchange); and (iii) one site is isotropic while the other possesses Ising magnetic anisotropy (reduces most often to collinear Ising exchange).²⁹⁰ For all other cases of intermediate anisotropy of interacting sites, the Lines model is believed to be a reasonable approximation. The Lines exchange parameters are the only unknown parameters in this approach and are usually found from a least-squares fit of the experimental magnetic data. Alternatively, the Lines exchange parameters can be extracted/estimated from broken-symmetry density functional theory calculations (BS-DFT).^{291,292} To this end, the anisotropic magnetic ions are replaced by the closest isotropic metal ions. Then the extracted BS-DFT exchange parameters J_{12} for a given pair of ions (1,2) in such a hypothetical complex is converted into the corresponding Lines parameter J_{12}^L for the original complex with the formula $J_{12}^L = (S_{i1}/S_{a1})(S_{i2}/S_{a2})J_{12}$, where the terms S_i and S_a stand for the spin of the corresponding isotropic ion and the genealogical spin of the anisotropic metal ion in the original compound, respectively. This approach was validated on several compounds.²⁹³

The POLY_ANISO module contains also several extensions going beyond the simple Lines model: (i) the three-axes exchange Hamiltonian containing three exchange parameters for each interacting pair, corresponding to the diagonal form (i.e., written in the main exchange axes) of symmetric anisotropic exchange Hamiltonian;²⁹⁴ (ii) antisymmetric or Dzyaloshinsky–Morya (DM) exchange interaction, requesting three parameters (the DM vector); (iii) the general anisotropic nine-parameter exchange model including both previous interactions; and (iv) biquadratic terms in the exchange interaction.²⁹⁴ Another extension of the Lines model concerns more involved (many-parameter) effective exchange interactions in the Lines approach instead of a single-parameter one.

The total magnetic interaction matrix is then written straightforwardly for the basis of the products of the on-site eigenstates obtained in the fragment *ab initio* calculations and then diagonalized.²⁹⁵ The obtained eigenstates alongside with the spin and magnetic dipole moment integrals expanded in

the obtained exchange-coupled basis are then further employed for the computation of the parameters of all magnetic Hamiltonians and magnetic properties.

5.5.2. Full Decomposition of Magnetic Exchange Interactions Using Irreducible Tensor Technique. The implemented models of magnetic interaction (e.g., Lines model) describe the exchange interaction between local pseudospins.^{296,297} The Lines parameters are not directly transferable between different compounds (given that their local pseudospins might differ). In order to overcome this problem, the full decomposition of all the interaction models implemented in the POLY_ANISO program has been developed and implemented using the irreducible tensor technique,²⁹⁸ for all interacting pairs. This results in a set of parameters $J(k_1, q_1, k_2, q_2)$, where k_i and q_i represent the rank and projection of the local irreducible tensor operator O_{k_i, q_i} on site i . The interaction Hamiltonian can be recovered exactly by summing up all contributions (eq 25). The parameters are given using the extended Stevens operator basis^{296,299,300} and could be used directly in connection with the EasySpin function in MATLAB.³⁰¹

$$\hat{H}_{\text{exch}}^{1,2} = \sum_{k_1, q_1, k_2, q_2} J_{k_1, q_1, k_2, q_2} O_{k_1, q_1} O_{k_2, q_2} \quad (25)$$

5.5.3. Thermodynamic Magnetic Properties. The POLY_ANISO module is able to compute basic static magnetic properties for polynuclear compounds. For the computation of the molar magnetization, the Zeeman matrix is built on the basis of several low-lying energy states (user-defined size) and diagonalized. The resulting eigenstates are used to compute molar magnetization where Zeeman states are being populated according to the Boltzmann distribution law. Contribution to the magnetization arising from the states which did not enter explicitly into the Zeeman matrix is considered within the second-order perturbation theory. The computation of molar magnetization (and torque) takes into account also the contribution of local excited states which were not accounted for exchange coupling. Molar magnetic susceptibility (tensor and powder) is computed using the zero-field limit of the molar magnetization, where the implemented expressions do not require the Zeeman Hamiltonian to be explicitly computed, enabling significant speedup in computation of these properties compared to the computation of molar magnetization. The magnetic susceptibility is computed in several formulations: (i) the derived formulas for zero-field limit, (ii) using the “experimental” formulation as M/B (inaccurate but employed quite often), and (iii) as derivative of the magnetization with respect to applied field dM/dB (i.e., the rigorous definition). Intermolecular interactions are accounted for in a mean-field approach, using a single parameter (zJ). This parameter is usually quite small in magnitude and influences magnetic susceptibility, torque, and magnetization at very low temperatures. For each temperature point, the main values and main axes of the susceptibility tensor are given.

This methodology has been successfully applied for the investigation of anisotropic magnetism in Dy_3 triangles,³⁰² Co_7 wheels,³⁰³ $\text{Ln}-(\text{N}_2)^{3-}-\text{Ln}$ radical-bridged dlanthanides,³⁰⁴ and many other compounds (see Figure 16). POLY_ANISO and SINGLE_ANISO are actively used also for the investigation of the structure of blocking barriers of single-

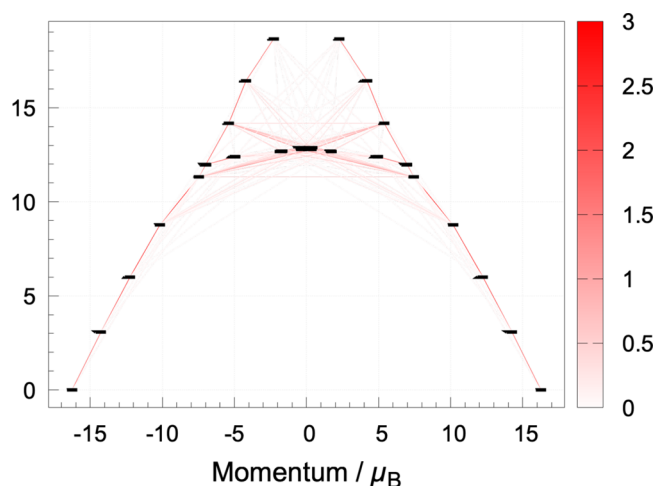


Figure 16. An example of application of the POLY_ANISO module for the *ab initio* construction of magnetization blocking barrier of a Co(II)–Gd(III)–Co(II) trinuclear complex.³⁰⁵ The magnetic relaxation path, outlining the blocking barrier, is traced by the red lines, whose intensity scales the transition magnetic dipole matrix elements between the connected multiplet states.

molecular magnets, molecules which display magnetic bistability of intramolecular origin.

5.6. Ultrahigh Precision Computer Spectroscopy. The accuracy of computer simulations can challenge that of experiments, suggesting that it may be worth computing rather than measuring some properties. This alternative way to achieve accurate reference data is pursued by some scientists using the OpenMolcas platform. In this context we would like to mention the open-ended implementation of the OpenMolcas platform in handling one-particle electronic basis functions with high angular momentum, allowing the evaluation of electron repulsion integrals and their storage in FCIDUMP format, using the same code used for the Stochastic-CASSCF approach, discussed in section 3.1. This feature has been used, for example, in the computational prediction of the carbon atom’s first ionization energy to within 1 cm^{-1} accuracy³⁰⁶ from computer spectroscopy.³⁰⁷ This calculation involved six fully correlated electrons in the neutral carbon atom, with an aug-cc-pCV8Z basis set (569 basis functions, including up to l angular functions). In the language of CAS spaces, this would be a CAS(6,569), which is by far the largest CAS calculation ever done to microhartree precision as far as we are aware.

6. ANALYSIS AND VISUALIZATION

As discussed above, OpenMolcas offers a broad range of quantum-chemical methods to describe large molecules with many correlated electrons and orbitals and to compute many excited electronic states efficiently. Setting up these calculations is a nontrivial task, requiring input from the user, who should have a sufficient understanding of the system under study and the method being applied. The analysis can be challenging if states with different characters mix, if multi-configurational character and double excitations are present, or if a large number of states are to be analyzed.

To help the user prepare and analyze calculations, OpenMolcas contains, or is easily interfaced with, suitable tools. Apart from widespread capabilities, like the computation of Mulliken populations and electric multipole moments,

OpenMolcas includes, for example, the LOPROP program³⁰⁸ for computing local properties and supports the generation of various types of orbitals—canonical, natural or localized with several methods. The generated orbitals, in the form of lists of coefficients, are usually not very informative, and some visualization tool becomes necessary in order to better appreciate the shape and structure of the orbitals. Traditionally this has been done by exporting the orbital and basis-set information in Molden³⁰⁹ format. However, it should be pointed out that there are several different ways to choose the orbitals (e.g., state-averaged and state-specific natural orbitals and natural transition orbitals) and that it is not always clear which orbital representation is optimally suited. Therefore, a number of tools have been developed that allow easily switching between these different representations.

Recent developments in OpenMolcas provide additional tools to visualize and manipulate the orbitals (section 6.1), as well as to analyze their properties (section 6.2), and more options for the analysis of wave functions and transitions, including tools that allow for a completely automatized analysis of the wave function character and provide a rigorous route to comparing the wave functions produced by different methods (sections 6.3 and 6.4). In this section we describe the most significant of these new capabilities.

6.1. Graphical Interface and Orbital Visualization.

OpenMolcas, as other high performance computing programs, requires numeric data as input and can produce a vast quantity of data as output. Raw numeric data (atomic coordinates, orbital coefficients, electron populations, bond orders, etc.) are often very difficult to comprehend. As a typical example, an essential step in CASSCF and related calculations is selecting the active space, a task for which an orbital viewer is of great help. With MOLCAS, the tools of choice have been either third-party programs capable of computing and rendering isosurfaces “on the fly”, from the basis set and orbital coefficients information (in Molden format), or more specific programs which rely on the precalculation of the volumetric data and use custom formats.

First, in order to make these tasks easier, a program with GUI: LUSCUS has been developed³¹⁰ as a stand-alone program (distributed under the Academic Free License (AFL) version 3.0³¹¹) convenient for manipulation and visualization. Although some data produced by quantum chemistry programs can be stored in standardized or well-

established formats, for complex data the formats are often unique, and thus GUIs are strongly bound to the computational code. LUSCUS uses a native data format (see Figure 17) to read or write visualizable data, which is supported by OpenMolcas. Other chemical formats can be used with LUSCUS since they are automatically converted to and from LUSCUS data format by external plug-ins. Plug-ins convert data on demand without the need of user intervention. Therefore, from the user’s point of view, LUSCUS is capable of manipulating a number of chemical formats, making it not only a graphical front-end for OpenMolcas but also a powerful general-purpose chemical viewer and editor.

Complementarily, a new stand-alone program has been developed to generate precomputed volumetric data: SAGIT (stand-alone grid independent transformer).³¹² This code is operated via command line and can be useful to generate volumetric data for many orbitals simultaneously or in batch mode, where a GUI is not needed; it can also be used as a plug-in for LUSCUS to visualize orbitals on the fly.

With the release of OpenMolcas, a new orbital viewer has been developed which tries to suit the most typical needs of OpenMolcas users. Pegamoid³¹³ is written in Python and is easily installable in modern computer systems. It can open orbital or volumetric files in a variety of formats generated by OpenMolcas. Most significantly, it can open, display, and save orbital files in the new HDF5 format generated by OpenMolcas, which has several advantages compared to other formats: (i) as outlined in section 2, it is a portable self-documented format that allows easy transfer and access of data, (ii) it is directly usable by OpenMolcas programs, e.g., as starting orbitals for the RASSCF program, and (iii) it is not affected by limitations in the Molden format, like the maximum angular momentum in basis functions or the mixture of Cartesian and spherical harmonic type of functions. With respect to formats with volumetric data, the main advantage is that its size is not excessive even with large basis sets and that the desired quantities to be visualized need not be precomputed.

Apart from simply viewing the orbitals saved in a particular file, Pegamoid (as well as LUSCUS) can also assign them to different orbital spaces (frozen, inactive, RAS1, RAS2, RAS3, secondary, deleted) and save them in a new file that can be used as input for OpenMolcas programs. When the orbital file contains the necessary information (e.g., an HDF5 file generated by a state-average RASSCF run), it is also possible to visualize, without further postprocessing, natural orbitals and occupations for the different electronic states, electron density differences, natural difference orbitals, and natural transition (or binatural) orbitals between the states³¹⁴ (see Figure 18).

Pegamoid’s goal is to be a quick and convenient tool for viewing orbitals, selecting active spaces and identifying states. While it has options to control the display quality and features, the generation of high-quality eye-catching pictures often requires the use of other packages that offer a wider range of options. For this purpose, Pegamoid can be used to save the desired volumetric data in the Gaussian .cube format,²¹ which can then be used by other programs to render pictures with customized colors, textures, backgrounds, and additional elements.

6.2. Property Integrals of Individual Orbitals. OpenMolcas supports the computation of property integrals of molecular orbitals in the SEWARD module, including the

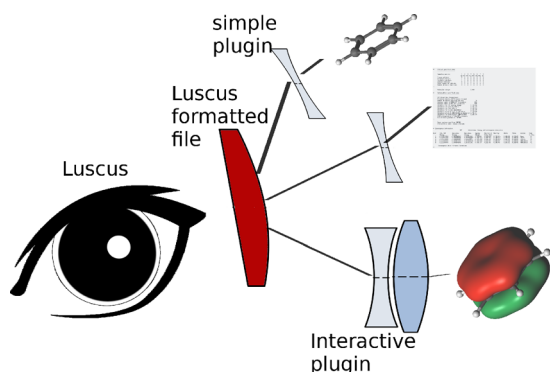


Figure 17. Interaction of LUSCUS and various data files: LUSCUS can only operate with .lus files (the native LUSCUS format) and separate plug-ins (both simple and interactive) are used to convert the data.

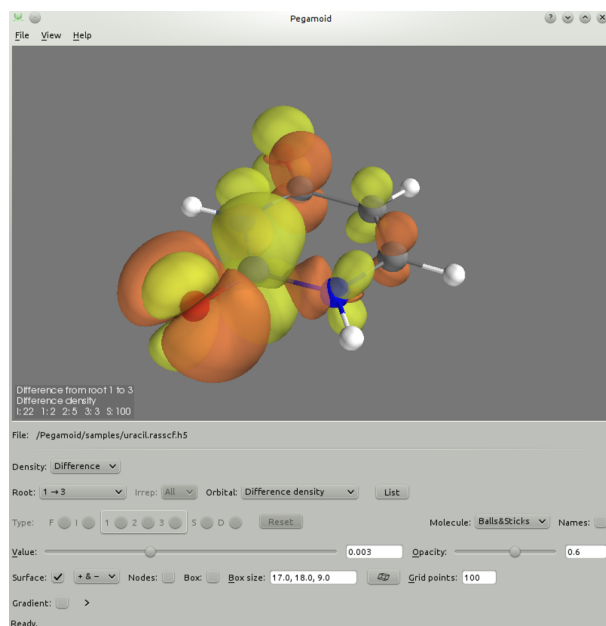


Figure 18. Pegamoid interface, showing the difference density between two electronic states of uracil (an $n \rightarrow \pi^*$ transition).

multipole moments, Cartesian moments, electric potential, electric field, electric field gradients, diamagnetic shielding, one-electron Darwin contact term, etc. It supports any orbitals calculated in SCF, RASSCF, CASPT2, or other modules. With natural orbitals, the sum of the occupation-number-weighted orbital property integral is the total electronic part of a property integral, so the occupation-number-weighted orbital property represents how much each orbital contributes to a property integral of an electronic state. For analysis purposes, one has the option of printing, for each molecular orbital, these property integrals weighted by the occupation number of each orbital or printing these property integrals for each orbital without the weighting. In case one is interested in the property integral for an unoccupied orbital, the nonweighted option is required, as otherwise any property integral would trivially be zero. This can be useful when analyzing Rydberg states to determine which orbitals are Rydberg orbitals. It can also be helpful when deciding which orbitals to include in the active space of an MCSCF calculation and when determining whether the excited states from different MCSCF calculations correspond to the same state.³¹⁵ For these examples, to determine how diffuse each orbital is, the second Cartesian moment $\langle r^2 \rangle$ and its components ($\langle x^2 \rangle$, $\langle y^2 \rangle$, $\langle z^2 \rangle$, $\langle xy \rangle$, $\langle yz \rangle$, $\langle xz \rangle$) of each orbital can be calculated. An example input file making use of this capability can be found in the [Supporting Information](#).

6.3. Binatural or Natural Transition Orbitals for Excitation Characterization. There is a frequent need to quantify the difference between two states and to visualize the difference for easily understood characterization. Assuming we have at hand correlated electronic wave functions, the usual difference density is often insufficient. However, recalling that the usual natural orbitals are the eigenfunctions of the one-electron reduced density matrix of a single state, a simple extension is to use the singular value decomposition (SVD) of the transition density matrix of two states to characterize their difference. This approach was used for single-determinant wave functions³¹⁶ and for TDDFT and CIS wave functions,³¹⁷

where the orbitals were named natural transition orbitals, and independently by Mayer.³¹⁸ An SVD has also been used to relate orbitals of fragments of a composite molecule.³¹⁹ Prior usage seems to have been proposed mostly for specific applications, but in ref 320 it was suggested to use orbitals computed as singular vectors of the one-electron transition density matrix as a technical tool to analyze the difference of pairs of general states, regardless of whether these were single-determinant states or indeed if they were actually computed to be eigenstates of any Hamiltonian. For general discussion of the SVD itself, see, e.g., the articles by Stewart.^{321,322}

The binatural orbitals, or natural transition orbitals, are obtained as the left and right singular functions of the reduced one-electron transition density matrix, γ^{PQ} . The binatural orbitals and their associated amplitudes encode in a compact way the whole γ^{PQ} and can be used to analyze the transition between two electronic states.

The states would usually be either two noninteracting, computed states, or they can be two different approximations. They could also be, e.g., states computed with and without some perturbation or indeed any two states that allowed us to compute the transition density matrix in a suitable basis—maybe but not necessarily obtained as an orbital basis that was used for the two states. The transition density matrices and the binatural orbitals are computed by the RASSI program within OpenMolcas.

There is one limitation: what is obtained is the difference of the states as expressed by a one-electron operator. One can easily extend this to form two-particle “binatural geminals”. Also, one might have use for “Dyson amplitudes”, as seen in [section 5.3](#), or “one-particle-two-holes” amplitudes, e.g., for core-hole states.

6.4. Detailed Analysis of Multireference Wave Functions. The wave function analysis module WFA³²³ does not only provide visualization methods but also computes a number of quantitative descriptors with the aim of eliminating personal bias in the assignment of state characters and allowing for an automated analysis of large data sets. WFA is based on the open-source wave function analysis package libwfa.^{314,324} One focus of libwfa is the analysis of excited states in terms of two-body electron–hole distributions within exciton theory.³²⁵ To visualize the excitations in real space, binatural or natural transition orbitals^{317,326} and the more compact electron and hole densities³¹⁴ are available. Electron–hole correlation effects can be elucidated using population analysis techniques.^{326,327} Central tools of libwfa are excited-state descriptors quantifying spatial and statistical properties of excited states such as exciton size,³²⁵ charge-transfer distance, and correlation coefficient.³²⁴ Furthermore, it supports the analysis of one-electron difference density matrices (1DDM) between different states, which is particularly important to study orbital relaxation effects.^{323,328,329} Finally, an effective number of unpaired electrons^{330,331} can be computed from natural orbital occupations. The WFA module is interfaced to the SCF, RASSCF, and RASSI modules of OpenMolcas. Through the RASSI interface, also other modules can be accessed such as the CASPT2 module and QCMAQUIS (DMRG and DMRG-NEVPT2, see [section 3.2](#)).

Previously, the described analysis methods were used to analyze single-reference computations addressing a wide range of phenomena, such as the analysis of electronic delocalization in DNA,³³² excitonic band structure in conjugated polymers,³²⁷ and the visualization of solvent effects in push–pull

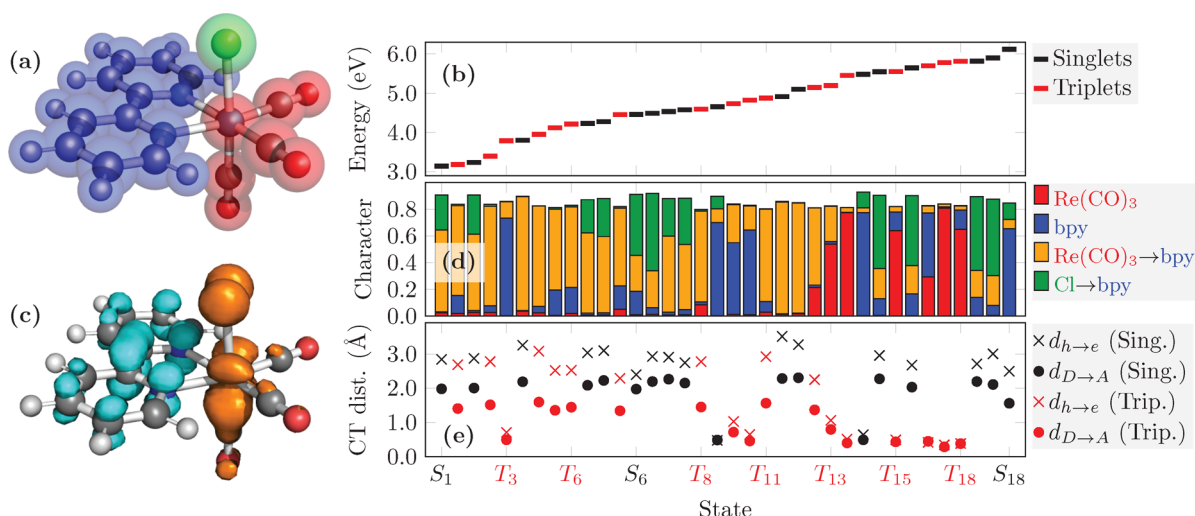


Figure 19. Analysis of the singlet and triplet excited-states of the $\text{Re}(\text{CO})_3(\text{bpy})\text{Cl}$ complex computed at the MS-CASPT2 level using the WFA module: (a) molecular structure and definition of the $\text{Re}(\text{CO})_3$ (red), bpy (blue), and Cl (green) fragments; (b) excitation energies; (c) electron (cyan) and hole (orange) densities of the S_1 state; (d) decomposition into different local and charge transfer contributions; (e) charge transfer distance using two different descriptors.

systems.³³³ We hope that through the new interface between OpenMolcas and libwfa, enabling the use of multireference methods, this scope can be significantly extended. Furthermore, the implemented analysis methods provide a rigorous route toward benchmarking excited-state calculations^{334,335} and can give new insight into specific failures of the different computational protocols employed.^{329,336}

Presenting a practical application of the WFA module, the excited states of the transition metal complex $\text{Re}(\text{CO})_3(\text{bpy})\text{Cl}$ are analyzed (Figure 19). Computations were performed at the MS-CASPT2 level using a CAS(12,12) active space considering 19 singlet and 18 triplet states. The excitation energies of these states are presented in Figure 19(b), illustrating the high density of low-lying states in this system. A direct analysis of these states in terms of canonical orbitals is not only tedious but is also quite challenging as the effects of different interacting configurations have to be disentangled. Therefore, we present here three alternative routes of analyzing these states, as implemented in the WFA module: a visual analysis of electron and hole densities, a fragment-based decomposition of the excitations, and an analysis in terms of statistical descriptors.

As a first option, the densities of the excited electron and the excitation hole, derived from the one-electron transition density matrix (1TDM),³¹⁴ are computed. These densities, computed for the S_1 state of the complex, are shown in Figure 19(c). This representation shows the main state character in an intuitive way, i.e., the hole (orange) is located on the Re and Cl atoms whereas the electron (cyan) is located on the bipyridyl (bpy) ligand. However, the problem of any visual analysis is the required time and the dependence of the outcome on the subjective reasoning of the person analyzing.

To overcome these problems of visual analysis, a completely automatized way to assign the state-character in transition metal complexes has been developed,^{329,335} and it is presented as a second option here. First, the system needs to be divided into different fragments; in the present case a useful partition is the $\text{Re}(\text{CO})_3$ unit (red), the chlorine atom (green), and the bpy ligand (blue), as represented in Figure 19(a). Subsequently, the excitation process is partitioned into different

local contributions on the individual fragments and charge transfer (CT) between them using a 1TDM population analysis procedure yielding the so-called charge-transfer numbers.^{314,326} The outcome of this analysis is presented in Figure 19(d). The left-most bar graph corresponding to the S_1 state shows that this state is predominantly of $\text{Re}(\text{CO})_3 \rightarrow \text{bpy}$ CT character (yellow bar, 61%) with a secondary contribution of $\text{Cl} \rightarrow \text{bpy}$ character (green bar, 26%). More generally, Figure 19(d) shows the low-energy states to be generally of $\text{Re}(\text{CO})_3 \rightarrow \text{bpy}$ character with the exception of T_3 , which is a locally excited state on bpy (blue bar).

A downside of the CT number analysis is that its application requires an *a priori* definition of the fragments used for the decomposition. When intuition is untrustworthy, it is possible to automatize the fragment definition process.³³⁵ Alternatively, we can move away from the population-analysis concept altogether leading to the third option, exemplified here through the computation of a CT distance in real space. Two different formulas are employed considering either (i) the distance $d_{h \rightarrow e}$ between the barycenters of hole and electron densities as computed from the 1TDM or (ii) the distance $d_{D \rightarrow A}$ between the barycenters of the detachment and attachment densities³³⁷ as computed from the 1DDM.³²⁴ The results are shown in Figure 19(e), and without going into too much detail, we want to mention two observations. First, the CT distance mirrors CT character as identified in Figure 19(d), i.e., the CT distances of the local states (red and blue bars) are close to zero while they are significantly enhanced for the CT states. Second, CT distances obtained from the 1TDM and 1DDM differ significantly where the latter are always lower. This difference can be interpreted to originate from orbital relaxation effects,^{323,328,329} i.e., the total amount of charge separation is lowered as the orbitals adjust to the primary excitation process.

7. ADDITIONAL FEATURES

In this final section on new options and utilities in OpenMolcas, we present developments for a new multiscale option, accurate and compact basis sets, symmetrization of wave functions, and simulations of muonic molecular systems.

7.1. Multiscale Simulations by Frozen-Density Embedding Theory. The toolbox of electron correlation methods present in OpenMolcas would not be complete without the possibility to combine them in a multiscale fashion. Among the different possibilities for multiscale modeling in OpenMolcas, the one based on frozen-density embedding theory (FDET)^{338–340} provides a robust tool to treat systems and problems of different nature. This multiscale approach is a first-principles description of a complex system as combination of two interacting subsystems. One portion of the system, subsystem *A*, is selected to be described at the molecular orbital level—e.g., through a Kohn–Sham determinant,³³⁸ or an interacting wave function³³⁹—whereas the second (subsystem *B*, so-called “environment”) is accessed through a simpler descriptor, namely its electron density. The interaction between the electrons of *A* with subsystem *B* is nonetheless accounted quantum mechanically through the action of the following (orbital-free) embedding potential:

$$v_{\text{emb}}[\rho_A, \rho_B, v_B^{\text{nuc}}](\mathbf{r}) = v_B^{\text{nuc}}(\mathbf{r}) + \int \frac{\rho_B(\mathbf{r}')}{|\mathbf{r}' - \mathbf{r}|} d\mathbf{r}' + \frac{\delta T_s^{\text{nad}}[\rho_A, \rho_B]}{\delta \rho_A(\mathbf{r})} + \frac{\delta E_{\text{xc}}^{\text{nad}}[\rho_A, \rho_B]}{\delta \rho_A(\mathbf{r})} + \frac{\delta \Delta F[\rho_A]}{\delta \rho_A(\mathbf{r})} \quad (26)$$

The first two terms in eq 26 represent electrostatic contributions due to the nuclei of system *B* and to its electron density $\rho_B(\mathbf{r})$, respectively. The next two terms are instead purely quantum mechanical and originate from the nonadditive contribution to the noninteracting kinetic energy functional $T_s[\rho]$ and the exchange–correlation functional $E_{\text{xc}}[\rho]$, respectively. By nonadditive contribution of a generic density functional $G[\rho]$, we refer to a bifunctional of the electron densities of *A* and *B*, namely to $G^{\text{nad}}[\rho_A, \rho_B] = G[\rho_A + \rho_B] - G[\rho_A] - G[\rho_B]$. Finally, the last term in eq 26 is not related to the interaction between the two subsystems, but it rather ensures consistency with the Hohenberg–Kohn theorem upon introduction of approximations in the description of subsystem *A*. This term is however neglected in most practical applications of the theory.³³⁹

The one-electron operator corresponding to the potential of eq 26 can then be added to the environment-free Hamiltonian (H_A) of the quantum mechanical method of choice for subsystem *A* in order to proceed with the electronic structure calculation. Naturally, this way to proceed simplifies the computational effort compared to the corresponding quantum mechanical calculation on the entire (*A* + *B*) system. One limitation of the current OpenMolcas implementation is the need to use explicitly basis functions on *B* as well as *A*. For true multiscale simulations, where for example $\rho_B(\mathbf{r})$ is obtained from statistical averages,³⁴¹ the use of a real-space representation is certainly desirable and will be implemented in a future release of the software. Nonetheless, it should be pointed out that the overhead for the presence of basis functions on *B* is somewhat handled intelligently so that correlation methods need not to include orbitals from subsystem *B* explicitly (see section S15).

If the exact functional forms for $T_s^{\text{nad}}[\rho_A, \rho_B]$, for $E_{\text{xc}}^{\text{nad}}[\rho_A, \rho_B]$, and for $\Delta F[\rho_A]$ were known, eq 26 would produce an exact quantum mechanical model for the interacting subsystems, but in practice various approximations to these functionals are available that guarantee a sufficient accuracy. Some of such approximate functionals are included in the current Open-

Molcas implementation of FDET^{342–345} as detailed in the software documentation. Noticeably, the construction of the embedding potential through eq 26 requires the user to make another important choice, namely that of which $\rho_B(\mathbf{r})$ is to be used. This is a key issue for the correct use of FDET, and despite the lack of a general answer to the question, the many studies present in the literature show the general trend that the results do not depend strongly on the choice of $\rho_B(\mathbf{r})$.³⁴⁶ In practice, with any physically justified $\rho_B(\mathbf{r})$, deviations in the predicted observables are smaller than the errors introduced by other sources, such as the basis set used, the choice of the approximants for $T_s^{\text{nad}}[\rho_A, \rho_B]$ and $E_{\text{xc}}^{\text{nad}}[\rho_A, \rho_B]$, or the quantum mechanical method selected to describe subsystem *A*.

As OpenMolcas is specialized in multiconfigurational wave function methods,⁷ the combination with FDET represents a somewhat unique tool for investigating complex systems especially in their excited states and for notorious *DFT-hard* situations. With this in mind, an effort has been put into the development of a variant of FDET, known as linearized FDET,³⁴³ that shows some advantages compared to the conventional FDET approach, as it inherits useful properties of the corresponding wave function method. Linearization consists of approximating the nonadditive functionals so that they become linear in $\rho_A(\mathbf{r})$, by means of a Taylor expansion around a reference density $\rho_A^{\text{ref}}(\mathbf{r})$, which can be assumed not to differ significantly from the stationary density of the embedded subsystem. Among the many advantages of linearized FDET, we point out the fact that the eigenstates of the embedded Hamiltonian are orthogonal, hence they can be directly related to the true ground and excited states of the embedded subsystem. Also, differences in the computed eigenenergies of the embedded Hamiltonian can be used to assign excitation energies in much the same way as it is done for the calculation on the isolated system *A*.

7.2. Development of New ANO Basis Sets. Basis sets based on the atomic natural orbitals (ANO) approach³⁴⁷ are the workhorse of the MOLCAS/OpenMolcas program packages. The ANO contraction scheme offers a fast convergence toward the uncontracted form of the basis set. Thus, ANO basis sets even in small contracted forms—say valence double- ζ plus polarization functions (VDZP)—usually are able to yield accurate results, which makes them the perfect choice for calculations where the bottleneck lies in the correlation part. With the focus on fast convergence by contraction and application in accurate correlated calculations, ANO basis sets were allowed to contain a larger number of primitive basis functions than other comparable basis sets.^{348,349}

Accompanying the nonrelativistic ANO-L basis set,³⁵⁰ the more compact ANO-S basis set³⁵¹ had been available, thus allowing more economic treatment of large molecular systems where the integral computation time can rival the correlation part. For relativistic calculations, however, so far only the relativistic core-correlated ANO-RCC basis set³⁵² had been developed for the second-order Douglas–Kroll–Hess (DKH2) Hamiltonian. The large size of this basis set in terms of primitive basis functions made integral calculations for extended systems rather costly. To make also relativistic calculations for large systems more economic, a new compact relativistic basis set, the ANO-XS basis set,³⁵³ has recently been developed. The number of primitive basis functions in the ANO-XS basis set is about half that of the ANO-RCC basis set. This greatly reduces the computational costs in the integral

ANO Basis Sets On an MOF Template

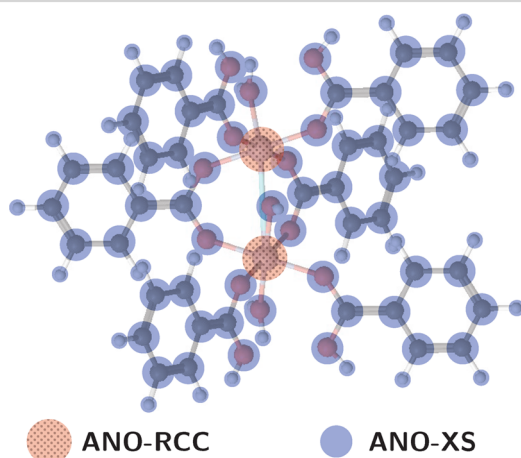


Figure 20. Basis set combination of ANO-RCC and ANO-XS for the calculation of an MOF template.

computation time, especially when used in combination with Cholesky decomposition.

The ANO-XS basis set is available for light atoms ($Z \leq 20$). Its main intent is to be used in combination with the larger ANO-RCC basis set in relativistic calculations containing heavy atoms such as the chromium complex shown in Figure 20, constituting a part of a metal–organic framework (MOF). When using the ANO-RCC basis set with VDZP contraction for all atoms, the total number of primitive basis functions is 4573. Replacing the basis set for all atoms except chromium with the ANO-XS basis set reduces the number to 2014.

7.3. Symmetrization of Wave Functions. At the early stage of quantum chemistry, the symmetry of molecules played an important role as an efficient way to reduce the size of the computational problems. Today this aspect is not as important, since the absolute majority of computed systems has no symmetry elements except of identity.

Many computational codes, including OpenMolcas, use only Abelian point groups (D_{2h} and subgroups) for calculations. In

this case the result of any symmetry operation on a matrix element is a multiplication by 1 or -1 .

If a molecule has a symmetry higher than D_{2h} , the computational code will use a lower symmetry, and as a result, the computed density or wave function can present a broken symmetry. In some cases, this deviation from symmetrical solution will be small, but in other cases this error will be significant.

Rewriting the computational codes for the purpose of handling an arbitrary point group is a rather complicated programming task. Instead, there is a more simple approach, which involves symmetrization of the computed wave function according to any specified symmetry, e.g., the symmetry of the molecular structure. The procedure of symmetrization of the wave function can be applied at the end of the calculation or during the iterative procedure of computing the wave function (e.g., in a self-consistent cycle). The details of the algorithm of symmetrization are described in ref 354. Prior to an SCF calculation the point group is determined. The orbital spaces for each irreducible representation (irrep) are then calculated for the supplied basis. At each iteration the symmetric orbitals are projected out and partner functions determined. Coefficients are then averaged over the partner functions. Since the dimension of each irrep space is known, the symmetrization step will also verify that the projected subspaces belong to the correct symmetry species. This is required since no restriction is placed on the rotations during the iterations, and large symmetry breaking may occur.

A mathematical library (libMSYM) has been designed for two independent tasks: automatic detection of the point group and symmetrization of the computed wave function according to a given symmetry.³⁵⁵ Version 2.0 of the library can be integrated into the OpenMolcas code and can produce SCF calculations with wave function symmetrized at any SCF cycle. The usage of libMSYM is especially important if approximate integrals are used in the calculations. Two examples below demonstrate the abilities of the library.

As a first example, in tetrafluoromethane (CF_4), belonging to the T_d point group, the HOMO orbitals belong to the T_1 irrep. After removing three electrons from the molecule and

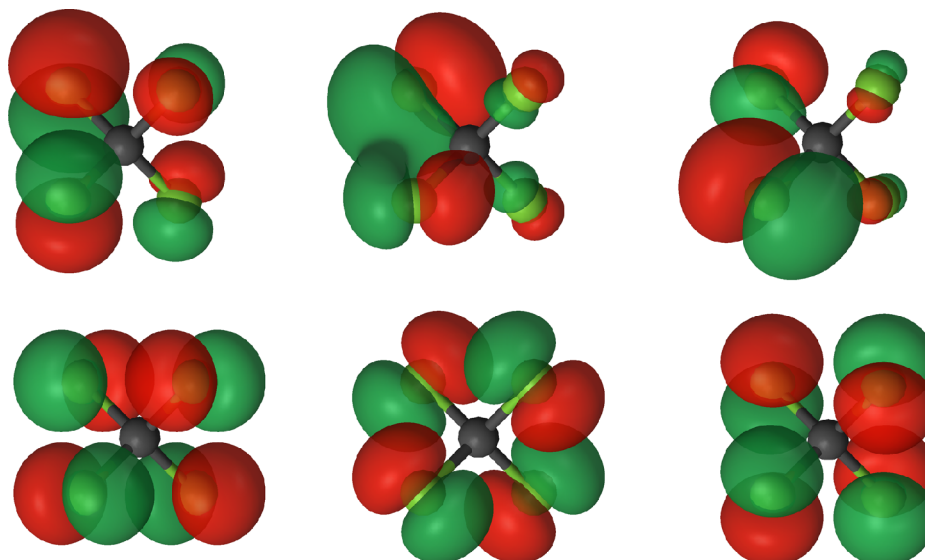


Figure 21. Orbitals for CF_4 (point group T_d) before (upper row) and after (lower row) symmetrization.

running a UHF/DFT calculation the symmetry will break even though T_1 is 3-dimensional. By applying symmetry restrictions in the SCF calculation the charges will be evenly distributed between 3 orbitals of T_1 symmetry as can be seen in Figure 21.

The second example is a symmetry-broken solution. The structure of the $(\text{NO}_2)_2$ dimer is totally symmetric and belongs to the D_{2h} point group. However, if we add a positive charge, the wave function (at the UHF level) becomes unstable and the electron is localized at one of the monomers. By enforcing the symmetry with the libMSYM library, we obtain a fully symmetric solution. The total dipole moment is of the order of 10^{-13} D.

7.4. Calculations of Muonic Atoms and Molecules.

The overwhelming majority of chemical studies, experimental and computational, are concerned with “normal” matter, constituted of electrons, protons, and neutrons. However, a large number of other elementary and composite particles are known which could, in principle, replace the ordinary Fermions, although their lifetimes are usually so short that the practical significance is doubtful. An outstanding case is that of the muon, whose lifetime of 2.2 μs has allowed its detection combined with normal matter. The muon is a lepton, with similar properties to the electron, but with a mass about 200 times larger. Muons can replace electrons in normal molecules, and due to their heavier mass, their density is concentrated much closer to the nuclei. The radiation emitted as a muon falls down to lower energy levels can give information about the nuclear charge distribution and, to some extent, about the electronic structure. Recent developments in muonic X-ray spectroscopy for nondestructive elemental analysis^{356–358} have spurred the interest of theoreticians to predict the properties of muonic atoms and molecules.

Calculations of systems including muons and electrons are now possible with OpenMolcas.³⁵⁹ There are a few issues to take care of. One-particle and exchange integrals are always vanishing between electrons and muons, since they are distinguishable, but Coulomb integrals are always nonzero, regardless of which particles they refer to. Due to the heavy mass of the muons, the Born–Oppenheimer approximation becomes less valid, especially for the lighter nuclei, which cannot be assumed infinitely heavier than the muons. To account for this, OpenMolcas allows including the so-called finite nuclear mass correction (FNMC)³⁶⁰ term to the kinetic energy. In addition, since the muonic density is much more concentrated close to the nucleus, the muonic energy levels are much more sensitive to the nuclear size and charge distribution, and a pointlike nuclear model is expected to be inaccurate. In OpenMolcas finite nuclear size effects can be included through a Gaussian charge distribution. Finally, the description of muons requires the use of specialized basis sets, with exponents much larger than those typically used for electronic basis functions. Such a basis set has been recently developed for elements from H to Ar and Cu.³⁵⁹ Initial calculations for atoms and molecules where one electron was replaced with one muon showed satisfactory agreement with experimentally available data, suggested a mislabeling of one of the peaks for Cu and allowed the estimation of the sensitivity of muonic X-ray energies to chemical environment.

8. SUMMARY

OpenMolcas—an open-source community development platform—is based on the source code of the MOLCAS package.

The program suite is now also a fully operational user’s alternative. This move has been done under the leadership of the (Open)Molcas developers to promote the use and the development of the multiconfigurational wave function paradigm. The report includes technical details of the development platform and also a large number of novel implementations. For the first part it was described how the OpenMolcas code is developed and managed. This arrangement will allow easier contributions from new developers and a more direct interaction with other software, as already exemplified by some of the interfaces reported in this work. For the second part it is reported an array of new options in OpenMolcas, which include new techniques in wave function models, tools for molecular dynamics and potential energy surface exploration, methods for computing spectroscopic and magnetic properties, utilities for graphical representation of results, and other additional new features. These items are summarized below.

The range of applicability of the CASSCF procedure has been extended by a number of new implementations and interfaces. The report describes in some detail the Stochastic-CASSCF approach, two DMRG options—the OpenMolcas–CheMPS2 and the OpenMolcas–QCMAQUIS interfaces—and new features available for the MC-PDFT method. Furthermore, new tools for exploration of the electronic PES and various types of MD have been implemented. More specifically, we report on availability of analytical nonadiabatic coupling vectors and associated optimization and characterization of conical intersections, on new options for the DYNAMIX module, and on two interfaces for molecular dynamics—SHARC for semiclassical dynamics and Quantics for on-the-fly quantum dynamics. A number of options and features have been implemented to improve the capacity of OpenMolcas to address issues associated with different types of spectroscopy. These options include the use of the exact semiclassical operator for the light–matter interaction, the treatment of core-holes, the generation of Dyson orbitals, the simulations of MCD spectra, the POLY_ANISO module for the simulation of magnetic properties of polynuclear complexes, and the use of OpenMolcas in association with ultra-accurate simulations. The OpenMolcas package has additionally been supplemented with a list of new tools for postcalculation analysis. These include LUSCUS—a general purpose GUI, a stand-alone grid generator SAGIT, the orbital visualizer Pegamoid, the generation of natural transition orbitals in the RASSI module, and the WFA module to analyze excited-state simulations. Finally, some additional features were described, such as the ANO-XS basis set, a multiscale option using frozen-density embedding techniques, implementation of higher point groups through the libMSYM library, and options to handle both the negatively charged muons and electrons at the same time.

To conclude, we have reported on the new development and application environment of the open-source quantum chemical electron structure and molecular dynamics simulation package OpenMolcas. This report described a robust software development environment. This and the documentation of a large array of new developments should stimulate more developers to join the OpenMolcas community, in particular those interested in multiconfigurational electron structure theory and various types of molecular dynamics and spectroscopies. Moreover, to the reader, and potential user, we hope that the case has been made that OpenMolcas—a free-of-charge tool—

can provide a strong and dynamic platform for state-of-the-art simulations. The user can virtually get access to new options and features as soon as the developer deems them stable for use in production calculations. Looking toward the future and new development one would in particular look forward to a robust implementation of a QM/MM interface, a better platform infrastructure to facilitate efficient massively parallel simulations, integral-direct RI techniques, and the use of new technologies, such as machine learning, to accelerate current procedures but also open for new ways in which *ab initio* data are used.

■ ASSOCIATED CONTENT

📄 Supporting Information

The Supporting Information is available free of charge on the ACS Publications website at DOI: [10.1021/acs.jctc.9b00532](https://doi.org/10.1021/acs.jctc.9b00532).

Example inputs for Stochastic-CASSCF, DMRG-CASPT2, DMRG-SCF, MPSSI, DMRG-NEVPT2, MC-PDFT, conical intersections, SHARC interface, light–matter interaction, Dyson orbitals, orbital properties, binatural orbitals, WFA, and FDET; computational details for DMRG-MRPT2 examples discussed in text; and discussion on convergence and performance for Fe(II)-porphyrin calculation with OpenMolcas–CheMPS2 (PDF)

Input files (ZIP)

■ AUTHOR INFORMATION

Corresponding Author

*E-mail: roland.lindh@kemi.uu.se.

ORCID

Ignacio Fdez. Galván: 0000-0002-0684-7689

Morgane Vacher: 0000-0001-9418-6579

Jochen Autschbach: 0000-0001-9392-877X

Jie J. Bao: 0000-0003-0197-3405

Sergey I. Bokarev: 0000-0003-0779-5013

Rebecca K. Carlson: 0000-0002-1710-5816

Sijia S. Dong: 0000-0001-8182-6522

Andreas Dreuw: 0000-0002-5862-5113

Luis Manuel Frutos: 0000-0003-1036-7108

Laura Gagliardi: 0000-0001-5227-1396

Angelo Giussani: 0000-0002-9452-7641

Leticia González: 0000-0001-5112-794X

Stefan Knecht: 0000-0001-9818-2372

Giovanni Li Manni: 0000-0002-3666-3880

Marcus Lundberg: 0000-0002-1312-1202

Philipp Marquetand: 0000-0002-8711-1533

Stefanie A. Mewes: 0000-0002-6538-9876

Jesper Norell: 0000-0003-1058-2588

Massimo Olivucci: 0000-0002-8247-209X

Markus Oppel: 0000-0001-6363-2310

Felix Plasser: 0000-0003-0751-148X

Markus Reiher: 0000-0002-9508-1565

Andrew M. Sand: 0000-0002-7166-2066

Igor Schapiro: 0000-0001-8536-6869

Prachi Sharma: 0000-0002-1819-542X

Donald G. Truhlar: 0000-0002-7742-7294

Liviu Ungur: 0000-0001-5015-4225

Alessio Valentini: 0000-0002-0882-9417

Tomasz A. Wesolowski: 0000-0001-5792-4616

Alexander Zech: 0000-0002-4332-8546

J. Patrick Zobel: 0000-0002-9601-7573

Roland Lindh: 0000-0001-7567-8295

Present Addresses

⁹Theoretical Division, Los Alamos National Laboratory, Los Alamos, NM 87545, USA.

¹⁴Materials Science Division and Center for Molecular Engineering, Argonne National Laboratory, Lemont, IL 60439, USA.

²¹Division of Chemical Physics, Chemical Center, Lund University, SE-221 00 Lund, Sweden.

²²Department of Chemistry, University of Washington, Seattle, WA 98195, USA.

³¹Department of Chemistry, Butler University, 4600 Sunset Avenue, Indianapolis, IN 46208, USA.

³³Chemical Sciences Division, Lawrence Berkeley National Laboratory, 1 Cyclotron Road, Berkeley, CA 94720, USA.

³⁴Theoretical Chemistry and Biology, School of Engineering Sciences in Chemistry, Biotechnology and Health (CBH), Royal Institute of Technology (KTH), SE-106 91 Stockholm, Sweden.

³⁵Lehrstuhl für Theoretische Chemie, Ruhr-Universität Bochum, D-44780 Bochum, Germany.

Funding

K.P. and Q.M.P. thank the Flemish Science Foundation (FWO) and KU Leuven Postdoctoral mandates (PDM/16/112) for funding. The computational resources and services used in DMRG-CASPT2 calculations were provided by the VSC (Flemish Supercomputer Center), funded by the Hercules Foundation and the Flemish Government-department EWI. The Zurich group was supported by the Schweizerischer Nationalfonds (Proj. no. 200021_182400). L.F. acknowledges the Austrian Science Fund FWF for a Schrödinger fellowship (Project no. J 3935). J.A. acknowledges support from the U.S. Department of Energy, Office of Basic Energy Sciences, Heavy Element Chemistry program, under grant DE-SC0001136. The work at the University of Minnesota was supported by the Air Force Office of Scientific Research under grant no. FA9550-16-1-0134 and by the National Science Foundation under grant no. CHE-1746186. M.G.D., L.K.S., M.V., M.L., M.G., E.K., and R.L. acknowledge financial support from the Stiftelsen Olle Engqvist Byggnätare, the Knut and Alice Wallenberg Foundation (grant no. KAW-2013.0020), and the Swedish Research Council (2012-3924). The project R-143-000-A65-133 of the National University of Singapore is gratefully acknowledged. The computational work for the ANISO section was fully performed on resources of the National Supercomputing Centre, Singapore (<https://www.nscg.sg>). R.L. and I.F.G. acknowledge funding from the Swedish Research Council (grant 2016-03398). L.Go., S.M., P.M., and M.Op. thank the University of Vienna for generous support and all the past SHARC developers. A.G. is thankful for funding from the European Union's Horizon 2020 research and innovation programme under the Marie Skłodowska-Curie Grant Agreement no. 658173. The Spanish MINECO grant CTQ2016-80600-P is acknowledged. The ERC Starting Grant "Photo-Mutant" is acknowledged. S.M., F.P., and L.Go. gratefully acknowledge funding from the Austrian Science Fund (FWF) within project I2883. M.Ol. is grateful for grants NSF CHE-CLP-1710191, NIH GM126627 01, a USIAS 2015 fellowship,

and a MIUR Department of Excellence grant. S.I.B. acknowledges financial support from the Deutsche Forschungsgemeinschaft, grant No. BO 4915/1-1. J.N. acknowledges financial support from the Swedish Research Council (contract VR 2015-03956) and the Helmholtz Virtual Institute VI419 “Dynamic Pathways in Multidimensional Landscapes”. A.Z., F.A., and T.A.W. acknowledge support from Fonds National Suisse (FNS) under grant 200020-172532.

Notes

The authors declare no competing financial interest.

ACKNOWLEDGMENTS

M.G.D., L.K.S., M.V., M.L., M.G., E.K., and R.L. thank Trond Saue for useful discussions.

REFERENCES

- (1) Free Software Foundation *GNU Lesser General Public License*, version 2.1. <https://www.gnu.org/licenses/old-licenses/lgpl-2.1.html> (accessed Sept 19, 2019).
- (2) Roos, B. O.; Karlström, G.; Malmqvist, P.-Å.; Sadlej, A. J.; Widmark, P.-O. MOLCAS: A General Purpose Quantum Chemistry Program System for Correlated Wavefunctions. In *Modern Techniques in Computational Chemistry: MOTTECC-91*; Clementi, E., Ed.; ESCOM Science Publishers: 1991; Chapter 10, pp 435–454.
- (3) Andersson, K.; Fülischer, M. P.; Malmqvist, P.-Å.; Olsen, J.; Roos, B. O.; Widmark, P.-O. MOLCAS: A general purpose quantum chemistry program system for correlated wavefunctions. In *Methods and Techniques in Computational Chemistry: METECC-94*; Clementi, E., Ed.; STEF: 1994; Chapter 7, pp 275–324.
- (4) Karlström, G.; Lindh, R.; Malmqvist, P.-Å.; Roos, B. O.; Ryde, U.; Veryazov, V.; Widmark, P.-O.; Cossi, M.; Schimmelpfennig, B.; Neogrady, P.; Seijo, L. MOLCAS: a program package for computational chemistry. *Comput. Mater. Sci.* **2003**, *28*, 222–239.
- (5) Veryazov, V.; Widmark, P.-O.; Serrano-Andrés, L.; Lindh, R.; Roos, B. O. 2MOLCAS as a development platform for quantum chemistry software. *Int. J. Quantum Chem.* **2004**, *100*, 626–635.
- (6) Aquilante, F.; De Vico, L.; Ferré, N.; Ghigo, G.; Malmqvist, P.-Å.; Neogrady, P.; Pedersen, T. B.; Pitoňák, M.; Reiher, M.; Roos, B. O.; Serrano-Andrés, L.; Urban, M.; Veryazov, V.; Lindh, R. MOLCAS 7: The Next Generation. *J. Comput. Chem.* **2010**, *31*, 224–247.
- (7) Aquilante, F.; Pedersen, T. B.; Veryazov, V.; Lindh, R. MOLCAS—a software for multiconfigurational quantum chemistry calculations. *Wiley Interdiscip. Rev.: Comput. Mol. Sci.* **2013**, *3*, 143–149.
- (8) Aquilante, F.; Autschbach, J.; Carlson, R. K.; Chibotaru, L. F.; Delcey, M. G.; De Vico, L.; Fdez. Galván, I.; Ferré, N.; Frutos, L. M.; Gagliardi, L.; Garavelli, M.; Giussani, A.; Hoyer, C. E.; Li Manni, G.; Lischka, H.; Ma, D.; Malmqvist, P. Å.; Müller, T.; Nenov, A.; Olivucci, M.; Pedersen, T. B.; Peng, D.; Plasser, F.; Pritchard, B.; Reiher, M.; Rivalta, I.; Schapiro, I.; Segarra-Martí, J.; Stenrup, M.; Truhlar, D. G.; Ungur, L.; Valentini, A.; Vancoillie, S.; Veryazov, V.; Vysotskiy, V. P.; Weingart, O.; Zapata, F.; Lindh, R. MOLCAS 8: New capabilities for multiconfigurational quantum chemical calculations across the periodic table. *J. Comput. Chem.* **2016**, *37*, 506–541.
- (9) Lotrich, V.; Flocke, N.; Ponton, M.; Yau, A. D.; Perera, A.; Deumens, E.; Bartlett, R. J. Parallel implementation of electronic structure energy, gradient, and Hessian calculations. *J. Chem. Phys.* **2008**, *128*, 194104.
- (10) te Velde, G.; Bickelhaupt, F. M.; Baerends, E. J.; Fonseca Guerra, C.; van Gisbergen, S. J. A.; Snijders, J. G.; Ziegler, T. Chemistry with ADF. *J. Comput. Chem.* **2001**, *22*, 931–967.
- (11) Shiozaki, T. BAGEL: Brilliantly Advanced General Electronic-structure Library. *Wiley Interdiscip. Rev.: Comput. Mol. Sci.* **2018**, *8*, No. e1331.
- (12) Genovese, L.; Videau, B.; Ospici, M.; Deutsch, T.; Goedecker, S.; Méhaut, J.-F. Daubechies wavelets for high performance electronic

structure calculations: The BigDFT project. *C. R. Mec.* **2011**, *339*, 149–164.

- (13) Stanton, J. F.; Gauss, J.; Cheng, L.; Harding, M. E.; Matthews, D. A.; Szalay, P. G. *CFOUR, Coupled-Cluster techniques for Computational Chemistry*. <http://cfour.de> (accessed Sept 19, 2019).

- (14) Lischka, H.; Müller, T.; Szalay, P. G.; Shavitt, I.; Pitzer, R. M.; Shepard, R. Columbus—A program system for advanced multi-reference theory calculations. *Wiley Interdiscip. Rev.: Comput. Mol. Sci.* **2011**, *1*, 191–199.

- (15) Aidas, K.; Angeli, C.; Bak, K. L.; Bakken, V.; Bast, R.; Boman, L.; Christiansen, O.; Cimiraglia, R.; Coriani, S.; Dahle, P.; Dalskov, E. K.; Ekström, U.; Enevoldsen, T.; Eriksen, J. J.; Ettenhuber, P.; Fernández, B.; Ferrighi, L.; Fliegl, H.; Frediani, L.; Hald, K.; Halkier, A.; Hättig, C.; Heiberg, H.; Helgaker, T.; Hennum, A. C.; Hettner, H.; Hjertenaes, E.; Host, S.; Høyvik, I.-M.; Iozzi, M. F.; Jansík, B.; Jensen, H. J. Aa; Jonsson, D.; Jørgensen, P.; Kauczor, J.; Kirpekar, S.; Kjaergaard, T.; Klopper, W.; Knecht, S.; Kobayashi, R.; Koch, H.; Kongsted, J.; Krapp, A.; Kristensen, K.; Ligabue, A.; Lutnaes, O. B.; Melo, J. I.; Mikkelsen, K. V.; Myhre, R. H.; Neiss, C.; Nielsen, C. B.; Norman, P.; Olsen, J.; Olsen, J. M. H.; Osted, A.; Packer, M. J.; Pawłowski, F.; Pedersen, T. B.; Provasi, P. F.; Reine, S.; Rinkevicius, Z.; Ruden, T. A.; Ruud, K.; Rybkin, V. V.; Salek, P.; Samson, C. C. M.; Sánchez de Merás, A.; Saue, T.; Sauer, S. P. A.; Schimmelpfennig, B.; Sneskov, K.; Steindal, A. H.; Sylvester-Hvid, K. O.; Taylor, P. R.; Teale, A. M.; Tellgren, E. I.; Tew, D. P.; Thorvaldsen, A. J.; Thøgersen, L.; Vahtras, O.; Watson, M. A.; Wilson, D. J. D.; Ziolkowski, M.; Ågren, H. The Dalton quantum chemistry program system. *Wiley Interdiscip. Rev.: Comput. Mol. Sci.* **2014**, *4*, 269–284.

- (16) Koster, A. M.; Geudtner, G.; Alvarez-Ibarra, A.; Calaminici, P.; Casida, M. E.; Carmona-Espindola, J.; Dominguez, V. D.; Flores-Moreno, R.; Gamboa, G. U.; Goursot, A.; Heine, T.; Ipatov, A.; de la Lande, A.; Janetzko, F.; del Campo, J. M.; Mejia-Rodriguez, D.; Reveles, J. U.; Vasquez-Perez, J.; Vela, A.; Zuniga-Gutierrez, B.; Salahub, D. R. *deMon2k, A software package for density functional theory (DFT) calculations*; 2018; Cinvestav, Mexico-City. <http://www.demon-software.com> (accessed Sept 19, 2019).

- (17) Saue, T.; Visscher, L.; Jensen, H. J. Aa.; Bast, R. *DIRAC, a relativistic ab initio electronic structure program*. <http://www.diracprogram.org> (accessed Sept 19, 2019).

- (18) Granovsky, A. A. *Firefly QC package*. <http://classic.chem.msu.su/gran/gamess> (accessed Sept 19, 2019).

- (19) Gordon, M. S.; Schmidt, M. W. Advances in electronic structure theory: GAMESS a decade later. In *Theory and Applications of Computational Chemistry*; Elsevier: 2005; Chapter 41, pp 1167–1189, DOI: 10.1016/B978-044451719-7/50084-6.

- (20) Guest, M. F.; Bush, I. J.; Van Dam, H. J. J.; Sherwood, P.; Thomas, J. M. H.; Van Lenthe, J. H.; Havenith, R. W. A.; Kendrick, J. The GAMESS-UK electronic structure package: algorithms, developments and applications. *Mol. Phys.* **2005**, *103*, 719–747.

- (21) Frisch, M. J.; Trucks, G. W.; Schlegel, H. B.; Scuseria, G. E.; Robb, M. A.; Cheeseman, J. R.; Scalmani, G.; Barone, V.; Petersson, G. A.; Nakatsuji, H.; Li, X.; Caricato, M.; Marenich, A. V.; Bloino, J.; Janesko, B. G.; Gomperts, R.; Mennucci, B.; Hratchian, H. P.; Ortiz, J. V.; Izmaylov, A. F.; Sonnenberg, J. L.; Williams-Young, D.; Ding, F.; Lipparini, F.; Egidi, F.; Goings, J.; Peng, B.; Petrone, A.; Henderson, T.; Ranasinghe, D.; Zakrzewski, V. G.; Gao, J.; Rega, N.; Zheng, G.; Liang, W.; Hada, M.; Ehara, M.; Toyota, K.; Fukuda, R.; Hasegawa, J.; Ishida, M.; Nakajima, T.; Honda, Y.; Kitao, O.; Nakai, H.; Vreven, T.; Throssell, K.; Montgomery, J. A., Jr.; Peralta, J. E.; Ogliaro, F.; Bearpark, M. J.; Heyd, J. J.; Brothers, E. N.; Kudin, K. N.; Staroverov, V. N.; Keith, T. A.; Kobayashi, R.; Normand, J.; Raghavachari, K.; Rendell, A. P.; Burant, J. C.; Iyengar, S. S.; Tomasi, J.; Cossi, M.; Millam, J. M.; Klene, M.; Adamo, C.; Cammi, R.; Ochterski, J. W.; Martin, R. L.; Morokuma, K.; Farkas, O.; Foresman, J. B.; Fox, D. J. *Gaussian 16*; 2016; Gaussian Inc.: Wallingford, CT.

- (22) Nakamura, H.; Xidos, J. D.; Chamberlin, A. C.; Kelly, C. P.; Valero, R.; Yang, K. R.; Thompson, J. D.; Li, J.; Hawkins, G. D.; Zhu, T.; Lynch, B. J.; Volobuev, Y.; Rinaldi, D.; Liotard, D. A.; Cramer, C. J.; Truhlar, D. G. HONDOPLUS-v.5.2, based on HONDO v.99.6;

University of Minnesota: Minneapolis, MN, 2013. <https://t1.chem.umn.edu/hondoplus> (accessed Sept 19, 2019).

(23) Bochevarov, A. D.; Harder, E.; Hughes, T. F.; Greenwood, J. R.; Braden, D. A.; Philipp, D. M.; Rinaldo, D.; Halls, M. D.; Zhang, J.; Friesner, R. A. Jaguar: A high-performance quantum chemistry software program with strengths in life and materials sciences. *Int. J. Quantum Chem.* **2013**, *113*, 2110–2142.

(24) Werner, H.-J.; Knowles, P. J.; Knizia, G.; Manby, F. R.; Schütz, M. Molpro: a general-purpose quantum chemistry program package. *Wiley Interdiscip. Rev.: Comput. Mol. Sci.* **2012**, *2*, 242–253.

(25) Kállay, M.; Nagy, P. R.; Rolik, Z.; Mester, D.; Samu, G.; Csontos, J.; Csóka, J.; Szabó, B. P.; Gyevi-Nagy, L.; Ladjanszki, I.; Szegedy, L.; Ladóczki, B.; Petrov, K.; Farkas, M.; Mezei, P. D.; Hégyel, B. MRCC, a quantum chemical program suite. <https://www.mrcc.hu> (accessed Sept 19, 2019).

(26) Valiev, M.; Bylaska, E. J.; Govind, N.; Kowalski, K.; Straatsma, T. P.; Van Dam, H. J. J.; Wang, D.; Nieplocha, J.; Apra, E.; Windus, T. L.; de Jong, W. A. NWChem: A comprehensive and scalable open-source solution for large scale molecular simulations. *Comput. Phys. Commun.* **2010**, *181*, 1477–1489.

(27) Pederson, M. R.; Jackson, K. A.; Porezag, D. V. NRMOL; Naval Research Laboratory Molecular Orbital Library. https://quantum.utep.edu/new_nrlmol/nrlmoldoc_main.html (accessed Sept 19, 2019).

(28) Neese, F. Software update: the ORCA program system, version 4.0. *Wiley Interdiscip. Rev.: Comput. Mol. Sci.* **2018**, *8*, No. e1327.

(29) Baker, J.; Wolinski, K.; Malagoli, M.; Kinghorn, D.; Wolinski, P.; Magyarfalvi, G.; Saebo, S.; Janowski, T.; Pulay, P. Quantum chemistry in parallel with PQS. *J. Comput. Chem.* **2009**, *30*, 317–335.

(30) Parrish, R. M.; Burns, L. A.; Smith, D. G. A.; Simmonett, A. C.; DePrince, A. E.; Hohenstein, E. G.; Bozkaya, U.; Sokolov, A. Yu.; Di Remigio, R.; Richard, R. M.; Gonthier, J. F.; James, A. M.; McAlexander, H. R.; Kumar, A.; Saitow, M.; Wang, X.; Pritchard, B. P.; Verma, P.; Schaefer, H. F.; Patkowski, K.; King, R. A.; Valeev, E. F.; Evangelista, F. A.; Turney, J. M.; Crawford, T. D.; Sherrill, C. D. Psi4 1.1: An Open-Source Electronic Structure Program Emphasizing Automation, Advanced Libraries, and Interoperability. *J. Chem. Theory Comput.* **2017**, *13*, 3185–3197.

(31) Sun, Q.; Berkelbach, T. C.; Blunt, N. S.; Booth, G. H.; Guo, S.; Li, Z.; Liu, J.; McClain, J. D.; Sayfutyarova, E. R.; Sharma, S.; Wouters, S.; Chan, G. K.-L. PySCF: the Python-based simulations of chemistry framework. *Wiley Interdiscip. Rev.: Comput. Mol. Sci.* **2018**, *8*, No. e1340.

(32) Shao, Y.; Gan, Z.; Epifanovsky, E.; Gilbert, A. T. B.; Wormit, M.; Kussmann, J.; Lange, A. W.; Behn, A.; Deng, J.; Feng, X.; Ghosh, D.; Goldey, M.; Horn, P. R.; Jacobson, L. D.; Kaliman, I.; Khaliullin, R. Z.; Kus, T.; Landau, A.; Liu, J.; Proynov, E. I.; Rhee, Y. M.; Richard, R. M.; Rohrdanz, M. A.; Steele, R. P.; Sundstrom, E. J.; Woodcock, H. L.; Zimmerman, P. M.; Zuev, D.; Albrecht, B.; Alguire, E.; Austin, B.; Beran, G. J. O.; Bernard, Y. A.; Berquist, E.; Brandhorst, K.; Bravaya, K. B.; Brown, S. T.; Casanova, D.; Chang, C.-M.; Chen, Y.; Chien, S. H.; Closser, K. D.; Crittenden, D. L.; Diedenhofen, M.; DiStasio, R. A.; Do, H.; Dutoi, A. D.; Edgar, R. G.; Fatehi, S.; Fusti-Molnar, L.; Ghysels, A.; Golubeva-Zadorozhnaya, A.; Gomes, J.; Hanson-Heine, M. W. D.; Harbach, P. H. P.; Hauser, A. W.; Hohenstein, E. G.; Holden, Z. C.; Jagau, T.-C.; Ji, H.; Kaduk, B.; Khistyayev, K.; Kim, J.; Kim, J.; King, R. A.; Klunzinger, P.; Kosenkov, D.; Kowalczyk, T.; Krauter, C. M.; Lao, K. U.; Laurent, A. D.; Lawler, K. V.; Levchenko, S. V.; Lin, C. Y.; Liu, F.; Livshits, E.; Lochan, R. C.; Luenser, A.; Manohar, P.; Manzer, S. F.; Mao, S.-P.; Mardirossian, N.; Marenich, A. V.; Maurer, S. A.; Mayhall, N. J.; Neuscammann, E.; Oana, C. M.; Olivares-Amaya, R.; O'Neill, D. P.; Parkhill, J. A.; Perrine, T. M.; Peverati, R.; Prociuk, A.; Rehn, D. R.; Rosta, E.; Russ, N. J.; Sharada, S. M.; Sharma, S.; Small, D. W.; Sodt, A.; Stein, T.; Stück, D.; Su, Y.-C.; Thom, A. J. W.; Tsuchimochi, T.; Vanovschi, V.; Vogt, L.; Vydrov, O.; Wang, T.; Watson, M. A.; Wenzel, J.; White, A.; Williams, C. F.; Yang, J.; Yeganeh, S.; Yost, S. R.; You, Z.-Q.; Zhang, I. Y.; Zhang, X.; Zhao, Y.; Brooks, B. R.; Chan, G. K. L.; Chipman, D. M.; Cramer, C. J.; Goddard, W. A.; Gordon, M. S.; Hehre, W. J.

Klamt, A.; Schaefer, H. F.; Schmidt, M. W.; Sherrill, C. D.; Truhlar, D. G.; Warshel, A.; Xu, X.; Aspuru-Guzik, A.; Baer, R.; Bell, A. T.; Besley, N. A.; Chai, J.-D.; Dreuw, A.; Dunietz, B. D.; Furlani, T. R.; Gwaltney, S. R.; Hsu, C.-P.; Jung, Y.; Kong, J.; Lambrecht, D. S.; Liang, W.; Ochsenfeld, C.; Rassolov, V. A.; Slipchenko, L. V.; Subotnik, J. E.; Van Voorhis, T.; Herbert, J. M.; Krylov, A. I.; Gill, P. M. W.; Head-Gordon, M. Advances in molecular quantum chemistry contained in the Q-Chem 4 program package. *Mol. Phys.* **2015**, *113*, 184–215.

(33) TeraChem; PetaChem, LLC: Los Altos Hills, CA. <http://www.petachem.com/products.html> (accessed Sept 19, 2019).

(34) Furche, F.; Ahlrichs, R.; Hättig, C.; Klopper, W.; Sierka, M.; Weigend, F. Turbomole. *Wiley Interdiscip. Rev.: Comput. Mol. Sci.* **2014**, *4*, 91–100.

(35) Pirhadi, S.; Sunseri, J.; Koes, D. R. Open source molecular modeling. *J. Mol. Graphics Modell.* **2016**, *69*, 127–143.

(36) git, a free and open source distributed version control system. <https://www.git-scm.com> (accessed Sept 19, 2019).

(37) CMake, an extensible, open-source system that manages the build process. <https://cmake.org> (accessed Sept 19, 2019).

(38) GitLab, a git-based fully featured platform for software development. <https://about.gitlab.com> (accessed Sept 19, 2019).

(39) HDF5, high-performance data management and storage suite. <https://www.hdfgroup.org/> (accessed Sept 19, 2019).

(40) Cížek, J. On the Correlation Problem in Atomic and Molecular Systems. Calculation of Wavefunction Components in Ursell-Type Expansion Using Quantum-Field Theoretical Methods. *J. Chem. Phys.* **1966**, *45*, 4256–4266.

(41) Purvis, G. D.; Bartlett, R. J. A full coupled-cluster singles and doubles model: The inclusion of disconnected triples. *J. Chem. Phys.* **1982**, *76*, 1910–1918.

(42) Raghavachari, K.; Trucks, G. W. Highly correlated systems. Excitation energies of first row transition metals Sc–Cu. *J. Chem. Phys.* **1989**, *91*, 1062–1065.

(43) Hartree, D. R. The Wave Mechanics of an Atom with a Non-Coulomb Central Field. Part I. Theory and Methods. *Math. Proc. Cambridge Philos. Soc.* **1928**, *24*, 89.

(44) Fock, V. Näherungsmethode zur Lösung des quantenmechanischen Mehrkörperproblems. *Z. Phys.* **1930**, *61*, 126–148.

(45) Roothaan, C. C. J. New Developments in Molecular Orbital Theory. *Rev. Mod. Phys.* **1951**, *23*, 69–89.

(46) Roothaan, C. C. J. Self-Consistent Field Theory for Open Shells of Electronic Systems. *Rev. Mod. Phys.* **1960**, *32*, 179–185.

(47) Roos, B. O.; Taylor, P. R.; Siegbahn, P. E. M. A complete active space SCF method (CASSCF) using a density matrix formulated super-CI approach. *Chem. Phys.* **1980**, *48*, 157–173.

(48) Roos, B. O. The complete active space SCF method in a Fock-matrix-based super-CI formulation. *Int. J. Quantum Chem.* **1980**, *18*, 175–189.

(49) Siegbahn, P. E. M.; Almlöf, J.; Heiberg, A.; Roos, B. O. The complete active space SCF (CASSCF) method in a Newton–Raphson formulation with application to the HNO molecule. *J. Chem. Phys.* **1981**, *74*, 2384–2396.

(50) Siegbahn, P.; Heiberg, A.; Roos, B.; Levy, B. A Comparison of the Super-CI and the Newton–Raphson Scheme in the Complete Active Space SCF Method. *Phys. Scr.* **1980**, *21*, 323–327.

(51) Kohn, W.; Sham, L. J. Self-Consistent Equations Including Exchange and Correlation Effects. *Phys. Rev.* **1965**, *140*, A1133–A1138.

(52) Peverati, R.; Truhlar, D. G. Quest for a universal density functional: the accuracy of density functionals across a broad spectrum of databases in chemistry and physics. *Philos. Trans. R. Soc. A* **2014**, *372*, 20120476.

(53) Yu, H. S.; He, X.; Li, S. L.; Truhlar, D. G. MN15: A Kohn–Sham global-hybrid exchange–correlation density functional with broad accuracy for multi-reference and single-reference systems and noncovalent interactions. *Chem. Sci.* **2016**, *7*, 5032–5051.

(54) Li Manni, G.; Carlson, R. K.; Luo, S.; Ma, D.; Olsen, J.; Truhlar, D. G.; Gagliardi, L. Multiconfiguration Pair-Density Functional Theory. *J. Chem. Theory Comput.* **2014**, *10*, 3669–3680.

- (55) Olsen, J.; Roos, B. O.; Jørgensen, P.; Jensen, H. J. Aa. Determinant based configuration interaction algorithms for complete and restricted configuration interaction spaces. *J. Chem. Phys.* **1988**, *89*, 2185–2192.
- (56) Malmqvist, P. Å.; Rendell, A.; Roos, B. O. The restricted active space self-consistent-field method, implemented with a split graph unitary group approach. *J. Phys. Chem.* **1990**, *94*, 5477–5482.
- (57) Ma, D.; Li Manni, G.; Gagliardi, L. The generalized active space concept in multiconfigurational self-consistent field methods. *J. Chem. Phys.* **2011**, *135*, 044128.
- (58) Li Manni, G.; Ma, D.; Aquilante, F.; Olsen, J.; Gagliardi, L. SplitGAS Method for Strong Correlation and the Challenging Case of Cr_2 . *J. Chem. Theory Comput.* **2013**, *9*, 3375–3384.
- (59) Carlson, R. K.; Li Manni, G.; Sonnenberger, A. L.; Truhlar, D. G.; Gagliardi, L. Multiconfiguration Pair-Density Functional Theory: Barrier Heights and Main Group and Transition Metal Energetics. *J. Chem. Theory Comput.* **2015**, *11*, 82–90.
- (60) Carlson, R. K.; Truhlar, D. G.; Gagliardi, L. Multiconfiguration Pair-Density Functional Theory: A Fully Translated Gradient Approximation and Its Performance for Transition Metal Dimers and the Spectroscopy of $\text{Re}_2\text{Cl}_8^{2-}$. *J. Chem. Theory Comput.* **2015**, *11*, 4077–4085.
- (61) Gagliardi, L.; Truhlar, D. G.; Li Manni, G.; Carlson, R. K.; Hoyer, C. E.; Bao, J. L. Multiconfiguration Pair-Density Functional Theory: A New Way To Treat Strongly Correlated Systems. *Acc. Chem. Res.* **2017**, *50*, 66–73.
- (62) Andersson, K.; Malmqvist, P. Å.; Roos, B. O.; Sadlej, A. J.; Wolinski, K. Second-order perturbation theory with a CASSCF reference function. *J. Phys. Chem.* **1990**, *94*, 5483–5488.
- (63) Andersson, K.; Malmqvist, P. Å.; Roos, B. O. Second-order perturbation theory with a complete active space self-consistent field reference function. *J. Chem. Phys.* **1992**, *96*, 1218–1226.
- (64) Malmqvist, P. Å.; Pierloot, K.; Moughal Shahi, A. R.; Cramer, C. J.; Gagliardi, L. The restricted active space followed by second-order perturbation theory method: Theory and application to the study of CuO_2 and Cu_2O_2 systems. *J. Chem. Phys.* **2008**, *128*, 204109.
- (65) Angeli, C.; Cimiraglia, R.; Evangelisti, S.; Leininger, T.; Malrieu, J.-P. Introduction of n -electron valence states for multi-reference perturbation theory. *J. Chem. Phys.* **2001**, *114*, 10252–10264.
- (66) Angeli, C.; Cimiraglia, R.; Malrieu, J.-P. N -electron valence state perturbation theory: a fast implementation of the strongly contracted variant. *Chem. Phys. Lett.* **2001**, *350*, 297–305.
- (67) Angeli, C.; Cimiraglia, R.; Malrieu, J.-P. n -electron valence state perturbation theory: A spinless formulation and an efficient implementation of the strongly contracted and of the partially contracted variants. *J. Chem. Phys.* **2002**, *117*, 9138–9153.
- (68) Angeli, C.; Borini, S.; Cestari, M.; Cimiraglia, R. A quasidegenerate formulation of the second order n -electron valence state perturbation theory approach. *J. Chem. Phys.* **2004**, *121*, 4043–4049.
- (69) Angeli, C.; Borini, S.; Cavallini, A.; Cestari, M.; Cimiraglia, R.; Ferrighi, L.; Sparta, M. Developments in the n -electron valence state perturbation theory. *Int. J. Quantum Chem.* **2006**, *106*, 686–691.
- (70) Angeli, C.; Cimiraglia, R.; Malrieu, J.-P. A Simple Approximate Perturbation Approach to Quasi-degenerate Systems. *Theor. Chem. Acc.* **2006**, *116*, 434–439.
- (71) Angeli, C.; Pastore, M.; Cimiraglia, R. New perspectives in multireference perturbation theory: the n -electron valence state approach. *Theor. Chem. Acc.* **2007**, *117*, 743–754.
- (72) Sharma, P.; Truhlar, D. G.; Gagliardi, L. Active Space Dependence in Multiconfiguration Pair-Density Functional Theory. *J. Chem. Theory Comput.* **2018**, *14*, 660–669.
- (73) Li Manni, G.; Smart, S. D.; Alavi, A. Combining the Complete Active Space Self-Consistent Field Method and the Full Configuration Interaction Quantum Monte Carlo within a Super-CI Framework, with Application to Challenging Metal-Porphyrins. *J. Chem. Theory Comput.* **2016**, *12*, 1245–1258.
- (74) Li Manni, G.; Alavi, A. Understanding the Mechanism Stabilizing Intermediate Spin States in Fe(II)-Porphyrin. *J. Phys. Chem. A* **2018**, *122*, 4935–4947.
- (75) Li Manni, G.; Kats, D.; Tew, D. P.; Alavi, A. Role of Valence and Semicore Electron Correlation on Spin Gaps in Fe(II)-Porphyrins. *J. Chem. Theory Comput.* **2019**, *15*, 1492–1497.
- (76) Bogdanov, N.; Li Manni, G.; Sharma, S.; Gunnarsson, O.; Alavi, A. New superexchange paths due to breathing-enhanced hopping in corner-sharing cuprates. 2018, preprint [arXiv:1803.07026]. <https://arxiv.org/abs/1803.07026> (accessed Sept 19, 2019).
- (77) Davidson, E. R. The iterative calculation of a few of the lowest eigenvalues and corresponding eigenvectors of large real-symmetric matrices. *J. Comput. Phys.* **1975**, *17*, 87–94.
- (78) Roos, B. A new method for large-scale CI calculations. *Chem. Phys. Lett.* **1972**, *15*, 153–159.
- (79) Booth, G. H.; Thom, A. J. W.; Alavi, A. Fermion Monte Carlo without fixed nodes: A game of life, death, and annihilation in Slater determinant space. *J. Chem. Phys.* **2009**, *131*, 054106.
- (80) Cleland, D.; Booth, G. H.; Alavi, A. Communications: Survival of the fittest: Accelerating convergence in full configuration-interaction quantum Monte Carlo. *J. Chem. Phys.* **2010**, *132*, 041103.
- (81) Cleland, D. M.; Booth, G. H.; Alavi, A. A study of electron affinities using the initiator approach to full configuration interaction quantum Monte Carlo. *J. Chem. Phys.* **2011**, *134*, 024112.
- (82) Overy, C.; Booth, G. H.; Blunt, N. S.; Shepherd, J. J.; Cleland, D.; Alavi, A. Unbiased reduced density matrices and electronic properties from full configuration interaction quantum Monte Carlo. *J. Chem. Phys.* **2014**, *141*, 244117.
- (83) Blunt, N. S.; Smart, S. D.; Kersten, J. A. F.; Spencer, J. S.; Booth, G. H.; Alavi, A. Semi-stochastic full configuration interaction quantum Monte Carlo: Developments and application. *J. Chem. Phys.* **2015**, *142*, 184107.
- (84) Booth, G. H.; Smart, S. D.; Alavi, A. Linear-scaling and parallelisable algorithms for stochastic quantum chemistry. *Mol. Phys.* **2014**, *112*, 1855–1869.
- (85) Booth, G. H.; Cleland, D.; Thom, A. J. W.; Alavi, A. Breaking the carbon dimer: The challenges of multiple bond dissociation with full configuration interaction quantum Monte Carlo methods. *J. Chem. Phys.* **2011**, *135*, 084104.
- (86) Blunt, N. S.; Smart, S. D.; Booth, G. H.; Alavi, A. An excited-state approach within full configuration interaction quantum Monte Carlo. *J. Chem. Phys.* **2015**, *143*, 134117.
- (87) Blunt, N. S.; Alavi, A.; Booth, G. H. Krylov-Projected Quantum Monte Carlo Method. *Phys. Rev. Lett.* **2015**, *115*, 050603.
- (88) Helgaker, T.; Jørgensen, P.; Olsen, J. *Molecular Electronic Structure Theory*; John Wiley & Sons: Chichester, England, 2000; DOI: 10.1002/9781119019572.
- (89) Aquilante, F.; Lindh, R.; Pedersen, T. B. Unbiased auxiliary basis sets for accurate two-electron integral approximations. *J. Chem. Phys.* **2007**, *127*, 114107.
- (90) Aquilante, F.; Pedersen, T. B.; Lindh, R. Low-cost evaluation of the exchange Fock matrix from Cholesky and density fitting representations of the electron repulsion integrals. *J. Chem. Phys.* **2007**, *126*, 194106.
- (91) Aquilante, F.; Pedersen, T. B.; Lindh, R.; Roos, B. O.; Sánchez de Merás, A.; Koch, H. Accurate ab initio density fitting for multiconfigurational self-consistent field methods. *J. Chem. Phys.* **2008**, *129*, 024113.
- (92) Aquilante, F.; Gagliardi, L.; Pedersen, T. B.; Lindh, R. Atomic Cholesky decompositions: A route to unbiased auxiliary basis sets for density fitting approximation with tunable accuracy and efficiency. *J. Chem. Phys.* **2009**, *130*, 154107.
- (93) Pedersen, T. B.; Aquilante, F.; Lindh, R. Density fitting with auxiliary basis sets from Cholesky decompositions. *Theor. Chem. Acc.* **2009**, *124*, 1–10.
- (94) Bednorz, J. G.; Müller, K. A. Possible high T_c superconductivity in the Ba–La–Cu–O system. *Z. Phys. B: Condens. Matter* **1986**, *64*, 189–193.

- (95) Peng, Y. Y.; Dellea, G.; Minola, M.; Conni, M.; Amorese, A.; Di Castro, D.; De Luca, G. M.; Kummer, K.; Salluzzo, M.; Sun, X.; Zhou, X. J.; Balestrino, G.; Le Tacon, M.; Keimer, B.; Braicovich, L.; Brookes, N. B.; Ghiringhelli, G. Influence of apical oxygen on the extent of in-plane exchange interaction in cuprate superconductors. *Nat. Phys.* **2017**, *13*, 1201–1206.
- (96) van Oosten, A. B.; Broer, R.; Nieuwpoort, W. C. Heisenberg exchange enhancement by orbital relaxation in cuprate compounds. *Chem. Phys. Lett.* **1996**, *257*, 207–212.
- (97) Muñoz, D.; Illas, F.; de, P. R.; Moreira, I. Accurate Prediction of Large Antiferromagnetic Interactions in High- T_c $\text{HgBa}_2\text{Ca}_{n-1}\text{Cu}_n\text{O}_{2n+2+\delta}$ ($n = 2,3$) Superconductor Parent Compounds. *Phys. Rev. Lett.* **2000**, *84*, 1579–1582.
- (98) de Graaf, C.; Sousa, C.; de, P. R.; Moreira, I.; Illas, F. Multiconfigurational Perturbation Theory: An Efficient Tool to Predict Magnetic Coupling Parameters in Biradicals, Molecular Complexes, and Ionic Insulators. *J. Phys. Chem. A* **2001**, *105*, 11371–11378.
- (99) Calzado, C. J.; Angeli, C.; Taratiel, D.; Caballol, R.; Malrieu, J.-P. Analysis of the magnetic coupling in binuclear systems. III. The role of the ligand to metal charge transfer excitations revisited. *J. Chem. Phys.* **2009**, *131*, 044327.
- (100) Fink, K.; Staemmler, V. A modified CAS-CI approach for an efficient calculation of magnetic exchange coupling constants. *Mol. Phys.* **2013**, *111*, 2594–2605.
- (101) White, S. R. Density matrix formulation for quantum renormalization groups. *Phys. Rev. Lett.* **1992**, *69*, 2863–2866.
- (102) White, S. R. Density-matrix algorithms for quantum renormalization groups. *Phys. Rev. B: Condens. Matter Mater. Phys.* **1993**, *48*, 10345–10356.
- (103) Östlund, S.; Rommer, S. Thermodynamic Limit of Density Matrix Renormalization. *Phys. Rev. Lett.* **1995**, *75*, 3537–3540.
- (104) Rommer, S.; Östlund, S. Class of ansatz wave functions for one-dimensional spin systems and their relation to the density matrix renormalization group. *Phys. Rev. B: Condens. Matter Mater. Phys.* **1997**, *55*, 2164–2181.
- (105) Vidal, G.; Latorre, J. I.; Rico, E.; Kitaev, A. Entanglement in Quantum Critical Phenomena. *Phys. Rev. Lett.* **2003**, *90*, 227902.
- (106) Verstraete, F.; Porras, D.; Cirac, J. I. Density Matrix Renormalization Group and Periodic Boundary Conditions: A Quantum Information Perspective. *Phys. Rev. Lett.* **2004**, *93*, 227205.
- (107) Barthel, T.; Chung, M.-C.; Schollwöck, U. Entanglement scaling in critical two-dimensional fermionic and bosonic systems. *Phys. Rev. A: At., Mol., Opt. Phys.* **2006**, *74*, 022329.
- (108) Schuch, N.; Wolf, M. M.; Verstraete, F.; Cirac, J. I. Entropy Scaling and Simulability by Matrix Product States. *Phys. Rev. Lett.* **2008**, *100*, 030504.
- (109) Schollwöck, U. The density-matrix renormalization group in the age of matrix product states. *Ann. Phys. (Amsterdam, Neth.)* **2011**, *326*, 96–192.
- (110) McCulloch, I. P. From density-matrix renormalization group to matrix product states. *J. Stat. Mech.: Theory Exp.* **2007**, *2007*, P10014–P10014a.
- (111) Keller, S.; Reiher, M. Spin-adapted matrix product states and operators. *J. Chem. Phys.* **2016**, *144*, 134101.
- (112) Bekenstein, J. D. Black Holes and Entropy. *Phys. Rev. D: Part. Fields* **1973**, *7*, 2333–2346.
- (113) Srednicki, M. Entropy and area. *Phys. Rev. Lett.* **1993**, *71*, 666–669.
- (114) Olivares-Amaya, R.; Hu, W.; Nakatani, N.; Sharma, S.; Yang, J.; Chan, G. K.-L. The ab-initio density matrix renormalization group in practice. *J. Chem. Phys.* **2015**, *142*, 034102.
- (115) Verstraete, F.; Garcia-Ripoll, J. J.; Cirac, J. I. Matrix Product Density Operators: Simulation of Finite-Temperature and Dissipative Systems. *Phys. Rev. Lett.* **2004**, *93*, 207204.
- (116) Crosswhite, G. M.; Doherty, A. C.; Vidal, G. Applying matrix product operators to model systems with long-range interactions. *Phys. Rev. B: Condens. Matter Mater. Phys.* **2008**, *78*, 035116.
- (117) Keller, S.; Dolfi, M.; Troyer, M.; Reiher, M. An efficient matrix product operator representation of the quantum chemical Hamiltonian. *J. Chem. Phys.* **2015**, *143*, 244118.
- (118) Chan, G. K.-L.; Keselman, A.; Nakatani, N.; Li, Z.; White, S. R. Matrix product operators, matrix product states, and ab initio density matrix renormalization group algorithms. *J. Chem. Phys.* **2016**, *145*, 014102.
- (119) Hubig, C.; McCulloch, I. P.; Schollwöck, U. Generic construction of efficient matrix product operators. *Phys. Rev. B: Condens. Matter Mater. Phys.* **2017**, *95*, 035129.
- (120) Battaglia, S.; Keller, S.; Knecht, S. Efficient Relativistic Density-Matrix Renormalization Group Implementation in a Matrix-Product Formulation. *J. Chem. Theory Comput.* **2018**, *14*, 2353–2369.
- (121) Knecht, S.; Legeza, Ö.; Reiher, M. Communication: Four-component density matrix renormalization group. *J. Chem. Phys.* **2014**, *140*, 041101.
- (122) Kurashige, Y.; Yanai, T. Second-order perturbation theory with a density matrix renormalization group self-consistent field reference function: Theory and application to the study of chromium dimer. *J. Chem. Phys.* **2011**, *135*, 094104.
- (123) Freitag, L.; Knecht, S.; Angeli, C.; Reiher, M. Multireference Perturbation Theory with Cholesky Decomposition for the Density Matrix Renormalization Group. *J. Chem. Theory Comput.* **2017**, *13*, 451–459.
- (124) Knecht, S.; Keller, S.; Autschbach, J.; Reiher, M. A Nonorthogonal State-Interaction Approach for Matrix Product State Wave Functions. *J. Chem. Theory Comput.* **2016**, *12*, 5881–5894.
- (125) Wouters, S.; Poelmans, W.; Ayers, P. W.; Van Neck, D. CheMPS2: A free open-source spin-adapted implementation of the density matrix renormalization group for ab initio quantum chemistry. *Comput. Phys. Commun.* **2014**, *185*, 1501–1514.
- (126) Knecht, S.; Hedegård, E. D.; Keller, S.; Kovyrshin, A.; Ma, Y.; Muolo, A.; Stein, C. J.; Reiher, M. New Approaches for *ab initio* Calculations of Molecules with Strong Electron Correlation. *Chimia* **2016**, *70*, 244–251.
- (127) Wouters, S.; Van Speybroeck, V.; Van Neck, D. DMRG-CASPT2 study of the longitudinal static second hyperpolarizability of all-trans polyenes. *J. Chem. Phys.* **2016**, *145*, 054120.
- (128) Freitag, L.; Ma, Y.; Baiardi, A.; Knecht, S.; Reiher, M. Analytical gradients and nonadiabatic couplings for the state-average density matrix renormalization group self-consistent field method. 2019, preprint [arXiv:1905.01558]. <https://arxiv.org/abs/1905.01558> (accessed Sept 19, 2019).
- (129) Phung, Q. M.; Wouters, S.; Pierloot, K. Cumulant Approximated Second-Order Perturbation Theory Based on the Density Matrix Renormalization Group for Transition Metal Complexes: A Benchmark Study. *J. Chem. Theory Comput.* **2016**, *12*, 4352–4361.
- (130) Nakatani, N.; Guo, S. Density matrix renormalization group (DMRG) method as a common tool for large active-space CASSCF/CASPT2 calculations. *J. Chem. Phys.* **2017**, *146*, 094102.
- (131) Knowles, P. J.; Handy, N. C. A determinant based full configuration interaction program. *Comput. Phys. Commun.* **1989**, *54*, 75–83.
- (132) Roos, B. O. The Complete Active Space Self-Consistent Field Method and its Applications in Electronic Structure Calculations. In *Ab Initio Methods in Quantum Chemistry Part 2*; Lawley, K. P., Ed.; Advances in Chemical Physics; John Wiley & Sons, Inc.: 1987; pp 399–445, DOI: 10.1002/9780470142943.ch7.
- (133) Schmidt, M. W.; Gordon, M. S. The Construction and Interpretation of MCSCF Wavefunctions. *Annu. Rev. Phys. Chem.* **1998**, *49*, 233–266.
- (134) Pierloot, K. Nondynamic Correlation Effects in Transition Metal Coordination Compounds. In *Computational Organometallic Chemistry*; Cundari, T. R., Ed.; CRC Press: 2001; pp 123–158.
- (135) Pierloot, K. The CASPT2 method in inorganic electronic spectroscopy: from ionic transition metal to covalent actinide complexes. *Mol. Phys.* **2003**, *101*, 2083–2094.

- (136) Veryazov, V.; Malmqvist, P. Å.; Roos, B. O. How to select active space for multiconfigurational quantum chemistry? *Int. J. Quantum Chem.* **2011**, *111*, 3329–3338.
- (137) González, L.; Escudero, D.; Serrano-Andrés, L. Progress and Challenges in the Calculation of Electronic Excited States. *ChemPhysChem* **2012**, *13*, 28–51.
- (138) Stein, C. J.; Reiher, M. Automated Selection of Active Orbital Spaces. *J. Chem. Theory Comput.* **2016**, *12*, 1760–1771.
- (139) Legeza, Ö.; Sólyom, J. Optimizing the density-matrix renormalization group method using quantum information entropy. *Phys. Rev. B: Condens. Matter Mater. Phys.* **2003**, *68*, 195116.
- (140) Rissler, J.; Noack, R. M.; White, S. R. Measuring orbital interaction using quantum information theory. *Chem. Phys.* **2006**, *323*, 519–531.
- (141) Stein, C. J.; von Burg, V.; Reiher, M. The Delicate Balance of Static and Dynamic Electron Correlation. *J. Chem. Theory Comput.* **2016**, *12*, 3764–3773.
- (142) Stein, C. J.; Reiher, M. Automated Identification of Relevant Frontier Orbitals for Chemical Compounds and Processes. *Chimia* **2017**, *71*, 170–176.
- (143) Stein, C. J.; Reiher, M. SCINE autoCAS; 2018. <https://scine.ethz.ch/download/autocas> (accessed May 2019).
- (144) Stein, C. J.; Reiher, M. autoCAS: A Program for Fully Automated Multiconfigurational Calculations. *J. Comput. Chem.* **2019**, *40*, 2216–2226.
- (145) SCINE: Software for Chemical Interaction Networks. <https://scine.ethz.ch> (accessed Sept 19, 2019).
- (146) Stålring, J.; Bernhardsson, A.; Lindh, R. Analytical gradients of a state average MCSCF state and a state average diagnostic. *Mol. Phys.* **2001**, *99*, 103–114.
- (147) Delcey, M. G.; Freitag, L.; Pedersen, T. B.; Aquilante, F.; Lindh, R.; González, L. Analytical gradients of complete active space self-consistent field energies using Cholesky decomposition: Geometry optimization and spin-state energetics of a ruthenium nitrosyl complex. *J. Chem. Phys.* **2014**, *140*, 174103.
- (148) Delcey, M. G.; Pedersen, T. B.; Aquilante, F.; Lindh, R. Analytical gradients of the state-average complete active space self-consistent field method with density fitting. *J. Chem. Phys.* **2015**, *143*, 044110.
- (149) Hu, W.; Chan, G. K.-L. Excited-State Geometry Optimization with the Density Matrix Renormalization Group, as Applied to Polyenes. *J. Chem. Theory Comput.* **2015**, *11*, 3000–3009.
- (150) Ma, Y.; Knecht, S.; Reiher, M. Multiconfigurational Effects in Theoretical Resonance Raman Spectra. *ChemPhysChem* **2017**, *18*, 384–393.
- (151) Veis, L.; Antalík, A.; Brabec, J.; Neese, F.; Legeza, Ö.; Pittner, J. Coupled Cluster Method with Single and Double Excitations Tailored by Matrix Product State Wave Functions. *J. Phys. Chem. Lett.* **2016**, *7*, 4072–4078.
- (152) Veis, L.; Antalík, A.; Legeza, Ö.; Alavi, A.; Pittner, J. The Intricate Case of Tetramethyleneethane: A Full Configuration Interaction Quantum Monte Carlo Benchmark and Multireference Coupled Cluster Studies. *J. Chem. Theory Comput.* **2018**, *14*, 2439–2445.
- (153) Faulstich, F. M.; Laestadius, A.; Kvaal, S.; Legeza, Ö.; Schneider, R. Analysis of The Coupled-Cluster Method Tailored by Tensor-Network States in Quantum Chemistry. 2018, preprint [arXiv:1802.05699]. <https://arxiv.org/abs/1802.05699> (accessed Sept 19, 2019).
- (154) Roca-Sanjuán, D.; Aquilante, F.; Lindh, R. Multiconfiguration second-order perturbation theory approach to strong electron correlation in chemistry and photochemistry. *Wiley Interdiscip. Rev.: Comput. Mol. Sci.* **2012**, *2*, 585–603.
- (155) Dyall, K. G. The choice of a zeroth-order Hamiltonian for second-order perturbation theory with a complete active space self-consistent-field reference function. *J. Chem. Phys.* **1995**, *102*, 4909–4918.
- (156) Guo, S.; Watson, M. A.; Hu, W.; Sun, Q.; Chan, G. K.-L. N-Electron Valence State Perturbation Theory Based on a Density Matrix Renormalization Group Reference Function, with Applications to the Chromium Dimer and a Trimer Model of Poly(*p*-Phenylenevinylene). *J. Chem. Theory Comput.* **2016**, *12*, 1583–1591.
- (157) Meyer, W. Configuration Expansion by Means of Pseudonatural Orbitals. In *Methods of Electronic Structure Theory*; Springer US: 1977; pp 413–446, DOI: [10.1007/978-1-4757-0887-5_11](https://doi.org/10.1007/978-1-4757-0887-5_11).
- (158) Siegbahn, P. E. M. Direct configuration interaction with a reference state composed of many reference configurations. *Int. J. Quantum Chem.* **1980**, *18*, 1229–1242.
- (159) Werner, H.-J.; Reinsch, E.-A. The self-consistent electron pairs method for multiconfiguration reference state functions. *J. Chem. Phys.* **1982**, *76*, 3144–3156.
- (160) Beebe, N. H. F.; Linderberg, J. Simplifications in the generation and transformation of two-electron integrals in molecular calculations. *Int. J. Quantum Chem.* **1977**, *12*, 683–705.
- (161) Aquilante, F.; Malmqvist, P. Å.; Pedersen, T. B.; Ghosh, A.; Roos, B. O. Cholesky Decomposition-Based Multiconfiguration Second-Order Perturbation Theory (CD-CASPT2): Application to the Spin-State Energetics of Co(III)(diiminato)(NPh). *J. Chem. Theory Comput.* **2008**, *4*, 694–702.
- (162) Aquilante, F.; Boman, L.; Boström, J.; Koch, H.; Lindh, R.; Sánchez de Merás, A.; Pedersen, T. B. Cholesky Decomposition Techniques in Electronic Structure Theory. In *Linear-Scaling Techniques in Computational Chemistry and Physics*; Springer Netherlands: 2011; pp 301–343, DOI: [10.1007/978-90-481-2853-2_13](https://doi.org/10.1007/978-90-481-2853-2_13).
- (163) Malmqvist, P. Å.; Roos, B. O.; Schimmelpfennig, B. The restricted active space (RAS) state interaction approach with spin-orbit coupling. *Chem. Phys. Lett.* **2002**, *357*, 230–240.
- (164) Gendron, F.; Pritchard, B.; Bolvin, H.; Autschbach, J. Magnetic Resonance Properties of Actinyl Carbonate Complexes and Plutonyl(VI)-tris-nitrate. *Inorg. Chem.* **2014**, *53*, 8577–8592.
- (165) Pierloot, K.; Phung, Q. M.; Domingo, A. Spin State Energetics in First-Row Transition Metal Complexes: Contribution of (3s3p) Correlation and Its Description by Second-Order Perturbation Theory. *J. Chem. Theory Comput.* **2017**, *13*, 537–553.
- (166) Phung, Q. M.; Feldt, M.; Harvey, J. N.; Pierloot, K. Toward Highly Accurate Spin State Energetics in First-Row Transition Metal Complexes: A Combined CASPT2/CC Approach. *J. Chem. Theory Comput.* **2018**, *14*, 2446–2455.
- (167) Harding, M. E.; Metzroth, T.; Gauss, J.; Auer, A. A. Parallel Calculation of CCSD and CCSD(T) Analytic First and Second Derivatives. *J. Chem. Theory Comput.* **2008**, *4*, 64–74.
- (168) Atanasov, M.; Zadrozny, J. M.; Long, J. R.; Neese, F. A theoretical analysis of chemical bonding, vibronic coupling, and magnetic anisotropy in linear iron(II) complexes with single-molecule magnet behavior. *Chem. Sci.* **2013**, *4*, 139–156.
- (169) Guo, Y.; Sivalingam, K.; Valeev, E. F.; Neese, F. SparseMaps—A systematic infrastructure for reduced-scaling electronic structure methods. III. Linear-scaling multireference domain-based pair natural orbital *N*-electron valence perturbation theory. *J. Chem. Phys.* **2016**, *144*, 094111.
- (170) Coughtrie, D. J.; Giereth, R.; Kats, D.; Werner, H.-J.; Köhn, A. Embedded Multireference Coupled Cluster Theory. *J. Chem. Theory Comput.* **2018**, *14*, 693–709.
- (171) Fleig, T.; Olsen, J.; Marian, C. M. The generalized active space concept for the relativistic treatment of electron correlation. I. Kramers-restricted two-component configuration interaction. *J. Chem. Phys.* **2001**, *114*, 4775–4790.
- (172) Schollwöck, U. The density-matrix renormalization group. *Rev. Mod. Phys.* **2005**, *77*, 259–315.
- (173) Marti, K. H.; Ondík, I. M.; Moritz, G.; Reiher, M. Density matrix renormalization group calculations on relative energies of transition metal complexes and clusters. *J. Chem. Phys.* **2008**, *128*, 014104.
- (174) Roos, B. O. Multiconfigurational quantum chemistry. In *Theory and Applications of Computational Chemistry*; Elsevier: 2005; pp 725–764, DOI: [10.1016/B978-044451719-7/50068-8](https://doi.org/10.1016/B978-044451719-7/50068-8).
- (175) Ruedenberg, K.; Cheung, L. M.; Elbert, S. T. MCSCF optimization through combined use of natural orbitals and the

Brillouin–Levy–Berthier theorem. *Int. J. Quantum Chem.* **1979**, *16*, 1069–1101.

(176) Werner, H.-J.; Meyer, W. A quadratically convergent MCSCF method for the simultaneous optimization of several states. *J. Chem. Phys.* **1981**, *74*, 5794–5801.

(177) Bao, J. J.; Gagliardi, L.; Truhlar, D. G. Multiconfiguration pair-density functional theory for doublet excitation energies and excited state geometries: the excited states of CN. *Phys. Chem. Chem. Phys.* **2017**, *19*, 30089–30096.

(178) Bao, J. L.; Gagliardi, L.; Truhlar, D. G. Self-Interaction Error in Density Functional Theory: An Appraisal. *J. Phys. Chem. Lett.* **2018**, *9*, 2353–2358.

(179) Sharma, P.; Bernales, V.; Truhlar, D. G.; Gagliardi, L. Valence $\pi\pi^*$ Excitations in Benzene Studied by Multiconfiguration Pair-Density Functional Theory. *J. Phys. Chem. Lett.* **2019**, *10*, 75–81.

(180) Gáspár, R. Über eine Approximation des Hartree-Fockschen Potentials Durch eine Universelle Potentialfunktion. *Acta Phys. Acad. Sci. Hung.* **1954**, *3*, 263–286.

(181) Vosko, S. H.; Wilk, L.; Nusair, M. Accurate spin-dependent electron liquid correlation energies for local spin density calculations: a critical analysis. *Can. J. Phys.* **1980**, *58*, 1200–1211.

(182) Perdew, J. P.; Burke, K.; Ernzerhof, M. Generalized Gradient Approximation Made Simple. *Phys. Rev. Lett.* **1996**, *77*, 3865–3868.

(183) Zhang, Y.; Yang, W. Comment on “Generalized Gradient Approximation Made Simple”. *Phys. Rev. Lett.* **1998**, *80*, 890–890a.

(184) Hoyer, C. E.; Ghosh, S.; Truhlar, D. G.; Gagliardi, L. Multiconfiguration Pair-Density Functional Theory Is as Accurate as CASPT2 for Electronic Excitation. *J. Phys. Chem. Lett.* **2016**, *7*, 586–591.

(185) Becke, A. D. Density-functional exchange-energy approximation with correct asymptotic behavior. *Phys. Rev. A: At, Mol, Opt. Phys.* **1988**, *38*, 3098–3100.

(186) Lee, C.; Yang, W.; Parr, R. G. Development of the Colle–Salvetti correlation-energy formula into a functional of the electron density. *Phys. Rev. B: Condens. Matter Mater. Phys.* **1988**, *37*, 785–789.

(187) Handy, N. C.; Cohen, A. J. Left–right correlation energy. *Mol. Phys.* **2001**, *99*, 403–412.

(188) Bao, J. J.; Gagliardi, L.; Truhlar, D. G. Weak Interactions in Alkaline Earth Metal Dimers by Pair-Density Functional Theory. *J. Phys. Chem. Lett.* **2019**, *10*, 799–805.

(189) Verma, P.; Truhlar, D. G. HLE16: A Local Kohn–Sham Gradient Approximation with Good Performance for Semiconductor Band Gaps and Molecular Excitation Energies. *J. Phys. Chem. Lett.* **2017**, *8*, 380–387.

(190) Verma, P.; Truhlar, D. G. HLE17: An Improved Local Exchange–Correlation Functional for Computing Semiconductor Band Gaps and Molecular Excitation Energies. *J. Phys. Chem. C* **2017**, *121*, 7144–7154.

(191) Sand, A. M.; Truhlar, D. G.; Gagliardi, L. Efficient algorithm for multiconfiguration pair-density functional theory with application to the heterolytic dissociation energy of ferrocene. *J. Chem. Phys.* **2017**, *146*, 034101.

(192) Odoh, S. O.; Li Manni, G.; Carlson, R. K.; Truhlar, D. G.; Gagliardi, L. Separated-pair approximation and separated-pair pair-density functional theory. *Chem. Sci.* **2016**, *7*, 2399–2413.

(193) Bao, J. L.; Odoh, S. O.; Gagliardi, L.; Truhlar, D. G. Predicting Bond Dissociation Energies of Transition-Metal Compounds by Multiconfiguration Pair-Density Functional Theory and Second-Order Perturbation Theory Based on Correlated Participating Orbitals and Separated Pairs. *J. Chem. Theory Comput.* **2017**, *13*, 616–626.

(194) Ghosh, S.; Cramer, C. J.; Truhlar, D. G.; Gagliardi, L. Generalized-active-space pair-density functional theory: an efficient method to study large, strongly correlated, conjugated systems. *Chem. Sci.* **2017**, *8*, 2741–2750.

(195) Bao, J. L.; Sand, A.; Gagliardi, L.; Truhlar, D. G. Correlated-Participating-Orbitals Pair-Density Functional Method and Application to Multiplet Energy Splittings of Main-Group Divalent Radicals. *J. Chem. Theory Comput.* **2016**, *12*, 4274–4283.

(196) Stoneburner, S. J.; Truhlar, D. G.; Gagliardi, L. MC-PDFT can calculate singlet–triplet splittings of organic diradicals. *J. Chem. Phys.* **2018**, *148*, 064108.

(197) Wilbraham, L.; Verma, P.; Truhlar, D. G.; Gagliardi, L.; Ciofini, I. Multiconfiguration Pair-Density Functional Theory Predicts Spin-State Ordering in Iron Complexes with the Same Accuracy as Complete Active Space Second-Order Perturbation Theory at a Significantly Reduced Computational Cost. *J. Phys. Chem. Lett.* **2017**, *8*, 2026–2030.

(198) Ghosh, S.; Sonnenberger, A. L.; Hoyer, C. E.; Truhlar, D. G.; Gagliardi, L. Multiconfiguration Pair-Density Functional Theory Outperforms Kohn–Sham Density Functional Theory and Multi-reference Perturbation Theory for Ground-State and Excited-State Charge Transfer. *J. Chem. Theory Comput.* **2015**, *11*, 3643–3649.

(199) Hoyer, C. E.; Gagliardi, L.; Truhlar, D. G. Multiconfiguration Pair-Density Functional Theory Spectral Calculations Are Stable to Adding Diffuse Basis Functions. *J. Phys. Chem. Lett.* **2015**, *6*, 4184–4188.

(200) Dong, S. S.; Gagliardi, L.; Truhlar, D. G. Excitation spectra of retinal by multiconfiguration pair-density functional theory. *Phys. Chem. Chem. Phys.* **2018**, *20*, 7265–7276.

(201) Bao, J. J.; Dong, S. S.; Gagliardi, L.; Truhlar, D. G. Automatic Selection of an Active Space for Calculating Electronic Excitation Spectra by MS-CASPT2 or MC-PDFT. *J. Chem. Theory Comput.* **2018**, *14*, 2017–2025.

(202) Ghosh, S.; Verma, P.; Cramer, C. J.; Gagliardi, L.; Truhlar, D. G. Combining Wave Function Methods with Density Functional Theory for Excited States. *Chem. Rev. (Washington, DC, U. S.)* **2018**, *118*, 7249–7292.

(203) Fleig, T.; Olsen, J.; Visscher, L. The generalized active space concept for the relativistic treatment of electron correlation. II. Large-scale configuration interaction implementation based on relativistic 2- and 4-spinors and its application. *J. Chem. Phys.* **2003**, *119*, 2963–2971.

(204) Tishchenko, O.; Zheng, J.; Truhlar, D. G. Multireference Model Chemistries for Thermochemical Kinetics. *J. Chem. Theory Comput.* **2008**, *4*, 1208–1219.

(205) Sand, A. M.; Hoyer, C. E.; Sharkas, K.; Kidder, K. M.; Lindh, R.; Truhlar, D. G.; Gagliardi, L. Analytic Gradients for Complete Active Space Pair-Density Functional Theory. *J. Chem. Theory Comput.* **2018**, *14*, 126–138.

(206) Sharma, P.; Bernales, V.; Knecht, S.; Truhlar, D. G.; Gagliardi, L. Density matrix renormalization group pair-density functional theory (DMRG-PDFT): singlet–triplet gaps in polyacenes and polyacetylenes. *Chem. Sci.* **2019**, *10*, 1716–1723.

(207) Zhou, C.; Gagliardi, L.; Truhlar, D. G. Multiconfiguration Pair-Density Functional Theory for Iron Porphyrin with CAS, RAS, and DMRG Active Spaces. *J. Phys. Chem. A* **2019**, *123*, 3389–3394.

(208) Freitag, L.; Keller, S.; Knecht, S.; Ma, Y.; Stein, C.; Reiher, M. A quick user guide to the SCINE-QCMAQUIS software suite for OpenMolcas; 2018. https://scine.ethz.ch/static/download/qcmaquis_manual.pdf (accessed Sept 19, 2019).

(209) Sand, A. M.; Hoyer, C. E.; Truhlar, D. G.; Gagliardi, L. State-interaction pair-density functional theory. *J. Chem. Phys.* **2018**, *149*, 024106.

(210) Dong, S. S.; Huang, K. B.; Gagliardi, L.; Truhlar, D. G. State-Interaction Pair-Density Functional Theory Can Accurately Describe a Spiro Mixed Valence Compound. *J. Phys. Chem. A* **2019**, *123*, 2100–2106.

(211) Finley, J.; Malmqvist, P.-Å.; Roos, B. O.; Serrano-Andrés, L. The multi-state CASPT2 method. *Chem. Phys. Lett.* **1998**, *288*, 299–306.

(212) Granovsky, A. A. Extended multi-configuration quasi-degenerate perturbation theory: The new approach to multi-state multi-reference perturbation theory. *J. Chem. Phys.* **2011**, *134*, 214113.

(213) Nakano, H. Quasidegenerate perturbation theory with multiconfigurational self-consistent-field reference functions. *J. Chem. Phys.* **1993**, *99*, 7983–7992.

- (214) Nakano, H. MCSCF reference quasidegenerate perturbation theory with Epstein–Nesbet partitioning. *Chem. Phys. Lett.* **1993**, *207*, 372–378.
- (215) Malhado, J. P.; Bearpark, M. J.; Hynes, J. T. Non-adiabatic dynamics close to conical intersections and the surface hopping perspective. *Front. Chem. (Lausanne, Switz.)* **2014**, *2*, DOI: 10.3389/fchem.2014.00097.
- (216) Jasper, A. W.; Kendrick, B. K.; Mead, C. A.; Truhlar, D. G. Non-Born–Oppenheimer Chemistry: Potential Surfaces, Couplings, and Dynamics. In *Modern Trends in Chemical Reaction Dynamics*; World Scientific: 2004; pp 329–391, DOI: 10.1142/9789812565426_0008.
- (217) Vacher, M.; Bearpark, M. J.; Robb, M. A. Direct methods for non-adiabatic dynamics: connecting the single-set variational multi-configuration Gaussian (vMCG) and Ehrenfest perspectives. *Theor. Chem. Acc.* **2016**, *135*, 187.
- (218) Maeda, S.; Ohno, K.; Morokuma, K. Updated Branching Plane for Finding Conical Intersections without Coupling Derivative Vectors. *J. Chem. Theory Comput.* **2010**, *6*, 1538–1545.
- (219) Fdez. Galván, I.; Delcey, M. G.; Pedersen, T. B.; Aquilante, F.; Lindh, R. Analytical State-Average Complete-Active-Space Self-Consistent Field Nonadiabatic Coupling Vectors: Implementation with Density-Fitted Two-Electron Integrals and Application to Conical Intersections. *J. Chem. Theory Comput.* **2016**, *12*, 3636–3653.
- (220) Lischka, H.; Dallos, M.; Szalay, P. G.; Yarkony, D. R.; Shepard, R. Analytic evaluation of nonadiabatic coupling terms at the MR-CI level. I. Formalism. *J. Chem. Phys.* **2004**, *120*, 7322–7329.
- (221) Anglada, J. M.; Boffill, J. M. A reduced-restricted-quasi-Newton–Raphson method for locating and optimizing energy crossing points between two potential energy surfaces. *J. Comput. Chem.* **1997**, *18*, 992–1003.
- (222) De Vico, L.; Olivucci, M.; Lindh, R. New General Tools for Constrained Geometry Optimizations. *J. Chem. Theory Comput.* **2005**, *1*, 1029–1037.
- (223) Vreven, T.; Bernardi, F.; Garavelli, M.; Olivucci, M.; Robb, M. A.; Schlegel, H. B. *Ab Initio* Photoisomerization Dynamics of a Simple Retinal Chromophore Model. *J. Am. Chem. Soc.* **1997**, *119*, 12687–12688.
- (224) Tully, J. C. Molecular dynamics with electronic transitions. *J. Chem. Phys.* **1990**, *93*, 1061–1071.
- (225) García-Iriepa, C.; Marazzi, M.; Zapata, F.; Valentini, A.; Sampedro, D.; Frutos, L. M. Chiral Hydrogen Bond Environment Providing Unidirectional Rotation in Photoactive Molecular Motors. *J. Phys. Chem. Lett.* **2013**, *4*, 1389–1396.
- (226) Gozem, S.; Melaccio, F.; Valentini, A.; Filatov, M.; Huix-Rotllant, M.; Ferré, N.; Frutos, L. M.; Angeli, C.; Krylov, A. I.; Granovsky, A. A.; Lindh, R.; Olivucci, M. Shape of Multireference, Equation-of-Motion Coupled-Cluster, and Density Functional Theory Potential Energy Surfaces at a Conical Intersection. *J. Chem. Theory Comput.* **2014**, *10*, 3074–3084.
- (227) Marchand, G.; Eng, J.; Schapiro, I.; Valentini, A.; Frutos, L. M.; Pieri, E.; Olivucci, M.; Léonard, J.; Gindensperger, E. Directionality of Double-Bond Photoisomerization Dynamics Induced by a Single Stereogenic Center. *J. Phys. Chem. Lett.* **2015**, *6*, 599–604.
- (228) Manathunga, M.; Yang, X.; Luk, H. L.; Gozem, S.; Frutos, L. M.; Valentini, A.; Ferré, N.; Olivucci, M. Probing the Photodynamics of Rhodopsins with Reduced Retinal Chromophores. *J. Chem. Theory Comput.* **2016**, *12*, 839–850.
- (229) Valentini, A.; Rivero, D.; Zapata, F.; García-Iriepa, C.; Marazzi, M.; Palmeiro, R.; Fdez. Galván, I.; Sampedro, D.; Olivucci, M.; Frutos, L. M. Optomechanical Control of Quantum Yield in *Trans–Cis* Ultrafast Photoisomerization of a Retinal Chromophore Model. *Angew. Chem., Int. Ed.* **2017**, *56*, 3842–3846.
- (230) Gueye, M.; Manathunga, M.; Agathangelou, D.; Orozco, Y.; Paolino, M.; Fusi, S.; Haacke, S.; Olivucci, M.; Léonard, J. Engineering the vibrational coherence of vision into a synthetic molecular device. *Nat. Commun.* **2018**, *9*, 313.
- (231) García-Iriepa, C.; Sampedro, D.; Mendicuti, F.; Léonard, J.; Frutos, L. M. Photoreactivity Control Mediated by Molecular Force Probes in Stilbene. *J. Phys. Chem. Lett.* **2019**, *10*, 1063–1067.
- (232) Schnedermann, C.; Yang, X.; Liebel, M.; Spillane, K. M.; Lugtenburg, J.; Fernández, I.; Valentini, A.; Schapiro, I.; Olivucci, M.; Kukura, P.; Mathies, R. A. Evidence for a vibrational phase-dependent isotope effect on the photochemistry of vision. *Nat. Chem.* **2018**, *10*, 449–455.
- (233) Schapiro, I.; Ryazantsev, M. N.; Frutos, L. M.; Ferré, N.; Lindh, R.; Olivucci, M. The Ultrafast Photoisomerizations of Rhodopsin and Bathorhodopsin Are Modulated by Bond Length Alternation and HOOP Driven Electronic Effects. *J. Am. Chem. Soc.* **2011**, *133*, 3354–3364.
- (234) Gozem, S.; Luk, H. L.; Schapiro, I.; Olivucci, M. Theory and Simulation of the Ultrafast Double-Bond Isomerization of Biological Chromophores. *Chem. Rev. (Washington, DC, U. S.)* **2017**, *117*, 13502–13565.
- (235) Vacher, M.; Farahani, P.; Valentini, A.; Frutos, L. M.; Karlsson, H. O.; Fdez. Galván, I.; Lindh, R. How Do Methyl Groups Enhance the Triplet Chemiexcitation Yield of Dioxetane? *J. Phys. Chem. Lett.* **2017**, *8*, 3790–3794.
- (236) Richter, M.; Marquetand, P.; González-Vázquez, J.; Sola, I.; González, L. SHARC: *Ab Initio* Molecular Dynamics with Surface Hopping in the Adiabatic Representation Including Arbitrary Couplings. *J. Chem. Theory Comput.* **2011**, *7*, 1253–1258.
- (237) Mai, S.; Marquetand, P.; González, L. A general method to describe intersystem crossing dynamics in trajectory surface hopping. *Int. J. Quantum Chem.* **2015**, *115*, 1215–1231.
- (238) Mai, S.; Marquetand, P.; González, L. Nonadiabatic dynamics: The SHARC approach. *Wiley Interdiscip. Rev.: Comput. Mol. Sci.* **2018**, *8*, No. e1370.
- (239) Mai, S.; Richter, M.; Heindl, M.; Menger, M. F. S. J.; Atkins, A.; Ruckebauer, M.; Plasser, F.; Oppel, M.; Marquetand, P.; González, L. SHARC2.0: *Surface Hopping Including Arbitrary Couplings – A Program Package for Non-Adiabatic Dynamics*; 2018. <https://www.sharc-md.org> (accessed Sept 19, 2019).
- (240) SHARC GitHub repository. <https://github.com/sharc-md/sharc> (accessed Sept 19, 2019).
- (241) Granucci, G.; Persico, M.; Toniolo, A. Direct semiclassical simulation of photochemical processes with semiempirical wave functions. *J. Chem. Phys.* **2001**, *114*, 10608–10615.
- (242) Plasser, F.; Ruckebauer, M.; Mai, S.; Oppel, M.; Marquetand, P.; González, L. Efficient and Flexible Computation of Many-Electron Wave Function Overlaps. *J. Chem. Theory Comput.* **2016**, *12*, 1207–1219.
- (243) Worth, G. A.; Giri, K.; Richings, G. W.; Burghardt, I.; Beck, M. H.; Jäckle, A.; Meyer, H.-D. *QUANTICS Package*, Version 1.1; University of Birmingham: Birmingham, U.K., 2015. <http://chemb125.chem.ucl.ac.uk/quantics/> (accessed Sept 19, 2019).
- (244) Worth, G. A.; Beck, M. H.; Jäckle, A.; Meyer, H.-D. *MCTDH Package*, Version 8.3; 2003. <http://www.pci.uni-heidelberg.de/tc/usr/mctdh/> (accessed Sept 19, 2019).
- (245) Burghardt, I.; Meyer, H.-D.; Cederbaum, L. S. Approaches to the approximate treatment of complex molecular systems by the multiconfiguration time-dependent Hartree method. *J. Chem. Phys.* **1999**, *111*, 2927–2939.
- (246) Richings, G. W.; Polyak, I.; Spinlove, K. E.; Worth, G. A.; Burghardt, I.; Lasorne, B. Quantum dynamics simulations using Gaussian wavepackets: the vMCG method. *Int. Rev. Phys. Chem.* **2015**, *34*, 269–308.
- (247) Although not implemented yet, one could read the relevant information instead from the HDF5 standard format files generated by OpenMolcas.
- (248) Köppel, H.; Schubert, B. The concept of regularized diabatic states for a general conical intersection. *Mol. Phys.* **2006**, *104*, 1069–1079.
- (249) Richings, G. W.; Worth, G. A. A Practical Diabatization Scheme for Use with the Direct-Dynamics Variational Multi-

Configuration Gaussian Method. *J. Phys. Chem. A* **2015**, *119*, 12457–12470.

(250) Collins, M. A.; Zhang, D. H. Application of interpolated potential energy surfaces to quantum reactive scattering. *J. Chem. Phys.* **1999**, *111*, 9924–9931.

(251) Frankcombe, T. J. Using Hessian update formulae to construct modified Shepard interpolated potential energy surfaces: Application to vibrating surface atoms. *J. Chem. Phys.* **2014**, *140*, 114108.

(252) Heß, B. A.; Marian, C. M.; Wahlgren, U.; Gropen, O. A mean-field spin-orbit method applicable to correlated wavefunctions. *Chem. Phys. Lett.* **1996**, *251*, 365–371.

(253) Bernadotte, S.; Atkins, A. J.; Jacob, C. R. Origin-independent calculation of quadrupole intensities in X-ray spectroscopy. *J. Chem. Phys.* **2012**, *137*, 204106.

(254) Guo, M.; Sørensen, L. K.; Delcey, M. G.; Pinjari, R. V.; Lundberg, M. Simulations of iron K pre-edge X-ray absorption spectra using the restricted active space method. *Phys. Chem. Chem. Phys.* **2016**, *18*, 3250–3259.

(255) Guo, M.; Källman, E.; Sørensen, L. K.; Delcey, M. G.; Pinjari, R. V.; Lundberg, M. Molecular Orbital Simulations of Metal 1s_{2p} Resonant Inelastic X-ray Scattering. *J. Phys. Chem. A* **2016**, *120*, 5848–5855.

(256) Sørensen, L. K.; Lindh, R.; Lundberg, M. Gauge origin independence in finite basis sets and perturbation theory. *Chem. Phys. Lett.* **2017**, *683*, 536–542.

(257) Sørensen, L. K.; Guo, M.; Lindh, R.; Lundberg, M. Applications to metal K pre-edges of transition metal dimers illustrate the approximate origin independence for the intensities in the length representation. *Mol. Phys.* **2017**, *115*, 174–189.

(258) List, N. H.; Kauczor, J.; Saue, T.; Jensen, H. J. Aa.; Norman, P. Beyond the electric-dipole approximation: A formulation and implementation of molecular response theory for the description of absorption of electromagnetic field radiation. *J. Chem. Phys.* **2015**, *142*, 244111.

(259) Sørensen, L. K.; Kieri, E.; Srivastav, S.; Lundberg, M.; Lindh, R. Implementation of a semiclassical light-matter interaction using the Gauss–Hermite quadrature: A simple alternative to the multipole expansion. *Phys. Rev. A: At., Mol., Opt. Phys.* **2019**, *99*, 013419.

(260) List, N. H.; Saue, T.; Norman, P. Rotationally averaged linear absorption spectra beyond the electric-dipole approximation. *Mol. Phys.* **2017**, *115*, 63–74.

(261) Hahn, J. E.; Scott, R. A.; Hodgson, K. O.; Doniach, S.; Desjardins, S. R.; Solomon, E. I. Observation of an electric quadrupole transition in the X-ray absorption spectrum of a Cu(II) complex. *Chem. Phys. Lett.* **1982**, *88*, 595–598.

(262) Josefsson, I.; Kunnus, K.; Schreck, S.; Föhlisch, A.; de Groot, F.; Wernet, P.; Odelius, M. Ab Initio Calculations of X-ray Spectra: Atomic Multiplet and Molecular Orbital Effects in a Multiconfigurational SCF Approach to the L-Edge Spectra of Transition Metal Complexes. *J. Phys. Chem. Lett.* **2012**, *3*, 3565–3570.

(263) Bokarev, S. I.; Dantz, M.; Suljoti, E.; Kühn, O.; Aziz, E. F. State-Dependent Electron Delocalization Dynamics at the Solute–Solvent Interface: Soft-X-Ray Absorption Spectroscopy and Ab Initio Calculations. *Phys. Rev. Lett.* **2013**, *111*, 083002.

(264) Pinjari, R. V.; Delcey, M. G.; Guo, M.; Odelius, M.; Lundberg, M. Restricted active space calculations of L-edge X-ray absorption spectra: From molecular orbitals to multiplet states. *J. Chem. Phys.* **2014**, *141*, 124116.

(265) Sergentu, D.-C.; Duignan, T. J.; Autschbach, J. Ab Initio Study of Covalency in the Ground versus Core-Excited States and X-ray Absorption Spectra of Actinide Complexes. *J. Phys. Chem. Lett.* **2018**, *9*, 5583–5591.

(266) Pinjari, R. V.; Delcey, M. G.; Guo, M.; Odelius, M.; Lundberg, M. Cost and sensitivity of restricted active-space calculations of metal L-edge X-ray absorption spectra. *J. Comput. Chem.* **2016**, *37*, 477–486.

(267) Nyvang, A.; Malmqvist, P. Å.; Veryazov, V. A generally-contracted Gaussian basis set for photochemistry and photophysics in the range 0–2 keV; Poster at Swedish Theoretical Chemistry meeting

2017; 2017. http://www.molcas.org/VV/poster2_Gothenburg.pdf (accessed Sept 19, 2019).

(268) Cederbaum, L. S.; Domcke, W.; Schirmer, J. Many-body theory of core holes. *Phys. Rev. A: At., Mol., Opt. Phys.* **1980**, *22*, 206–222.

(269) Delcey, M. G.; Sørensen, L. K.; Vacher, M.; Couto, R. C.; Lundberg, M. Efficient calculations of a large number of highly excited states for multiconfigurational wavefunctions. *J. Comput. Chem.* **2019**, *40*, 1789–1799.

(270) Malmqvist, P.-Å.; Roos, B. O. The CASSCF state interaction method. *Chem. Phys. Lett.* **1989**, *155*, 189–194.

(271) Olsen, J.; Jørgensen, P.; Simons, J. Passing the one-billion limit in full configuration-interaction (FCI) calculations. *Chem. Phys. Lett.* **1990**, *169*, 463–472.

(272) Grell, G.; Bokarev, S. I.; Winter, B.; Seidel, R.; Aziz, E. F.; Aziz, S. G.; Kühn, O. Multi-reference approach to the calculation of photoelectron spectra including spin-orbit coupling. *J. Chem. Phys.* **2015**, *143*, 074104.

(273) Grell, G.; Bokarev, S. I.; Winter, B.; Seidel, R.; Aziz, E. F.; Aziz, S. G.; Kühn, O. Erratum: "Multi-reference approach to the calculation of photoelectron spectra including spin-orbit coupling" [*J. Chem. Phys.* **143**, 074104 (2015)]. *J. Chem. Phys.* **2016**, *145*, 089901.

(274) Malmqvist, P. Å. Calculation of transition density matrices by nonunitary orbital transformations. *Int. J. Quantum Chem.* **1986**, *30*, 479–494.

(275) Cremaschi, P. A theoretical analysis of the four-photon ionization spectrum of the nitric oxide molecule. *J. Chem. Phys.* **1981**, *75*, 3944–3953.

(276) Moguelevski, A.; Wilke, M.; Grell, G.; Bokarev, S. I.; Aziz, S. G.; Engel, N.; Raheem, A. A.; Kühn, O.; Kiyani, I. Y.; Aziz, E. F. Ultrafast Spin Crossover in [Fe^{II}(bpy)₃]²⁺: Revealing Two Competing Mechanisms by Extreme Ultraviolet Photoemission Spectroscopy. *ChemPhysChem* **2017**, *18*, 465–469.

(277) Golnak, R.; Bokarev, S. I.; Seidel, R.; Xiao, J.; Grell, G.; Atak, K.; Unger, I.; Thürmer, S.; Aziz, S. G.; Kühn, O.; Winter, B.; Aziz, E. F. Joint Analysis of Radiative and Non-Radiative Electronic Relaxation Upon X-ray Irradiation of Transition Metal Aqueous Solutions. *Sci. Rep.* **2016**, *6*, 24659.

(278) Norell, J.; Grell, G.; Kühn, O.; Odelius, M.; Bokarev, S. I. Photoelectron shake-ups as a probe of molecular symmetry: 4d XPS analysis of I₃⁻ in solution. *Phys. Chem. Chem. Phys.* **2018**, *20*, 19916–19921.

(279) Josefsson, I.; Eriksson, S. K.; Ottosson, N.; Öhrwall, G.; Siegbahn, H.; Hagfeldt, A.; Rensmo, H.; Björneholm, O.; Odelius, M. Collective hydrogen-bond dynamics dictates the electronic structure of aqueous I₃⁻. *Phys. Chem. Chem. Phys.* **2013**, *15*, 20189.

(280) Piepho, S. B.; Schatz, P. N. *Group theory in spectroscopy*; John Wiley & Sons: New York, 1983.

(281) Neese, F.; Solomon, E. I. MCD C-Term Signs, Saturation Behavior, and Determination of Band Polarizations in Randomly Oriented Systems with Spin S ≥ 1/2. Applications to S = 1/2 and S = 5/2. *Inorg. Chem.* **1999**, *38*, 1847–1865.

(282) Buckingham, A. D.; Stephens, P. J. Magnetic Optical Activity. *Annu. Rev. Phys. Chem.* **1966**, *17*, 399–432.

(283) Stephens, P. J. Theory of Magnetic Circular Dichroism. *J. Chem. Phys.* **1970**, *52*, 3489.

(284) Gendron, F.; Fleischauer, V. E.; Duignan, T. J.; Scott, B. L.; Löble, M. W.; Cary, S. K.; Kozimor, S. A.; Bolvin, H.; Neidig, M. L.; Autschbach, J. Magnetic circular dichroism of UCl₆⁻ in the ligand-to-metal charge-transfer spectral region. *Phys. Chem. Chem. Phys.* **2017**, *19*, 17300–17313.

(285) Bolvin, H. Theoretical Determination of the Excited States and of g-Factors of the Creutz–Taube Ion, [(NH₃)₅-Ru-pyrazine-Ru(NH₃)₅]³⁺. *Inorg. Chem.* **2007**, *46*, 417–427.

(286) MCD-molcas, tools for calculating MCD spectra with OpenMolcas. <https://github.com/jautschbach/mcd-molcas.git> (accessed Sept 19, 2019).

(287) Heit, Y. N.; Sergentu, D.-C.; Autschbach, J. Magnetic circular dichroism spectra of transition metal complexes calculated from

restricted active space wavefunctions. *Phys. Chem. Chem. Phys.* **2019**, *21*, 5586–5597.

(288) Gnuplot 4.6: an interactive plotting program. <http://gnuplot.sourceforge.net> (accessed Sept 19, 2019).

(289) Lines, M. E. Orbital Angular Momentum in the Theory of Paramagnetic Clusters. *J. Chem. Phys.* **1971**, *55*, 2977–2984.

(290) Chibotaru, L. F.; Iwahara, N. Ising exchange interaction in lanthanides and actinides. *New J. Phys.* **2015**, *17*, 103028.

(291) Noodleman, L.; Case, D. A.; Aizman, A. Broken symmetry analysis of spin coupling in iron–sulfur clusters. *J. Am. Chem. Soc.* **1988**, *110*, 1001–1005.

(292) Shoji, M.; Koizumi, K.; Kitagawa, Y.; Kawakami, T.; Yamanaka, S.; Okumura, M.; Yamaguchi, K. A general algorithm for calculation of Heisenberg exchange integrals J in multispin systems. *Chem. Phys. Lett.* **2006**, *432*, 343–347.

(293) Langley, S. K.; Wielechowski, D. P.; Vieru, V.; Chilton, N. F.; Moubaraki, B.; Abrahams, B. F.; Chibotaru, L. F.; Murray, K. S. A $\{Cr^{III}_2Dy^{III}_2\}$ Single-Molecule Magnet: Enhancing the Blocking Temperature through 3d Magnetic Exchange. *Angew. Chem., Int. Ed.* **2013**, *52*, 12014–12019.

(294) Bencini, A.; Gatteschi, D. *Electron Paramagnetic Resonance of Exchange Coupled Systems*; Springer Berlin Heidelberg: 1990; DOI: 10.1007/978-3-642-74599-7.

(295) Chibotaru, L. F. Theoretical Understanding of Anisotropy in Molecular Nanomagnets. In *Molecular Nanomagnets and Related Phenomena*; Springer Berlin Heidelberg: 2014; pp 185–229, DOI: 10.1007/430_2014_171.

(296) Chibotaru, L. F.; Ungur, L. Ab initio calculation of anisotropic magnetic properties of complexes. I. Unique definition of pseudospin Hamiltonians and their derivation. *J. Chem. Phys.* **2012**, *137*, 064112.

(297) Chibotaru, L. F. In *Ab Initio Methodology for Pseudospin Hamiltonians of Anisotropic Magnetic Complexes*; Rice, S. A., Dinner, A. R., Eds.; Advances in Chemical Physics; John Wiley & Sons, Inc.: 2013; Vol. 153, pp 397–519, DOI: 10.1002/9781118571767.ch6.

(298) Varshalovich, D. A.; Moskalev, A. N.; Khersonskii, V. K. *Quantum Theory of Angular Momentum*; World Scientific: 1988; DOI: 10.1142/0270.

(299) Rudowicz, C. Transformation relations for the conventional O_k^q and normalised O_k^q Stevens operator equivalents with $k = 1$ to 6 and $J - k \leq q \leq k$. *J. Phys. C: Solid State Phys.* **1985**, *18*, 1415–1430.

(300) Rudowicz, C.; Chung, C. Y. The generalization of the extended Stevens operators to higher ranks and spins, and a systematic review of the tables of the tensor operators and their matrix elements. *J. Phys.: Condens. Matter* **2004**, *16*, 5825–5847.

(301) Stoll, S.; Schweiger, A. EasySpin, a comprehensive software package for spectral simulation and analysis in EPR. *J. Magn. Reson.* **2006**, *178*, 42–55.

(302) Chibotaru, L. F.; Ungur, L.; Soncini, A. The Origin of Nonmagnetic Kramers Doublets in the Ground State of Dysprosium Triangles: Evidence for a Toroidal Magnetic Moment. *Angew. Chem., Int. Ed.* **2008**, *47*, 4126–4129.

(303) Chibotaru, L. F.; Ungur, L.; Aronica, C.; Elmoll, H.; Pilet, G.; Luneau, D. Structure, Magnetism, and Theoretical Study of a Mixed-Valence $Co^{II}_3Co^{III}_4$ Heptanuclear Wheel: Lack of SMM Behavior despite Negative Magnetic Anisotropy. *J. Am. Chem. Soc.* **2008**, *130*, 12445–12455.

(304) Vieru, V.; Iwahara, N.; Ungur, L.; Chibotaru, L. F. Giant exchange interaction in mixed lanthanides. *Sci. Rep.* **2016**, *6*, 24046.

(305) Ungur, L.; Thewissen, M.; Costes, J.-P.; Wernsdorfer, W.; Chibotaru, L. F. Interplay of Strongly Anisotropic Metal Ions in Magnetic Blocking of Complexes. *Inorg. Chem.* **2013**, *52*, 6328–6337.

(306) Dattani, N. S.; Li Manni, G.; Feller, D.; Koput, J. Submitted for publication.

(307) Dattani, N. Computer Spectrometers. In *Proceedings of the 72nd International Symposium on Molecular Spectroscopy*; 2017; DOI: 10.15278/isms.2017.MI08.

(308) Gagliardi, L.; Lindh, R.; Karlström, G. Local properties of quantum chemical systems: The LoProp approach. *J. Chem. Phys.* **2004**, *121*, 4494–4500.

(309) Schaftenaar, G.; Noordik, J. H. Molden: A pre- and post-processing program for molecular and electronic structures. *J. Comput.-Aided Mol. Des.* **2000**, *14*, 123–134.

(310) Kováčević, G.; Veryazov, V. LUSCUS: molecular viewer and editor for MOLCAS. *J. Cheminf.* **2015**, *7*, 16.

(311) Williams, S. In *Free As in Freedom: Richard Stallman's Crusade for Free Software*, 1st ed.; Petrycki, L., Ed.; O'Reilly & Associates, Inc.: Sebastopol, CA, USA, 2002.

(312) SAGIT, a grid generator distributed under the LGPL license. <https://sourceforge.net/projects/sagit/> (accessed Sept 19, 2019).

(313) Pegamoid, an orbital viewer especially suited for use with OpenMolcas. <https://pypi.org/project/Pegamoid> (accessed Sept 19, 2019).

(314) Plasser, F.; Wormit, M.; Dreuw, A. New tools for the systematic analysis and visualization of electronic excitations. I. Formalism. *J. Chem. Phys.* **2014**, *141*, 024106.

(315) Dong, S. S.; Gagliardi, L.; Truhlar, D. G. Nature of the 1^1B_u and 2^1A_g Excited States of Butadiene and the Goldilocks Principle of Basis Set Diffuseness. *J. Chem. Theory Comput.* **2019**, *15*, 4591–4601.

(316) Amos, A. T.; Hall, G. G. Single Determinant Wave Functions. *Proc. R. Soc. London, Ser. A* **1961**, *263*, 483–493.

(317) Martin, R. L. Natural transition orbitals. *J. Chem. Phys.* **2003**, *118*, 4775–4777.

(318) Mayer, I. Identifying a pair of interacting chromophores by using SVD transformed CIS wave functions. *Chem. Phys. Lett.* **2007**, *443*, 420–425.

(319) Kawata, I.; Nitta, H. An excited state paired interacting orbital method. *J. Chem. Phys.* **2012**, *136*, 064109.

(320) Malmqvist, P. Å.; Veryazov, V. The binatural orbitals of electronic transitions. *Mol. Phys.* **2012**, *110*, 2455–2464.

(321) Stewart, G. W. On the Early History of the Singular Value Decomposition. *SIAM Rev.* **1993**, *35*, 551–566.

(322) Stewart, G. W. The decompositional approach to matrix computation. *Comput. Sci. Eng.* **2000**, *2*, 50–59.

(323) Plasser, F.; Mewes, S. A.; Dreuw, A.; González, L. Detailed Wave Function Analysis for Multireference Methods: Implementation in the Molcas Program Package and Applications to Tetracene. *J. Chem. Theory Comput.* **2017**, *13*, 5343–5353.

(324) Plasser, F.; Thomitzni, B.; Bäßler, S. A.; Wenzel, J.; Rehn, D. R.; Wormit, M.; Dreuw, A. Statistical analysis of electronic excitation processes: Spatial location, compactness, charge transfer, and electron–hole correlation. *J. Comput. Chem.* **2015**, *36*, 1609–1620.

(325) Bäßler, S. A.; Plasser, F.; Wormit, M.; Dreuw, A. Exciton analysis of many-body wave functions: Bridging the gap between the quasiparticle and molecular orbital pictures. *Phys. Rev. A: At, Mol, Opt. Phys.* **2014**, *90*, 052521.

(326) Plasser, F.; Lischka, H. Analysis of Excitonic and Charge Transfer Interactions from Quantum Chemical Calculations. *J. Chem. Theory Comput.* **2012**, *8*, 2777–2789.

(327) Mewes, S. A.; Mewes, J.-M.; Dreuw, A.; Plasser, F. Excitons in poly(*para* phenylene vinylene): a quantum-chemical perspective based on high-level ab initio calculations. *Phys. Chem. Chem. Phys.* **2016**, *18*, 2548–2563.

(328) Plasser, F.; Bäßler, S. A.; Wormit, M.; Dreuw, A. New tools for the systematic analysis and visualization of electronic excitations. II. Applications. *J. Chem. Phys.* **2014**, *141*, 024107.

(329) Plasser, F.; Dreuw, A. High-Level Ab Initio Computations of the Absorption Spectra of Organic Iridium Complexes. *J. Phys. Chem. A* **2015**, *119*, 1023–1036.

(330) Head-Gordon, M. Characterizing unpaired electrons from the one-particle density matrix. *Chem. Phys. Lett.* **2003**, *372*, 508–511.

(331) Plasser, F.; Pašalić, H.; Gerzabek, M. H.; Libisch, F.; Reiter, R.; Burgdörfer, J.; Müller, T.; Shepard, R.; Lischka, H. The Multiradical Character of One- and Two-Dimensional Graphene Nanoribbons. *Angew. Chem., Int. Ed.* **2013**, *52*, 2581–2584.

(332) Nogueira, J. J.; Plasser, F.; González, L. Electronic delocalization, charge transfer and hypochromism in the UV absorption spectrum of polyadenine unravelled by multiscale

computations and quantitative wavefunction analysis. *Chem. Sci.* **2017**, *8*, 5682–5691.

(333) Kautny, P.; Glöckhofer, F.; Kader, T.; Mewes, J.-M.; Stöger, B.; Fröhlich, J.; Lumpi, D.; Plasser, F. Charge-transfer states in triazole linked donor–acceptor materials: strong effects of chemical modification and solvation. *Phys. Chem. Chem. Phys.* **2017**, *19*, 18055–18067.

(334) Mewes, S. A.; Plasser, F.; Krylov, A.; Dreuw, A. Benchmarking Excited-State Calculations Using Exciton Properties. *J. Chem. Theory Comput.* **2018**, *14*, 710–725.

(335) Mai, S.; Plasser, F.; Dorn, J.; Fumanal, M.; Daniel, C.; González, L. Quantitative wave function analysis for excited states of transition metal complexes. *Coord. Chem. Rev.* **2018**, *361*, 74–97.

(336) Mewes, S. A.; Plasser, F.; Dreuw, A. Universal Exciton Size in Organic Polymers is Determined by Nonlocal Orbital Exchange in Time-Dependent Density Functional Theory. *J. Phys. Chem. Lett.* **2017**, *8*, 1205–1210.

(337) Head-Gordon, M.; Grana, A. M.; Maurice, D.; White, C. A. Analysis of Electronic Transitions as the Difference of Electron Attachment and Detachment Densities. *J. Phys. Chem.* **1995**, *99*, 14261–14270.

(338) Wesolowski, T. A.; Warshel, A. Frozen density functional approach for ab initio calculations of solvated molecules. *J. Phys. Chem.* **1993**, *97*, 8050–8053.

(339) Wesolowski, T. A. Embedding a multideterminantal wave function in an orbital-free environment. *Phys. Rev. A: At., Mol., Opt. Phys.* **2008**, *77*, 012504.

(340) Wesolowski, T. A.; Shedge, S.; Zhou, X. Frozen-Density Embedding Strategy for Multilevel Simulations of Electronic Structure. *Chem. Rev. (Washington, DC, U. S.)* **2015**, *115*, 5891–5928.

(341) Laktionov, A.; Chemineau-Chalaye, E.; Wesolowski, T. A. Frozen-density embedding theory with average solvent charge densities from explicit atomistic simulations. *Phys. Chem. Chem. Phys.* **2016**, *18*, 21069–21078.

(342) Zech, A.; Aquilante, F.; Wesolowski, T. A. Homogeneity properties of the embedding potential in frozen-density embedding theory. *Mol. Phys.* **2016**, *114*, 1199–1206.

(343) Zech, A.; Aquilante, F.; Wesolowski, T. A. Orthogonality of embedded wave functions for different states in frozen-density embedding theory. *J. Chem. Phys.* **2015**, *143*, 164106.

(344) Aquilante, F.; Wesolowski, T. A. Self-consistency in frozen-density embedding theory based calculations. *J. Chem. Phys.* **2011**, *135*, 084120.

(345) Prager, S.; Zech, A.; Aquilante, F.; Dreuw, A.; Wesolowski, T. A. First time combination of frozen density embedding theory with the algebraic diagrammatic construction scheme for the polarization propagator of second order. *J. Chem. Phys.* **2016**, *144*, 204103.

(346) Humbert-Droz, M.; Zhou, X.; Shedge, S. V.; Wesolowski, T. A. How to choose the frozen density in Frozen-Density Embedding Theory-based numerical simulations of local excitations? *Theor. Chem. Acc.* **2014**, *133*, 1405.

(347) Almlöf, J.; Taylor, P. R. General contraction of Gaussian basis sets. I. Atomic natural orbitals for first- and second-row atoms. *J. Chem. Phys.* **1987**, *86*, 4070–4077.

(348) Dunning, T. H. Gaussian basis sets for use in correlated molecular calculations. I. The atoms boron through neon and hydrogen. *J. Chem. Phys.* **1989**, *90*, 1007–1023.

(349) Jensen, F. Polarization consistent basis sets: Principles. *J. Chem. Phys.* **2001**, *115*, 9113–9125.

(350) Widmark, P.-O.; Malmqvist, P.-Å.; Roos, B. O. Density matrix averaged atomic natural orbital (ANO) basis sets for correlated molecular wave functions. *Theor. Chim. Acta* **1990**, *77*, 291–306.

(351) Pierloot, K.; Dumez, B.; Widmark, P.-O.; Roos, B. O. Density matrix averaged atomic natural orbital (ANO) basis sets for correlated molecular wave functions. *Theor. Chim. Acta* **1995**, *90*, 87–114.

(352) Roos, B. O.; Lindh, R.; Malmqvist, P.-Å.; Veryazov, V.; Widmark, P.-O. Main Group Atoms and Dimers Studied with a New Relativistic ANO Basis Set. *J. Phys. Chem. A* **2004**, *108*, 2851–2858.

(353) Widmark, P.-O.; Zobel, J. P.; Vysotskiy, V. P.; Tsuchiya, T.; Veryazov, V. New compact density matrix averaged ANO basis sets for relativistic calculations. *J. Chem. Phys.* **2018**, *149*, 194102.

(354) Johansson, M.; Veryazov, V. Automatic procedure for generating symmetry adapted wavefunctions. *J. Cheminf.* **2017**, *9*, 8.

(355) *msym*, a library for symmetrization distributed under the MIT license. <https://gitlab.com/mcodev31/libmsym> (accessed Sept 19, 2019).

(356) Ninomiya, K.; Nagatomo, T.; Kubo, K.; Ito, T. U.; Higemoto, W.; Kita, M.; Shinohara, A.; Strasser, P.; Kawamura, N.; Shimomura, K.; Miyake, Y.; Saito, T. Development of Nondestructive and Quantitative Elemental Analysis Method Using Calibration Curve between Muonic X-ray Intensity and Elemental Composition in Bronze. *Bull. Chem. Soc. Jpn.* **2012**, *85*, 228–230.

(357) Terada, K.; Ninomiya, K.; Osawa, T.; Tachibana, S.; Miyake, Y.; Kubo, M. K.; Kawamura, N.; Higemoto, W.; Tsuchiyama, A.; Ebihara, M.; Uesugi, M. A new X-ray fluorescence spectroscopy for extraterrestrial materials using a muon beam. *Sci. Rep.* **2015**, *4*, 5072.

(358) Ninomiya, K.; Kubo, M. K.; Nagatomo, T.; Higemoto, W.; Ito, T. U.; Kawamura, N.; Strasser, P.; Shimomura, K.; Miyake, Y.; Suzuki, T.; Kobayashi, Y.; Sakamoto, S.; Shinohara, A.; Saito, T. Nondestructive Elemental Depth-Profiling Analysis by Muonic X-ray Measurement. *Anal. Chem.* **2015**, *87*, 4597–4600.

(359) Ugandi, M.; Fdez. Galván, I.; Widmark, P.-O.; Lindh, R. Uncontracted basis sets for ab initio calculations of muonic atoms and molecules. *Int. J. Quantum Chem.* **2018**, *118*, No. e25755.

(360) Mohallem, J. R.; Diniz, L. G.; Dutra, A. S. Separation of motions of atomic cores and valence electrons in molecules. *Chem. Phys. Lett.* **2011**, *501*, 575–579.